Structural Mechanisms of Experience-Dependent Synaptic Plasticity in the Mouse Visual Cortex

by

Rachel W. Schecter

B.A. Cell Biology and Neuroscience
Rutgers University, 2005

SUBMITTED TO THE DEPARTMENT OF BRAIN AND COGNITIVE SCIENCES IN PARTIAL FULFILLMENT OF THE REQUIREMENTS FOR THE DEGREE OF

DOCTOR OF PHILOSOPHY IN NEUROSCIENCE
AT THE
MASSACHUSETTS INSTITUTE OF TECHNOLOGY

JUNE 2016

Signature of Author Signature redacted

Department of Brain and Cognitive Sciences
March 4, 2016

Certified by Signature redacted

Mark F. Bear
Picower Professor of Neuroscience
Thesis Supervisor

Accepted by Signature redacted

Matthew A. Wilson
Sherman Fairchild Professor of Neuroscience and Picower Scholar
Director of Graduate Education of Brain and Cognitive Sciences

Structural Mechanisms of Experience-Dependent Synaptic Plasticity in the Mouse Visual Cortex

by

Rachel W. Schecter

Submitted to the Department of Brain and Cognitive Sciences on March 3, 2016
in Partial Fulfillment of the Requirements of the Degree of
Doctor of Philosophy in Neuroscience

ABSTRACT

Changes in the sensory experience of an animal shapes behavior through synaptic plasticity. Modification in the strength of synaptic drive can result from adjustments in the strength of existing synapses, creation of new synapses, or removal of existing ones and involves presynaptic, postsynaptic, and extrasynaptic mechanisms. Ocular dominance (OD) plasticity following brief periods of monocular deprivation (MD) is a classic example of experience-dependent change, which leads to a rapid weakening of cortical responsiveness to the deprived eye and a strengthening of responsiveness to the non-deprived eye. Though there is clear anatomical reorganization following long periods of lid suture, only recently has brief periods (3 days) of MD has been shown to drive structural plasticity of thalamic input to binocular visual cortex. The exact molecular and synaptic mechanisms responsible for rapid OD shifts remain unclear. In my thesis work, I address the requirement of proper microglial functioning via the fractalkine receptor (CX3CR1) in OD plasticity following 3 days of MD. I first identify increased lysosomal content in microglia within layer 4 (L4) of binocular visual cortex following MD, which suggests microglia participate in this structural rearrangement. As it is currently believed that a major axis of communication between neurons and microglia occurs via fractalkine and its specific receptor CX3CR1, I investigated OD plasticity within the CX3CR1 KO mouse. My experiments reveal increased lysosomal content, structural plasticity of thalamocortical synapses, and OD shifts measured with visually evoked potentials (VEPs) all occur normally in this mutant mouse as a result of 3 days of MD with only subtle differences when compared to WT mice. I conclude that, while microglia may have a role in the anatomical and functional experience-dependent cortical plasticity driven by brief lid suture, it does not require CX3CR1.

Thesis Supervisor: Mark F. Bear, Ph.D.
Picower Professor of Neuroscience

RACHEL W. SCHECTER

RachelWS@mit.edu

EDUCATION

Massachusetts Institute of Technology (MIT; Cambridge, MA) **2016**

Ph.D. in Neuroscience, Department of Brain and Cognitive Sciences

Doctoral Thesis: Structural Mechanisms of Experience-Dependent Synaptic Plasticity in the Mouse Visual Cortex

Rutgers University (RU; New Brunswick, NJ) **2005**

B.A. in Cell Biology and Neuroscience, School of Arts and Sciences

Highest Honors, Henry Rutgers Scholar

RESEARCH EXPERIENCE

SCIENTIST: Bear Laboratory (MIT; Cambridge, MA) 2011 – present

- Conceptualized and executed a novel project to study the interplay between neurons and immune-derived microglia, resulting in manuscript and 3 follow-up projects
- Acquired, analyzed, and interpreted large data sets for publications and presentations
- Collaboration with the Erisir Lab at University of Virginia on novel project; coordinated sharing of tissue samples, data reconciliation, and translated goals across fields
- Presented monthly with a didactic focus on conveying accurate technical concepts to both expert and general audiences
- Maintained portfolio of $1 million of microscopy equipment including training all users

SCIENTIST: Nedivi Laboratory (MIT; Cambridge, MA) 2006 – 2011

- Investigated synapse dynamics that lead to learning disability
- Optimized protocols to increase viral titers and protein yields by an order of magnitude
- Expertize featured in the BBC television series *Horizon: What Makes a Genius?*

LEADERSHIP

CAREER FAIR COORDINATOR 2015
UNDERGRADUATE MENTOR/SUPERVISOR 2010 - 2012
TEACHING ASSISTANT & COURSE DIRECTOR 2006 - 2009

- Earned Angus MacDonald Excellence in Undergraduate Teaching Award
- *Neurobiology Lab* (2 semesters)
- *Developmental Neurobiology*
- *Summer Splash Neuroscience* (2 semesters)

PRESENTATION

- Boston University Seminar Series — speaker, 2016
- Boston Interactive Glia Group — poster, 2016
- Integrative Neuronal Systems — poster, 2013

ACKNOWLEDGEMENTS

Firstly, I would like to thank my advisor, Mark F. Bear, for his guidance and support. Through his mentorship, I have learned how to do great science by generating simple, testable hypotheses that lead to clear – yet meticulous – presentations. I would also like to thank my committee members: Troy Littleton, Weifeng Xu, and Beth Stevens. Their constructive input has guided me towards better experiments and interpretations. Furthermore, thank you to Alev Erisir, a wonderful collaborator, teacher, and host.

Throughout my research, I have had exceptional mentorship from a variety of sources. Arnie has provided incredible support in science and life, always offering to help in any way he could. I benefited from both great high school science teachers – Mrs. DeSantis and Mrs. Robinson – and mentors who gave me a strong foundation for how to perform experiments – Sven, Tad, Jason, Barbara, and Dr. Carr. I am grateful to all of the colleagues who provided exceptional experimental help: Ming, Jeff, Eitan, Rob, Sam, Alan, and Joanne. The Bear Lab is a great place to go to work everyday, and that is possible because of Suzanne, Amanda, Emily (GC), and Erik (Sklarmagedon). Furthermore, the comradery offered by Laura, Ben, Mike, Asha, Jifang, Miquel, Tkay, Aurore, Becca, Hector, and Peter has supported and entertained me.

I am particularly thankful for the great friendships I have had within the department that will continue long after graduation. Caroline, Josh, and Lauren have been there from my first day of graduate school to my last, acting as friends and my own science family. The nights spent hanging out around Caroline's dining table fighting with Josh over musical control kept me laughing and provided some of my fondest memories. Danielle is always an island of normalcy in a sea of crazy. I would not have survived this without the life and science advice of Emily (O) and Lena; I joined the Bear Lab largely because I loved them so much and there were many days that the only thing that got me up in the morning was knowing Emily would be waiting for me with coffee at Area Four.

I am lucky to have had great roommates who are great friends. Jen, Mary, Denecia, Jeannette, and Alex: the best part of my long tenure in Cambridge is being here long enough to find them. My life would lack so much, including but not limited to The Bachelor, Vermont trips, the ability to do headstands, and cookies. They make me happier than any apartment of my own ever could. Summer and Jane have always been there when I needed it, even if it's just to whine about politics or go to a yoga class. Emily (I) was the first friend I made at MIT and often the only thing that kept me going was getting home on Friday and joining her on the couch. Seeing so many new bands together has given me tinnitus, but I don't regret a single one of those nights.

I have a great extended family – as well as friends are family by choice – that I know always root for my success: The Bakers, The Byrds, The Dukelows, The Wards (4x), The LaPellas, The Cunninghams, The Bernhagens, The Schecters, and my grandmother. Sara and Matt have provided a science-free oasis whenever I needed it. There is no way I could have made it without the support of Lynn.

Most important of all is my immediate family, and my perseverance and resourcefulness is directly attributable to the three of them. My father always nurtured my science side, encouraging questions and finding experiments to do together. Nothing made him prouder than seeing me pursue a PhD, and I wish he could be here for the culmination. My sister Meredith has always been supportive, whether that means late night texts or holding down the fort in New Jersey, and I cannot imagine my life without her in it to keep me balanced. Lastly, my mother deserves recognition most of all. Her empathy is her best and worst quality, and she has shared in my lowest points where I was sure I couldn't go on and I am so glad that she can now experience the pride and relief. I owe everything I have done, and will ever do, to them.

TABLE OF CONTENTS

Chapter I

Structural plasticity mechanisms of ocular dominance plasticity in the primary visual cortex

Chapter II

Microglial CX3CR1 is not required for proper structural synaptic remodeling in experience-dependent plasticity

Chapter III

Axon branch dynamics of specifically labeled deprived-eye thalamic input as a consequence of brief MD

Chapter IV

CPG15 is implicated in mediating proper spine dynamics and protein synthesis

Chapter V

Implications and future directions

List of Figures

CHAPTER I

Structural plasticity mechanisms of ocular dominance shifts in the primary visual cortex

---

INTRODUCTION

The capacity for learning and memory is a hallmark of animals which requires the ability to learn from experience and adapt in response to environmental changes. The needs of each individual require circuitry that is capable of adapting to the specific experience of the organism. The mammalian brain is particularly evolved to have a tremendous ability to alter responses to changes in the world it senses, a capacity that exceeds computers and approaches 1 petabite of information (Bartol et al., 2015).

Synaptic plasticity, wherein the connections between neurons in the brain are strengthened or weakened and new connections formed and lost, is a substrate for experience-dependent modifications in the brain. While this process occurs throughout an animal's lifetime, the capacity for change is not constant; early in development when the brain is beginning to experience sensory input, multiple mechanisms are accessible to massively sculpt circuits. This increased capacity for remodeling circuitry decreases sharply with age, and identifying the molecular, cellular, and structural mechanisms that allow for malleability is one long-standing goal of neuroscience.

OCULAR DOMINANCE PLASTICITY

A pre-eminent model system for studying experience-dependent changes is the visual cortex because of the vast history of anatomical and physiological studies performed in the system. Over 50 years ago, David Hubel and Torsten Wiesel produced one of the first examples of how experience can directly alter the circuits of the brain. By manipulating simple characteristics of the visual experience of kittens, they observed a robust functional and structural reorganization of the visual area of the brain. In mammals, binocular vision is generated by input from each eye converging on individual neurons in the primary visual cortex. The relative responsiveness of individual neurons to stimulation of either eye can be measured and then compared to the relative responsiveness after visual input has been manipulated. They termed this model of experience-dependent plasticity of the primary visual cortex ocular dominance (OD) plasticity.

Hubel and Wiesel demonstrated that in kittens with normal vision, approximately 80% of cortical neurons within primary visual cortex (V1) respond to stimulation of both eyes (Hubel and Wiesel, 1962). When one eye is deprived of patterned vision after the eyelid is sutured closed for months – a manipulation termed monocular deprivation (MD) – responses driven by the eye that had been deprived are dramatically reduced: the majority of neurons shift their responsiveness toward the non-deprived eye (Wiesel and Hubel, 1963). This finding has been repeated across a variety of manipulations which degrade the image from one eye. Induction of strabismus by artificially misaligning the eyes produces a similarly strong OD shift (Hubel and Wiesel, 1965). A more recent study degraded the quality of vision from one eye using an over-correcting contact lens and produced an OD shift equivalent to monocular lid suture (Rittenhouse et al., 2006). Interestingly, this loss of vision is specifically due to a decorrelation of activity between the two eyes and not merely a result of the absence of high-quality visual input, as reducing the input through both eyes equally with binocular deprivation fails to induce an OD shift ((Wiesel and Hubel, 1965), (Gordon and Stryker, 1996), (Frenkel and Bear, 2004)).

This loss of binocularity has been observed in both physiology and anatomy. The early experiments of Hubel and Wiesel measured OD shifts using electrophysiological recordings of individual cortical neurons (single-unit) within V1. Long-term monocular deprivation of cats and monkeys results in a virtual loss of cortical responsiveness to the formerly deprived eye in V1 ((Wiesel and Hubel, 1963), (LeVay et al., 1980)). Ensuing experiments showed that changes following MD can be detected as early as 6 hours after lid suture in kittens (Mioche and Singer, 1989) and following only 1 day of MD in the mouse (Liu et al., 2008). OD plasticity has since been detected across species and via diverse methods including optical intrinsic imaging (Hofer et al., 2006b), calcium imaging (Mrsic-Flogel et al., 2007), and immediate-early gene induction (Tagawa et al., 2005).

In cats, monkeys, and humans, representations of binocular visual space are projected to the visual cortex contralateral to the visual hemifield and organized into alternating patches known as ocular dominance columns. Using transsynaptic eye tracers, the columns can be labeled; their size reflects the extent of geniculocortical arbors subserving the labeled eye. MD results in a decrease of columnar size in cortex downstream of the deprived eye and an increase in the area being fed by afferents of the non-deprived eye ((Hubel and Wiesel, 1968), (LeVay et al., 1980), (Shatz and Stryker, 1978)). This result

can be detected at the level of individual neurons: in monocularly deprived kittens, reconstructions of geniculocortical axons serving the deprived eye had shorter arbors and were less complex ((Friedlander et al., 1991), (Antonini and Stryker, 1993)). Eventually, these effects are detectable within the geniculate itself: cells receiving input from the deprived eye have smaller somas than those receiving input from the non-deprived eye ((Wiesel and Hubel, 1963), (Kupfer and Palmer, 1964)).

The OD shift also bears functional consequences that can be measured by proficiency in behavioral tasks. Rodents subjected to a visual discrimination task following long periods of MD showed a dramatic loss of acuity in the deprived eye ((Prusky et al., 2000), (Iny et al., 2006)), while performance through the non-deprived eye was enhanced (Iny et al., 2006). Behavioral assays in kittens have recapitulated these findings ((Mitchell et al., 1977), (Mitchell, 1988)), demonstrating that changes in ocular dominance result in behaviorally meaningful changes in sensory processing.

THE MOUSE VISUAL SYSTEM

The classic work of OD plasticity describing the shift in ocular dominance was performed in cat and monkey. However, recent attention has shifted study to the mouse visual cortex. Mice provide an advantage over other species due to their relative abundance and the available tools developed in recent decades to aid in manipulating their genetics. This has allowed for rapid progress and more elegantly controlled experimental design, where biochemical and electrophysiological studies are coordinated both *in vivo* and *ex vivo*. Transgenic technologies have provided a way to investigate the involvement of the presence or absence of specific gene products on the function of the visual cortex.

The visual system of a mouse shares a similar organization to higher-order mammals. Representations of the visual hemifield project contralaterally from each eye (**Fig. 1.1a**). Visual information is transmitted from retina ganglion cells (RGC) to the dorsal lateral geniculate nucleus of the thalamus (dLGN). The eye-specific inputs are segregated into a core region receiving information from the ipsilateral eye and a shell region receiving information from the contralateral eye (**Fig. 1.1c**). The dLGN projects to the visual cortex, where eye-specific inputs converge onto pyramidal neurons of layer 4 as well as sending

collaterals to more superficial layers. Unlike some other mammals, mice lack segregated ocular dominance columns: the majority of neurons in binocular cortex receive input from both eyes with varying degrees of dominance (**Fig. 1.1b**) ((Drager, 1974), (Mrsic-Flogel et al., 2007)).

Most importantly, the qualities of the visual system found in most mammals are highly reproducible in mice. Mouse visual cortex contains all major receptive field types characterized in cats and monkeys ((Drager, 1975), (Mangini and Pearlman, 1980), (Metin et al., 1988)). Experiments that have systemically mapped the retinotopic organization of the contralateral visual field in mouse V1 using single-unit and intrinsic imaging have shown a similar organization to that of carnivores ((Drager, 1975), (Schuett et al., 2002)).

DEPRIVED-EYE DEPRESSION

The earliest consequence of MD is the loss of responsiveness to visual stimulation of the formerly deprived eye. The most well characterized synaptic mechanism for weakening of synaptic transmission is long-term depression (LTD). While it was initially characterized in the hippocampus ((Dudek and Bear, 1992), (Mulkey and Malenka, 1992)), it was also found in visual cortex (Kirkwood et al., 1993). The classic form of LTD result from weak activation of N-methyl-D-aspartate (NMDA) receptors, which then leads to dephosphorylation and internalization of α-amino-3-hydroxy-5-methyl-4-isoxazoleproprionate (AMPA) receptors (Heynen et al., 2003).

Biochemical and electrophysiological measurements of V1 following brief MD have detected these same signatures of LTD. The induction of an OD shift is NMDAR-dependent (Bear et al., 1990) and triggers dephosphorylation of AMPA receptors at a site that is essential to the expression of LTD (Heynen et al., 2003). This was followed by a studies demonstrating disruption of AMPA receptor endocytosis results in both a lack of OD plasticity *in vivo* and disruption of cortical LTD *in vitro* ((Lee et al., 2002), (Ahmadian et al., 2004), (Waung et al., 2008), (Yoon et al., 2009)). Furthermore, changes induced by MD *in vivo* occlude induction of LTD in subsequent visual cortical slices *ex vivo* (Heynen et al., 2003). These findings demonstrate that MD and LTD share similar molecular mechanisms that are necessary for deprived-eye depression following MD.

While the electrophysiological mechanisms are detectable rapidly after MD (Frenkel and Bear, 2004), deprived-eye depression can also be observed anatomically. As described earlier, in cats and monkeys, the ocular dominance columns subserving the deprived eye shrink ((Hubel and Wiesel, 1968), (LeVay et al., 1980), (Shatz and Stryker, 1978)). Though they lack the ocular dominance columns that aid in measurements of gross anatomy, mice also show less axon volume of the deprived geniculocortical axons following long periods of MD (Antonini et al., 1999). Recently, anatomical changes following MD were detected at the level of individual synapses. Quantitative immuno-electron microscopy (EM) measured thalamocortical synapses in mice and found that the synaptic density and thalamocortical terminal size decreases significantly after just 3 days of MD (Coleman et al., 2010).

Post-Synaptic Structural Plasticity of Dendritic Spines

The synapse is comprised of a pre-synaptic and post-synaptic component. In the CNS, a lot of experimental attention has been focused on post-synaptic mechanisms of excitatory synaptic transmission, most of which occurs within dendritic spines. Tiny protrusions extending approximately 1mm from the dendrite, spines act as compartments for the post-synaptic machinery including neurotransmitter receptors and the signaling components required for synaptic plasticity ((Koch and Zador, 1993), (Harris, 1999)).

Their discrete structures allow for relatively easy imaging and quantitation, and they have been repeatedly shown to correlate with excitatory synapse dynamics. An increase in the size of a spine may indicate an increase in synaptic strength, as spine volume correlates with the size of the postsynaptic density (PSD) area ((Harris and Stevens, 1989), (Knott et al., 2006)) and the larger the PSD the more glutamate receptors it contains ((Kharazia and Weinberg, 1999), (Takumi et al., 1999)). Spine sprouting and retraction is associated with synapse formation and elimination, respectively, both *in vivo* and *in vitro* ((Trachtenberg et al., 2002), (Knott et al., 2006), (Svoboda and Yasuda, 2006), (Arellano et al., 2007)), and the number of spines predicts the number of synapses (Braitenberg et al., 1998). Tetanic stimulation, glutamate uncaging, or other forms of long-term potentiation (LTP) induction – in addition to increasing synaptic strength – increases the number and size of spines ((Van

Harreveld and Fifkova, 1975), (Maletic-Savatic et al., 1999), (Ivanco et al., 2000), (Matsuzaki et al., 2004), (Lang et al., 2004), (Engert and Bonhoeffer, 1999)). Just like synapse dynamics, spine dynamics are bidirectional: induction of LTD results in spine removal and shrinkage ((Zhou et al., 2004), (Nagerl et al., 2004), (Okamoto et al., 2004)) and blocking AMPA receptors reduces spine density (McKinney et al., 1999).

Further, the molecular mechanisms that play key roles in synaptic plasticity also control spine stability. Blocking CaMKII, a kinase repeatedly shown to be required for synaptic plasticity and learning and increased AMPAR currents ((Giese et al., 1998), (Frankland et al., 2001)), prevents the stabilization of increased spine volume (Matsuzaki et al., 2004). Increasing activated CaMKII potentiates synaptic transmission and causes the formation of new spines (Jourdain et al., 2003). The actin cytoskeleton is the main structural component of the spine ((Fifkova and Morales, 1992), (Matus, 2000)), and increasing the rates of actin polymerization biochemically or via LTP induction increases both spine and synapse formation ((Zito et al., 2004), (Okamoto et al., 2004), (Lin et al., 2005)), while decreasing actin polymerization through LTD induction reduces spine volume (Okamoto et al., 2004). The amount of actin filament may serve as a mechanism for trafficking new proteins within the spine (Kaech et al., 2001), which is especially important for the expression of synaptic weakening, namely metabotropic glutamate receptor (mGluR) dependent LTD. Local protein synthesis is required for expression of mGluR LTD (Huber et al., 2000), as well as subsequent changes in spine morphology (Vanderklish and Edelman, 2002). Protein synthesis is also a necessary for sustained synaptic strengthening: late-phase LTP and its corresponding spine expansion requires functional protein synthesis ((Bradshaw et al., 2003), (Yang et al., 2008), (Tanaka et al., 2008)).

Many forms of experience-dependent plasticity affect the shape and presence of spines, and spine motility peaks during critical periods of sensory circuit development ((Dunaevsky et al., 1999), (Lendvai et al., 2000)). Removing visual sensory experience via dark rearing results in altered spine morphology and decreased spine density in V1 (Wallace and Bear, 2004), while light hyperstimulation leads to increased densities (Parnavelas et al., 1973); increased whisker stimulation has the same effect on neurons in the barrel cortex (Knott et al., 2002). General stimulation by enriched environments results in increased size and density of dendritic spines ((Greenough et al., 1973), (Diamond et al., 1975)). Targeted deprivations like whisker trimming increased the number of dynamic spines, though the

overall spine density was unchanged (Trachtenberg et al., 2002). Interestingly, the effect is most pronounced at the border between deprived and spared barrels columns (Wilbrecht et al., 2010). In a particularly dramatic demonstration of spine behavior following sensory deprivation, retinal lesion induces almost a complete turnover of spines in the deafferented area coincident with functional recovery (Keck et al., 2008). All of these results demonstrate a strong case for dendritic spines reflecting synaptic strength and circuit dynamics.

PRE-SYNAPTIC STRUCTURAL PLASTICITY OF AXONS

Axon terminals are the structural and functional complement to dendritic spines. In the same way that spines reflect the synaptic structures they contain, axonal boutons reflect the presence of presynaptic machinery. Boutons identified by light microscopy are almost always found to contain synapses when analyzed by electron microscopy ((Somogyi et al., 1978), (Schuz and Munster, 1985)), and the size of the bouton is correlated to the size of the active zone inside ((Harris and Sultan, 1995), (Schikorski and Stevens, 1997)).

Initial work on post-developmental axon plasticity used post-mortem tracing studies to measure the extent of individual axons following deprivation. Kittens subjected to either long-term (1 month) or moderate-term (1 week) MD resulted in restructuring of thalamocortical axons which mirrors physiology; axons serving the deprived eye show reduced complexity and branch elimination while axons serving the open eye have expanded arbors (Antonini and Stryker, 1993). A subsequent study in mice using long-term MD (~1 month) also showed atrophied axons driven by the deprived eye (Antonini et al., 1999). Later experimental findings demonstrated sensory deprivation leads to large-scale axon arbor changes of intracortical connections ((Darian-Smith and Gilbert, 1994), (Florence et al., 1998), (Trachtenberg and Stryker, 2001)). Studies of the mossy fibers of the hippocampus have also shown that axon dynamics are influenced by the same cellular mechanisms that are required for synaptic plasticity: axon arbor rearrangement requires activity and synaptic transmission (Galimberti et al., 2006)) and changes in axon bouton dynamics require functional AMPA receptors and protein synthesis (De Paola et al., 2003).

Despite this evidence that axon terminals are involved in circuit plasticity, most anatomical studies have been dendrite- and spine-centric. When compared to dendrites,

CNS axons have much larger synaptic territories; their arbors often extend millimeters away from their somas, and their boutons, which contain presynaptic machinery, are tens of microns apart. The diameter of an axon is also half the size of a dendrite. These qualities introduce technical difficulties to quantifying structural changes. In order to assess full arbors or at least enough of the axon to track multiple boutons, large volumes of tissue must be included and the resolution of microscopy must be higher. These issues were addressed with the advent and popularity of two-photon microscopy. By exciting a narrow focal plane with an infrared laser, light scatter is minimized and excitation can reach deep into tissue (Denk et al., 1990) and the nature of the laser localization decreases photodamage, allowing tissue viability to be maintained (Squirrell et al., 1999). Combined with transgenic technology to sparsely label neurons, the past decade has yielded exciting data revealing the naturalistic and experience-dependent changes in axonal structure.

Longitudinal *in vivo* studies of adult cortex without any sensory manipulation show that lengths of axons are largely stable, and over one month, add and subtract 4% of their branches ((De Paola et al., 2006), (Stettler et al., 2006)). Both studies found boutons to be more dynamic, though the rates of which vary as to whether the axons are intracortical or thalamocortical in origin and whether they were en passant or terminaux (De Paola et al., 2006). When comparing the activity of axons and dendrites in normally raised juvenile mice, axon terminals were more stable than spines (Majewska et al., 2006). This lack of basal presynaptic structural dynamics gave support for the theory that the immediate structural dynamics underlying synaptic plasticity are predominantly on the dendritic side of the synapse, with changes to the axonal side lagging behind.

However, horizontal axon remodeling occurs within 24 hours of retinal lesion (Yamahachi et al., 2009). Fast axonal remodeling is not limited to corticocortical projections, as thalamocortical terminal remodeling is a consequence of brief MD (Coleman et al., 2010). This parallels physiological plasticity, as thalamocortical synaptic transmission solely accounts for OD shifts after 3 days of MD (Khibnik et al., 2010). Furthermore, monocular inactivation with TTX, a similar manipulation of vision but one that does not induce an OD shift, also does not induce removal of thalamocortical terminals (Coleman et al., 2010). Thus there is a relationship between structural rearrangement and physiological plasticity, but demonstrating how and when axonal structural plasticity is a major expression

mechanism of rapid experience-dependent synaptic plasticity is an exciting, and yet unanswered, topic of study.

MICROGLIA IN STRUCTURAL SYNAPTIC PLASTICITY

For over 100 years, the synapse was defined as a two-party transaction between neurons (Ramón y Cajal et al., 1988). However, the brain consists of an equal number of non-neuronal glia as neurons themselves ((Herculano-Houzel et al., 2007); though the exact quantities are still in active debate). A redefinition of the synapse to include astrocytes (Araque et al., 1999) and microglia (Schafer et al., 2013) as important components of a "quad-partite" synapse has occurred in the last decade. Astrocytes have been shown to have a role in information processing, mainly by removing excess glutamate via glutamate transporters (Danbolt, 2001), along with other important functions detailed in many comprehensive reviews ((Allen and Barres, 2005), (Perea and Araque, 2010), (Theodosis et al., 2008)).

As they share a lineage with the immune system and macrophages, microglia have long been studied for their phagocytotic ability to clear damage after injury or apoptotic cells in beginning stages of brain development – they are present early in the embryonic brain – and later in life during pathological conditions. For the times in between when the brain is healthy, microglia had been believed to be "resting", waiting for an insult to become "active" wherein the cell morphology changes drastically to reflect a pathological state: surveying processes are retracted and the soma size becomes larger (Thomas, 1992). This view was upended in 2005 when Nimmerjahn and colleagues imaged microglia in an intact mouse brain and found microglia to be highly dynamic. Their processes are fast moving and short lived, allowing the total microglia population to scan the entire brain every few hours (Nimmerjahn et al., 2005). Furthermore, microglia made contact to all cortical and synaptic elements, a finding that has been repeated in postmortem murine studies showing that 94% of microglial processes are in direct apposition to a synaptic component ((Tremblay et al., 2010), (Nimmerjahn et al., 2005), (Wake et al., 2009)).

It is very clear that microglia are physical bystanders to synaptic transmission, but are they actual participants? Excitingly, microglia have the capacity to detect and respond to

synaptic activity. In organotypic hippocampal slices, modulating activity with TTX or LTP induction results in increased or decreased microglial motility, respectively (Grinberg et al., 2011), and *in vivo*, increased inhibition via GABA application induces increased microglial sampling (Nimmerjahn et al., 2005). Microglia are also particularly responsive to altered sensory activity. Global sensory deprivation with dark exposure reduces microglia movement, yet increases the area of contact with synaptic elements (Tremblay et al., 2010); microglial contact was likely to result in spine shrinkage, and these microglia contained inclusions of pre and postsynaptic material (Tremblay et al., 2010). Eliminating visual activity with binocular enucleation or TTX reduces microglial synaptic contact as well (Wake et al., 2009). Microglia are preferentially attracted to neurons with naturally high levels of spontaneous activity, and increasing activity with glutamate uncaging attracts microglial processes (Li et al., 2012). Microglia have the capability to express every known neurotransmitter (Pocock and Kettenmann, 2007), though knowing when and where they are expressed and how it impacts specific microglia activity is still largely unknown.

Experiments changing the balance of retinal ganglion cell (RGC) input into the developing dorsal lateral geniculate nucleus (dLGN) have been especially revealing of how modulating experience affects microglial behavior. During eye-specific segregation of the dLGN in mice, microglia engulf RGC presynaptic terminals ((Paolicelli et al., 2011), (Schafer et al., 2012)) and inhibition of microglia with minocycline also reduces proper segregation of the inputs (Schafer et al., 2012). This behavior is activity-dependent: there is increased microglial phagocytosis of RGC inputs after eyeball injection of TTX and decreased phagocytosis of inputs after injection of forskolin (Schafer et al., 2012).

Furthermore, disruption of the ability of microglia to sense their environment results in improper wiring. Microglial motility is especially dependent upon purinoception, with an inverse correlation to the concentration of ATP in its microenvironment ((Haynes et al., 2006), (Davalos et al., 2005), (Li et al., 2012)). Their mesodermal origin results in expression of receptors specifically for signaling components originally defined in innate immune signaling.

On the body side of the blood brain barrier, the complement signaling system exists to tag pathogens for rapid removal, and reduces the negative charge of the pathogenic membrane to enhance phagocytosis. Within the developing brain, complement signaling is redirected for structural synaptic plasticity: immature, unnecessary synapses are tagged for

removal via microglial engulfment. The complement system ultimately converges on C3, with C1q often acting upstream. During CNS development, C1q is expressed by neurons, localized to synapses that will be eliminated (Stevens et al., 2007). KO mice that lack components of the complement signaling cascade – C1q, C3, or C3R (the microglial-specific receptor for C3) – have improperly segregated dLGNs and increased RGC synapses (Stevens et al., 2007), (Schafer et al., 2012)). C1q and C3R KO animals also show a failure to prune synapses, with more presynaptic boutons and synapse density, increased spontaneous excitatory transmission, and propensity towards seizure ((Chu et al., 2010), (Schafer et al., 2012)).

Along with physically removing pre and post-synaptic components, microglia can also influence synaptic plasticity indirectly via release of a host of diverse neuroactive signals. In addition to the complement system, microglia can secrete many cytokines classically found in the immune system, including Tumor necrosis factor (TNFα), which when expressed by microglia at low levels acts as an effector of synaptic scaling, a uniform adjustment of synaptic strength ((Stellwagen and Malenka, 2006), (Pascual et al., 2012)). Microglia are also a major source of trophic factors in the brain, which increases cell survival and neurogenesis, as well as promotes learning-dependent synapse formation (Parkhurst et al., 2013). They can also potentially participate directly in synaptic transmission by releasing NO, glutamate, ATP, and other neurotransmitters ((Kettenmann et al., 2011), (Pascual et al., 2012)). Microglia can impact neuronal excitability by modulating the NMDAR glycine binding site (Hayashi et al., 2006) or changing chloride gradients which convert inhibitory responses to excitatory responses (Coull et al., 2005).

Microglia are in an ideal position to respond to altered sensory experience. They are in place coincident with the first waves of synaptogenesis (Kettenmann et al., 2011), and are sensitive to highly local changes in activity via a host of receptors that are dynamically expressed. This is not purely a position of observation, as they can influence synaptic transmission themselves by releasing various factors or directly phagocytosing synapses. This perspective is largely an accepted fact in the developing and degenerating brain, however there remains unanswered question as to what role microglia have in experience-dependent structural synaptic plasticity in the mature, healthy brain.

MICROGLIAL RECEPTOR CX3CR1 IN SYNAPTIC PLASTICITY

While there are many different mechanisms for microglia to observe and influence synaptic plasticity, there has been recent evidence that suggests fractalkine (CX3CL1) and the fractalkine receptor (CX3CR1) is involved in synaptic function. Fractalkine is a chemokine signal synthesized by neurons of the forebrain as a transmembrane protein that can be cleaved by cathepsin S or metalloproteases, releasing a soluble isoform which contains the chemokine domain ((Garton et al., 2001), (Sheridan and Murphy, 2013)). Fractalkine binds exclusively to the fractalkine receptor, a G_i-protein coupled receptor expressed by myeloid cells throughout the body ((Combadiere et al., 1998), (Harrison et al., 1998)). Within the brain, microglia are the only expressers of CX3CR1, allowing for a highly selective signal between neurons and microglia (Jung et al., 2000).

The specificity of the fractalkine signal between neurons and microglia led to studies investigating the impact of disruption of this signaling axis. A major tool for these experiments was the creation of a mouse line where the CX3CR1 gene is replaced by GFP; all microglia in the homozygotes of this mouse line lack expression of CX3CR1 and are labeled with GFP (Jung et al., 2000). The CX3CR1 heterozygote mouse has been used for many imaging studies and has been important to demonstrate that microglia contact synaptic elements ((Nimmerjahn et al., 2005), (Tremblay et al., 2010)). The CX3CR1 KO mice have been used to investigate the importance of fractalkine signaling on the neuronal circuitry of the non-pathological brain. As a chemokine that definitionally induces chemotaxis, many groups have investigated the impact of CX3CR1 deficiency on basal motility of microglia. In CX3CR1 KO retinal explants, microglia processes have slower-moving spontaneous motility (Liang et al., 2009), and in CX3CR1 KO hippocampal microglia, slower ATP-induced motion (Pagani et al., 2015). Possibly as a consequence of decreased microglial velocity, there is a transient reduction in microglial density within the hippocampus of CX3CR1 KO animals in the first month after birth (Paolicelli et al., 2011).

This study from the Gross Lab provided several lines of evidence for the involvement of fractalkine in hippocampal synaptic plasticity. Paolicelli *et al.* found that in the CX3CR1 KO mice, there is an increase in both hippocampal dendritic spines and PSD95 puncta (Paolicelli et al., 2011). The authors followed up on this finding in a subsequent paper, wherein they show CX3CR1 KOs contain less multisynapse boutons than WT animals (Zhan

et al., 2014). Together, this data suggests that without fractalkine signaling to microglia, there is a deficit of synaptic pruning that prevents the normal strengthening and maturation of specific synapses. They also showed an increase in immature synapses electrophysiologically by measuring spontaneous EPSCs (sEPSCs) that result from action potentials; in WT animals, the amplitude of sEPSCs increases during development as functional synapses are added to neuronal circuits, but this does not occur in KO animals even by P40 ((Paolicelli et al., 2011), (Zhan et al., 2014)). This synaptic deficit has functional impacts on hippocampal circuitry: KO animals have transient increased LTD and resistance to pharmacologically-induced seizures (Paolicelli et al., 2011). As expected, the circuitry deficits in mice that lack CX3CR1 interferes with their ability to learn. CX3CR1 KO animals perform normally in tone-dependent fear conditioning (which reflects amygdala function), but poorly in context-dependent fear conditioning (which reflects hippocampal function) (Rogers et al., 2011). These results demonstrate the importance of fractalkine signaling in proper hippocampal circuit function from the level of individual synapses to global behavioral function. Whether these deficits are the direct result of a lack of fractalkine signaling to microglia or a product of the decreased motility, recruitment, and density of CX3CR1 KO microglia is not entirely clear; however the reduction of hippocampal microglial density is transient and only occurs in juvenile mice, while many of the synaptic phenotypes persist into adulthood ((Paolicelli et al., 2011), (Zhan et al., 2014), (Rogers et al., 2011)).

The fractalkine receptor is also required for proper synaptic function throughout the brain. The overall long-range connectivity of CX3CR1 KO brains is compromised, with less coherence between brain regions (Zhan et al., 2014). CX3CR1 KO mice do not show increased motor performance on repeated trials of a rotorod task (Rogers et al., 2011), are seemingly averse to social interaction with other animals (Zhan et al., 2014), and spend increased time grooming (Zhan et al., 2014). In the developing mouse somatosensory cortex, microglia enter developing barrels of thalamocortical inputs, and this process is delayed in CX3CR1 KO animals (Hoshiko et al., 2012). Similar to hippocampal data, electrophysiology of acute barrel cortex slices reveal that CX3CR1 KO thalamocortical synapses are functionally immature, with a delayed GluN2B to GluN2A switch and lack of increase in the AMPAR to NMDAR ratio (Hoshiko et al., 2012).

These studies show that the fractalkine signaling pathway is required for proper neuronal circuit formation throughout the brain. Although it is evident that CX3CR1 KO mice show synaptic plasticity deficits during development, the question remains as to how experience-dependent plasticity occurs without the fractalkine receptor. As proper microglial motility requires the chemotaxic properties of fractalkine and CX3CR1 KO hippocampi have increased synapse density and decreased multisynapse presynaptic terminals, there would be similar synaptic deficits predicted within the visual cortex with CX3CR1 KO; specifically, that these animals would be unable to target and remove synapses subserving a deprived input, like those from a lid-sutured eye.

Involvement of Microglia in OD Plasticity

The experiments that follow in Chapter 2 were designed to critically test the role of microglia and CX3CR1 in visual cortical experience-dependent synaptic plasticity. We used OD plasticity of the juvenile mouse visual cortex as a model system because it is a classic example of deprivation that has been mechanistically well characterized from the neuron perspective. Furthermore, using this model system we are able to track changes in the primary visual circuit from the synaptic level all the way to functional outcomes.

As suggested in the previous section, we hypothesized that fractalkine signaling from neurons to microglia would be required for normal OD plasticity, as the CX3CR1 KO mouse has previously been shown to have synaptic plasticity deficits in the hippocampus and somatosensory cortex. We used this same mouse to ask if CX3CR1 is required 1) for the visual cortical plasticity observed following monocular deprivation and/or 2) for proper development of the visual system. We investigated if fractalkine signaling is required to drive the consequences of brief periods of monocular deprivation, namely a reduced density of thalamocortical synapses and the depression of deprived-eye visually evoked potentials (VEPs) within layer 4 of the binocular primary visual cortex ((Coleman et al., 2010), (Frenkel and Bear, 2004)). In addition, we measured a form of visual cortical strengthening, stimulus-selective response potentiation (SRP), which shares many of the hallmark characteristics of LTP (Frenkel et al., 2006) and therefore acts as a complement to deprived-eye depression. In parallel, we investigated the requirement of CX3CR1 on the normal development of the visual system including segregation of retinal input to the thalamus –

which requires other microglial signals such as C3 and C1q ((Stevens et al., 2007), (Schafer et al., 2012)) – and functional visual acuity.

Our investigation of the fractalkine receptor was part of a bigger question: are microglia required for or involved in OD plasticity? If our results showed that CX3CR1 blocked the consequences of lid suture that drive deprived-eye depression, we could conclude that microglia are required for OD plasticity; this could be because microglia were unable to detect the signals that flag synapses for change, unable to effect synaptic change, or simply not in place in the cortex to participate due to chemotaxic deficits. Conversely, if CX3CR1 KO animals are indistinguishable from WT animals, the overall role of microglia in visual cortical plasticity remains, though we can conclude that fractalkine signaling through microglia specifically is not required in OD plasticity.

We addressed this possibility experimentally by asking if we could detect any change in the microglia themselves at the cortical location where synapses are removed. We predicted that if microglia are involved in OD plasticity, there would be a measurable phenotypic change of microglia in WT animals following MD. This would be the first data to show that microglia are activated in response to lid suture, and would suggest that they have some involvement in visual cortical plasticity. Furthermore, by including CX3CR1 KO mice in this experiment, we can draw conclusions if lid sutured CX3CR1 KO mice lacked the same microglial activation seen in WT animals. In addition to lacking an OD shift, this would suggest that CX3CR1 is required specifically for microglia to detect the changes in activity that drive visual cortical plasticity.

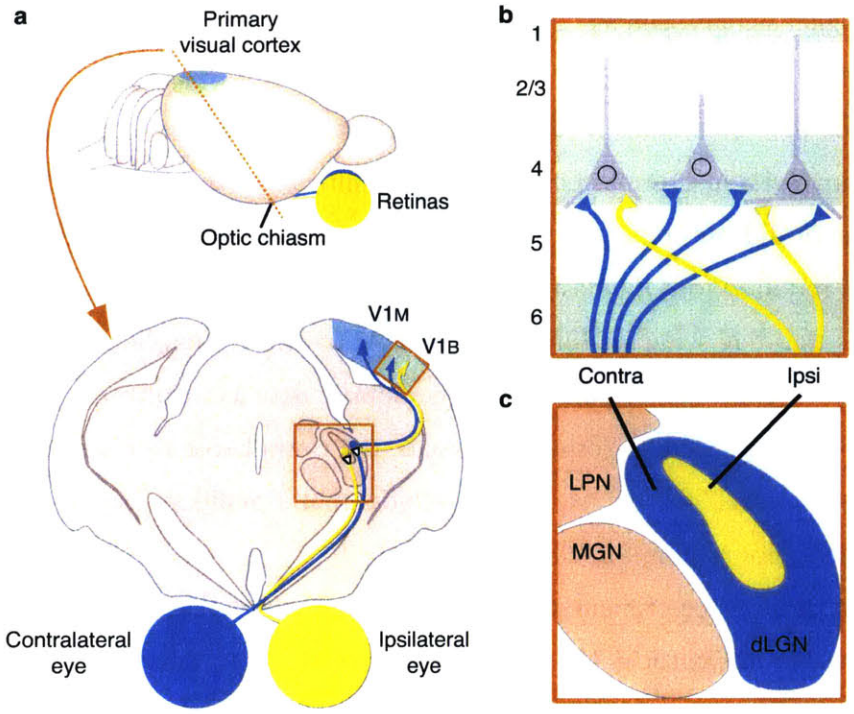

FIGURE 1.1: ORGANIZATION OF THE MOUSE VISUAL SYSTEM

a, (*top panel*) The mouse brain is depicted in profile. The primary visual cortex (*blue shading, monocular; green shading, binocular*) is located just rostral of the cerebellum and dorsal-medial in the cortex. A coronal slice (*bottom panel*) showing how visual information is received by the retina of each eye before being projected to the **c,** dorsal LGN, where it is then relayed to **b,** primary visual cortex. The majority of RGC cells project to the contralateral brain hemisphere, forming a shell of input in the dLGN (***c,*** *blue*) surrounding the fewer inputs from the ipsilateral eye (***c,*** *yellow*). **d,** The thalamocortical axons then travel to the primary visual cortex, synapsing onto pyramidal neurons in layer 4, with collateral projections to more superficial layers.

CHAPTER II

Microglial CX3CR1 is not required for proper structural synaptic remodeling in experience-dependent plasticity

---

Electron Microscopy experiments and analysis in this chapter were done in collaboration with Erin Maher and Alev Erisir at the Department of Psychology, University of Virginia.

ABSTRACT

Brief monocular deprivation (MD) shifts ocular dominance (OD) in primary visual cortex (V1) via depression of responses to the deprived eye and potentiation of responses to the open eye. A recent study showed rapid structural plasticity of thalamic input to binocular visual cortex following 3 days of lid suture. Microglia have been implicated in activity-dependent circuit refinement during development, and we found that they have increased phagocytotic activity as a result of lid suture. Here we address the extent to which the consequences of MD are dependent upon signaling through the fractalkine microglial receptor CX3CR1. CX3CR1 KO mice have been shown to express various synaptic plasticity deficits, however we found they expressed normal visual cortical plasticity as measured by stimulus-selective response potentiation (SRP) and 3 days of MD. We used quantitative electron microscopy (EM) to determine how the lack of fractalkine signaling impacts the synapses underlying the OD shift. Within layer 4 of binocular visual cortex following MD, WT and CX3CR1 brains have decreased densities of thalamocortical synapses and an increase in the density of intracortical synapses. As microglia within layer 4 of binocular visual cortex – the region that undergoes structural remodeling of thalamic input – are activated following MD, we believe microglia may be involved in mediating OD shifts. However, these results show that CX3CR1 is not required for this form of experience-dependent plasticity.

INTRODUCTION

While cell types other than principal neurons have been identified in the brain for over a century, the traditional view of the synapse has been primarily limited to neurons. Constraining the synapse to presynaptic structures and postsynaptic densities (Ramón y Cajal et al., 1988) is myopic and limits the field's ability to truly characterize how synapses function and change, and further, how disease states develop and are treated. Recent progress has been made which views the synapse as a dynamic structure that contains many cell types including astrocytes (Araque et al., 1999) and, most recently, microglia ((Ajami et al., 2007), (Tremblay and Majewska, 2011)). This more nuanced, complex definition has been termed the "quad-partite synapse" (Schafer et al., 2013) and is an exciting new avenue with which to investigate synaptic plasticity.

Microglia are the interface between the immune system and neurotransmission. Originating from the developmental circulatory system of the yolk sac, these mesoderm-derived cells colonize the brain prior to vascularization, even before monocytes exist outside of the brain (Alliot et al., 1999). A second wave of colonization occurs through the first and second trimester, as monocytes from the circulatory system invade the cortex and migrate into different cortical layers (Rezaie and Male, 1999). They are in place before apoptosis, during which they contact and engulf dying neurons and play a crucial role in developmental programmed cell death (Frade and Barde, 1998). Microglia also phagocytose axons that need to be pruned, such as those that are nonmylenated in the corpus callosum (Berbel and Innocenti, 1988), those that are injured in nerve axotomy of the peripheral nervous system (Cullheim and Thams, 2007), and in the cortex after lesion (Trapp 2007). Their influence over neurons is not limited to phagocytosis of damaged cells; microglia also release growth factors and superoxide ions to promote survival ((Mallat et al., 1989), (Shimojo et al., 1991), (Elkabes et al., 1996)).

While microglial behaviors during programmed cell death and neurodegeneration are well explored, there has been recent attention to their role in creating properly connected neural circuits. In the healthy brain, microglia are highly active, having multiple short-lived processes with dynamic actin skeletons regulated by Ionizing Ca-binding Adaptor Protein (Iba-1) that move at the incredibly fast speed of 1.5 microns a minute ((Nimmerjahn et al., 2005), (Kettenmann et al., 2011)). This constant surveillance occurs in an activity-

dependent manner ((Davalos et al., 2005), (Nimmerjahn et al., 2005) (Tremblay et al., 2010)). This also extends to primary sensory cortices and sensory experience: for example, when a mouse is deprived of light, microglial processes become less motile and contain more phagocytotic inclusions, and these effects are reversed after the animal is re-exposed to light (Tremblay et al., 2010) and the distribution of microglial cells within the barrel cortex changes after whisker lesion (Hoshiko et al., 2012). Electron microscopy has revealed that vesicles within microglia are immunoreactive for SNAP 25 and PSD-95, suggesting that microglia engulf both pre and postsynaptic components in the healthy adult rodent brain (Paolicelli et al., 2011), although a recent study suggests that microglial contact occurs predominantly on the presynaptic side (Sogn et al., 2013).

In order to have a dynamic, complex view of what is going on at each synapse contacted, microglia express many neuronal receptors and channels (Kettenmann et al., 2011). Reciprocally, microglia can also influence synaptic plasticity via release of cytokines ((Hanisch, 2002), (Mallat et al., 1994)), many of which are involved in learning and memory. Complement signaling – traditionally viewed as part of the immune system that enhances the ability of phagocytic cells to engulf pathogens – has recently been shown to be required for developmental experience-dependent circuit refinement. Neurons, expressing the complement proteins C1q and C3, and microglia, expressing the complement receptor C3R, is required for removing unwanted synapses ((Stevens et al., 2007), (Schafer et al., 2012), (Chu et al., 2010)).

When investigating synaptic plasticity in the adult brain, fractalkine (or CX3CL1) signaling has drawn attention. It is a putative neuron-to-microglia signal expressed exclusively by neurons (though astrocytes may also express fractalkine during inflammatory conditions (Maciejewski-Lenoir et al., 1999)) and, within the brain, the receptor (CX3CR1) is expressed exclusively by microglia (Nishiyori et al., 1998). A membrane-bound chemotaxic cytokine, it is constitutively expressed by neurons and is posited as a tonic "stop" signal to microglia (Harrison et al., 1998). Fractalkine can be cleaved into a soluble form by matrix metalloproteinases or Cathepsin S (Clark et al., 2007); although the influence of these different forms is not clear, both are capable of binding to CX3CR1 ((Chapman et al., 2000), (Haskell et al., 1999)). The fractalkine receptor is a metabotropic receptor coupled to a $G\alpha_i$ subunit whose sole ligand is CX3CL1, and whose activation is capable of modulating diverse signaling cascades including cell growth and phosphorylation of ERK

(Biber et al., 2007). The fractalkine signaling axis also has synaptic effects: in hippocampal slice experiments, CX3CL1 application decreases excitatory transmission via a mechanism that occludes LTD ((Ragozzino et al., 2006), (Maggi et al., 2009)). This prevents LTP induction by inhibiting NMDAR calcium influx and GluR1 dephosphorylation ((Deiva et al., 2004), (Ragozzino et al., 2006), (Maggi et al., 2009)).

Many studies have used a transgenic mouse in which the CX3CR1 gene is replaced with the GFP gene (Jung et al., 2000), hereafter referred to as a CX3CR1 KO, to interrogate the impact of the loss of fractalkine signaling on the brain. CX3CR1 KOs have synaptic plasticity deficits in the developing hippocampus: there is a lack of LTP (Rogers et al., 2011) and a transient increase in LTD (Paolicelli et al., 2011), as well as a persistent decrease in AP-induced EPSCs (Paolicelli et al., 2011). These electrophysiological phenotypes are also reflected in structure, as KO animals have 50% less multisynapse boutons (Zhan et al., 2014) as well as a transient increase in dendritic spines that, interestingly, becomes dissociated from the physiology as the spine phenotype disappears over time but the decreased evoked EPSCs does not (Zhan et al., 2014). On a global brain scale, these synaptic abnormalities result in a miswired brain, with decreased coherence between brain areas and subsequent reduced functional connectivity. The KO mouse demonstrates various behavioral abnormalities included altered fear conditioning (Rogers et al., 2011), compromised rotarod motor learning (Rogers et al., 2011), deficient water maze performance (Rogers et al., 2011), increased grooming (Zhan et al., 2014), and aversion to social interaction (Zhan et al., 2014).

Because *in vivo* studies thus far have manipulated sensory experience with paradigms that reduce general levels of neuronal activity, yet fail to induce obvious functional changes, we used short monocular deprivation to drive an ocular dominance shift in CX3CR1 KO mice. Rapid OD plasticity in mice is characterized by the selective depression of deprived-eye responses as measured where the inputs from the two eyes converge onto neurons in cortical layer 4 of binocular visual cortex. This decrease in excitatory synaptic transmission is a product of many synaptic plasticity mechanisms, including synapse weakening in the form of LTD ((Heynen et al., 2003), (Malenka and Bear, 2004)), as well as synapse elimination (Coleman et al., 2010). The requirement for each mechanism and the molecular machinery underlying each – especially synapse elimination – is not clear. We used the CX3CR1 KO mouse to probe the requirement of fractalkine signaling on experience-dependent plasticity within primary visual cortex following a brief period of MD. Our *in*

vivo electrophysiology and quantitative structural results show that CX3CR1 KO OD shifts that are similar to WT animals. While we find that microglia are activated following lid suture and therefore may be involved with the cortical response to MD, the fractalkine receptor is not required for ocular dominance plasticity in juvenile animals.

RESULTS

BRIEF LID SUTURE INCREASES LYSOSOME CONTENT WITHIN MICROGLIA BUT DOES NOT AFFECT MIGRATION

Three days of monocular lid suture results in decreased thalamocortical synaptic input to layer 4 of binocular primary visual cortex ((Khibnik et al., 2010), (Coleman et al., 2010)). We hypothesized that if microglia are required for this process, there might be increased microglia recruitment to the location of this change in input. However, we did not find any difference in the density of Iba1-stained microglia in layer 4 of binocular V1 in WT animals whether or not they had undergone MD (**Fig. 2.1b**; *WT: 192.50 ± 28.17 cells per mm^2; WT+MD: 183.33 ± 24.00 cells per mm^2; ANOVA MD condition: p = 0.968).* We did find decreased microglial soma size as a result brief MD in WT mice that is not statistically significant (**Fig. 2.1c**; *WT: 81.81 ± 2.87 mm^2; WT+MD: 73.26 ± 2.51 mm^2; ANOVA MD condition: p = 0.004, WT vs WT+MD: p = 0.059*). We believe this trend may be a consequence of increased microglial projection volume, which enables increased parenchymal scanning following MD.

If microglia respond to MD, they should show signs of activation. When phagosomes engulf material, the endosome containing the foreign material fuses with lysosomes containing digestive enzymes (Peri and Nusslein-Volhard, 2008). The presence of CD68, a lysosome membrane protein expressed in cells of myeloid origin (Song et al., 2011), has been used as a measure of microglial activation ((Tanaka et al., 2013), (Schafer et al., 2012)). For this reason, we quantified the CD68 immunoreactivity within microglia somas to determine if there was increased lysosomal content following MD (**Fig. 2.1a**). We found a striking effect of microglia-specific CD68 staining in animals that underwent 3 days of MD (**Fig. 2.1d**; *WT: 7.41 ± 1.40 % soma size; WT+MD: 16.25 ± 2.19 % soma size; ANOVA*

MD condition < 0.001, WT p = 0.003), and increased CD68 staining within individual microglia somas (**Fig. 2.1e**; *Mann-Whitney U Test WT vs WT+MD < 0.001*).

Many previous studies have found a microglia recruitment deficit as a result of CX3CR1 KO, which is in line with its chemoattractant function. In these animals, there is a transient deficit in microglia density in the developing hippocampus (Paolicelli et al., 2011) and increased microglia density in the white matter of the motor cortex (Ueno et al., 2013). However, a study of the mouse somatosensory cortex found no difference in microglia density in layer 4; the authors do report a recruitment deficit, but at a finer level reflective of the thalamic input, suggesting that there may be small, specific microdomains (Hoshiko et al., 2012). Our findings are in line with the somatosensory data: we found no significant difference between the layer 4 microglia density in WT and CX3CR1 KO mice (**Fig. 2.1b**; *KO: 171.25 ± 18.95 cells per mm^2; ANOVA genotype: p = 0.572*). Also like WT animals, KO animals have no recruitment difference following lid suture (**Fig. 1b**; *KO+MD: 178.57 ± 23.58 cells per mm^2; ANOVA genotype MD interaction: p = 0.720*). Microglial have significantly smaller soma sizes following MD without CX3CR1, similar to WT animals (**Fig. 2.1c**; *KO: 88.16 ± 3.45 mm^2; KO+MD: 76.93 ± 4.59 mm^2; p = 0.014*).

Lysosomal content per animal also increases after MD in KO animals (**Fig. 2.1d**; *KO: 7.76 ± 1.05 % soma size; KO+MD: 14.04 ± 1.95 % soma size*). On an individual microglial cell basis, there is a significant difference following MD in the KO animals (**Fig. 2.1e**; *Mann-Whitney U Test KO vs KO+MD: p < 0.001*). However, when comparing microglia of WT animals that have undergone MD to microglia of KO animals that have undergone MD, there is significantly less lysosome content in KO+MD microglia (**Fig. 2.1e**; *Mann-Whitney U Test WT+MD vs KO+MD: p = 0.001*). This leads us to conclude that CX3CR1 deficient microglia are capable of reacting to changes in activity and upregulating their phagocytotic machinery, but at a rate slightly less than WT microglia.

CX3CR1 IS NOT REQUIRED FOR SEGREGATION OF RETINAL GENICULATE INPUTS INTO THE LGN

During early postnatal development, the mouse LGN develops from a structure containing large areas of overlap between the retinal ganglion cell projections from each eye to one that is distinctly segregated. Prior to eye opening, axons segregate roughly into eye-

specific areas ((Dhande et al., 2011), (Huberman et al., 2008)). Then between eye opening (P10) until P20, the number of axons that innervate each LGN neuron decreases and ipsilateral eye projections are pruned away to leave a small core of remaining input that is surrounded by contralateral eye projections ((Chen and Regehr, 2000), (Jaubert-Miazza et al., 2005)). Increased area of overlap within the LGN between the two eyes is indicative of a synaptic pruning deficit ((Bjartmar et al., 2006), (Stevens et al., 2007), (Pham et al., 2001)). Microglia participate in this process, enveloping the projections that are pruned away (Schafer et al., 2012) in a manner which requires proper immune signaling ((Stevens et al., 2007), (Boulanger, 2009)). This raises the possibility that LGN segregation will be disrupted after knock out of CX3CR1, which has important implications for proper binocular cortical development and can influence interpretations of results relating to ocular dominance plasticity, and also reflects the role of CX3CR1 during development.

In order to measure LGN segregation, we labeled eye-specific inputs with an anterograde tracer (CTB) conjugated to a different fluorophore (Alexa 555 or 647) in littermate mice (**Fig. 2.2a and 2.2b**). We chose to analyze brains from P28 – P30 mice, which are complementary in age to our electrophysiology studies and at an age where the LGN has completed its development. We found no significant difference between either the areas occupied by the contralateral eye (**Fig. 2.2c**; *WT: 83.91 ± 1.88, KO: 83.88 ± 2.91 percent of total dLGN; p = 0.585*) or ipsilateral eye (**Fig. 2.2c**; *WT: 17.65 ± 3.09, KO: 18.57 ± 2.27 percent of total dLGN area; p = 0.528*). Furthermore, we did not see an increased area of overlapping projections (**Fig. 2.2c**; *WT: 2.08 ± 0.29, KO: 2.48 ± 0.52 percent total dLGN area; p = 0.482*), the hallmark of disrupted LGN segregation. This confirms that, at the retinal ganglion level, microglia lacking CX3CR1 are still capable of sculpting circuits during visual system development.

JUVENILE AND ADULT CX3CR1 KO MICE HAVE INTACT VISUAL ACUITY

Before CX3CR1 KO mice can be assessed for visual cortical synaptic plasticity, it is important to confirm that they have the same quality of vision as has been shown previously in wild-type animals. Like LGN segregation, the quality of vision is also a reflection of the proper developmental wiring of the visual system. Visually evoked potentials (VEPs) offer a

way to quantify visual function in mice at the level of the primary visual cortex and these recordings have been demonstrated to match previously reported behavioral measures of visual acuity ((Prusky and Douglas, 2003), (Muhammed, 2009)).

Juvenile CX3CR1 KO and WT littermate mice (P18) were implanted with VEP recording electrodes within layer 4 of binocular primary visual cortex, a depth that yields the maximum negative-going VEP ((Huang et al., 1999), (Sawtell et al., 2003)). Amplitudes of evoked responses to four different spatial frequencies (0.05, 0.2, 0.5, and 0.7 cycles per degree) were recorded from P21 to P31 during binocular stimulation with a uniquely oriented visual grating stimulus (**Fig. 2.3a**). We found no differences between VEP magnitudes of WT or KO animals at any of the spatial frequencies tested (**Fig. 2.3b, Supplementary Table 2.1**; *WT vs. KO: 0.05 cyc/degree $p = 0.776$, 0.2 cyc/degree $p = 0.908$, 0.5 cyc/degree $p = 0.278$, 0.7 cyc/degree $p = 0.358$*). Over the 10 days of testing, there was a gradual increase in VEP magnitude particularly at low spatial frequencies in both genotypes (*ANOVA animal age: 0.05 cyc/degree $p < 0.001$, 0.2 cyc/degree $p < 0.001$, 0.5 cyc/degree $p = 0.141$, 0.7 cyc/degree $p = 0.043$*).

We considered that a visual acuity deficit may become apparent over time in CX3CR1 KO animals and thus assessed visual acuity in adult mice. Animals were implanted with VEP electrodes as before, but at P25. VEPs were recorded in juvenile mice (at P28) across 8 spatial frequencies (0.05, 0.1, 0.2, 0.3, 0.4, 0.5, 0.6, and 0.7 cycles per degree) in order to get an acuity curve (**Fig. 2.3c, Supplementary Table 2.2**). One month later at P60, these animals were recorded across the same spatial frequencies. We do not detect a difference in visual acuity of WT and CX3CR1 KO mice as either juveniles or adult animals (**Fig 2.3d, Supplementary Table 2.2**; *ANOVA animal age, P28: $p = 0.360$; P60: $p = 0.192$*). This data shows that the quality of vision of CX3CR1 KO animals is approximately equal to that of WT animals.

JUVENILE AND ADULT CX3CR1 KO MICE ARE CAPABLE OF STIMULUS-SELECTIVE RESPONSE POTENTIATION

Stimulus-selective response potentiation (SRP) is a form of cortical visual learning induced by daily presentations of a visual stimulus of a particular orientation (Frenkel et al., 2006). Like LTP, this plasticity is input-specific (i.e. eye specific), and requires NMDAR

signaling and AMPAR insertion (Frenkel et al., 2006). Importantly, inducing thalamocortical LTP occludes this visual plasticity (Cooke and Bear, 2010). As LTP mechanisms are necessary and sufficient to account for SRP, SRP is an appropriate measure of geniculocortical LTP.

Using the standard VEP implantation surgery, littermate mice aged P25-P31 were binocularly presented with a phase-reversing sinusoidal grating stimulus of a specific orientation, repeated for 7 days (**Fig. 2.4a**). On the final day of SRP induction, the mice were presented with a stimulus of a novel orientation randomly interleaved with the familiar stimulus to confirm that SRP was specific to the trained stimulus. As shown previously in WT animals, the amplitude of VEPs evoked by the familiar visual stimulus increases across presentation days to approximately double that evoked by a novel stimulus ((Frenkel et al., 2006), (Cooke and Bear, 2010)).

In order to measure the quality of SRP during the visual system critical period, we began SRP induction a week earlier than our lab had previously tried. To our surprise, the timeline of SRP induction in WT mice was very different than previously detected: the VEP doubled after only one day of stimulus exposure (**Fig. 2.4b, 2.4c, and Supplementary Table 2.3;** *WT day 1 vs. WT day 2:* $p < 0.001$), a plateau that was unaffected by the additional days of training, and is specific to the trained stimuli (**Supplementary Table 2.3;** *WT day 7 vs WT day 7 novel:* $p < 0.001$). Juvenile CX3CR1 KO animals had SRP induction that was indistinguishable with WT animals (**Fig 2.4b, 2.4c, Supplementary Table 2.3;** *ANOVA genotype:* $p = 0.659$).

We repeated SRP induction with these animals using uniquely oriented spatial frequencies one month later (**Fig. 2.4a, 2.4d, 2.4e, Supplementary Table 2.3**). In adult mice using our lab-standard SRP timeline beginning in animals approximately 2 months of age, we found the classically reported incremental SRP induction approaching a plateau around 5 - 7 days of training in WT animals (**Fig. 2.4d, 2.4e, Supplementary Table 2.3**). Adult CX3CR1 KO animals also undergo SRP over 7 days and is equivalent to adult WT animals (**Fig. 2.4d, 2.4 e, Supplementary Table 2.3**; *ANOVA genotype* = 0.778).

While we found an age-dependent difference in SRP induction, which raises intriguing possibilities about visual cortical potentiation in WT animals, we did not find any

differences in CX3CR1 KO SRP. This leads us to conclude that the visual circuit does not require CX3CR1 in order to produce LTP-like synaptic plasticity.

BRIEF LID SUTURE INDUCES AN OCULAR DOMINANCE SHIFT IN WT AND CX3CR1 KO MICE

It has been repeatedly shown that ocular dominance in primary visual cortex as measured by VEPs can be strongly shifted by suturing the contralateral eyelid in juvenile mice (Frenkel and Bear, 2004). The ratio of VEP amplitudes evoked by stimulation of each eye provides a reliable index of ocular dominance and is in close agreement with single-unit recordings ((Hanover et al., 1999), (Huang et al., 1999)). VEPs have many advantages as an *in vivo* functional readout: the data are quantitative, they are less subject to sampling bias than single-unit recordings, and they can be recorded over days in awake animals, avoiding confounds of anesthesia. Because of these qualities, they are ideal to reveal kinetics of synaptic plasticity.

Juvenile mice (P25) were implanted with VEP recording electrodes in the binocular primary visual cortex within layer 4. Phase-reversing grating stimuli were presented monocularly to each eye and the amplitude of evoked responses was recorded. During baseline recordings at P28, we consistently observed that the ratio of contralateral eye VEP amplitude to ipsilateral eye VEP amplitude (the C/I ratio) for both WT and KO animals was approximately 2 (**Fig. 2.5b**; *WT pre-MD C/I ratio: 1.81 ± 0.24mV, KO pre-MD C/I ratio = 2.00 ± 0.17mV; ANOVA genotype: p = 0.778),* reflecting the published contralateral eye dominance in mice. Prior to MD, the amplitude of VEPs driven by the contralateral eye were no different between the genotypes (**Fig. 2.5a**; *WT contra pre-MD: 76.41 ± 7.53mV; KO contra pre-MD: 78.47 ± 7.75mV; ANOVA genotype: p = 0.487*), nor by the ipsilateral eye (**Fig. 2.5a**; *WT ipsi pre-MD: p = 53.87 ± 7.15mV, KO ipsi pre-MD: p = 45.22 ± 7.09mV; ANOVA genotype: p = 0.661*).

After 3 days of MD, an ocular dominance shift was manifested as both depression of deprived-eye VEP amplitudes (**Fig. 2.5a**; *WT contra post-MD: 42.67 ± 7.96mV, p = 0.003; KO contra post-MD: 57.12 ± 14.08mV, p = 0.044; ANOVA MD condition p < 0.001*) and potentiation of open-eye VEP amplitudes (**Fig 2.5a**; *WT ipsi post-MD: 74.59 ± 11.99mV, p = 0.031; KO ipsi post-MD: 72.36 ± 11.21mV, p = 0.007; ANOVA MD*

condition $p < 0.001$), with no significant differences between WT and KO animals (*contralateral ANOVA MD x genotype interaction: $p = 0.396$; ipsilateral ANOVA MD x genotype interaction: $p = 0.644$*). This ratio of responses driven by each eye was rapidly shifted as a consequence of contralateral eyelid closure, such that after 3 days of MD, the C/I ratio became approximately 1 for both genotypes (**Fig 2.5b**; *WT post-MD C/I ratio: 0.92 ± 0.27, $p = 0.010$; KO post-MD C/I ratio: 0.84 ± 0.16, $p = 0.001$; ANOVA MD x genotype interaction: $p = 0.540$).*

BRIEF LID SUTURE REDUCES THALAMOCORTICAL SYNAPSE DENSITY AND SIZE IN WT BRAINS, BUT ONLY REDUCES DENSITY IN CX3CR1 KO MICE

We were surprised that a brief period of MD induced an ocular dominance shift as measured by VEPs in CX3CR1 KO animals indistinguishable from WT animals, considering that KO microglia phagocytose less than WT animals after 3 days of lid suture (**Fig. 2.1**). However, the microglial activation phenotype in KO animals is slight and KO animals have electrophysiological OD shifts similar to WT animals, suggesting there may be no requirement for fractalkine signaling in experience-dependent visual cortical plasticity. As the VEP is a field recording of Layer 4 which contains both feedforward and feedback input, we investigated how 3 days of MD effects WT and KO brains at the level of individual synapses using quantitative immuno-electron microscopy (EM).

We used the vesicular glutamate transporter (VGluT2) antibody to specifically label thalamocortical synaptic terminals in the mouse (**Fig. 2.6a and 2.6b**; (Coleman et al., 2010), (Nahmani and Erisir, 2005)). This allows specific analysis on presynaptic input that originates from the LGN and a separate analysis on intracortical (horizontal) input, which remain unstained. Previous studies have shown that 3 days of MD results in a structural OD shift wherein thalamocortical synapses are less dense and their presynaptic terminals are smaller (Coleman et al., 2010). We confirmed this finding: in layer 4 (L4) of binocular visual cortex in WT animals, there is a significant *decrease* in the volumetric density of VGluT2 labeled synapses normalized to total volumetric density of each brain that had undergone 3 days of MD (**Fig. 2.7b**; *WT: 0.23 ± 0.01, WT+MD: 0.16 ± 0.02, $p = 0.005$*) but no impact on volumetric density of all synapses (**Fig. 2.7a**; *WT: $0.98 \pm 0.12\ nm^3$, WT+MD: $1.10 \pm 0.11\ nm^3$; $p < 0.05$*). In KO brains following 3 days of MD, we also find a

significant decreased in the normalized density of VGlut2 labeled synapses (**Fig. 2.7e**; *KO: 0.28 ± 0.02, KO+MD: 0.23 ± 0.01, $p = 0.003$*) and no change in the synaptic density of all synapses (**Fig. 2.7d;** *KO: 0.79 ± 0.03 nm^3; KO+MD: 0.80 ± 0.02 nm^3; $p < 0.05$*).

Between the genotypes during normal sensory experience, there is a non-significant trend towards KO brains having a *decrease* in the total volumetric density when compared to WT brains (**Fig. 2.7g**; *WT: $9.79^{10} \pm 0.12^{10}$, KO: $7.92^{10} \pm 0.32^{10}$, $p < 0.05$*). However, when looking specifically at labeled synapses, KO brains have significantly *higher* normalized volumetric densities (**Fig. 2.7h**; *WT: 0.23 ± 0.01, KO: 0.28 ± 0.02, $p = 0.02$*), yet *smaller* thalamic terminals (**Fig. 2.7i;** *Mann-Whitney U Test: $p = 0.004$*).

In addition to the lower density of labeled synapses in WT animals, there is a significant decrease in the size of the thalamocortical presynaptic terminals after MD (**Fig. 2.7c**; *WT: median = 0.30 mm^2, WT+MD: median = 0.24 mm^2, Mann-Whitney U Test: $p < 0.001$*). Yet in CX3CR1 KO animals, there is no change in the size of labeled terminals following MD (**Fig. 2.7f**; *KO: median = 0.27 mm^2, KO+MD: median = 0.27 mm^2, Mann-Whitney U Test: $p = 0.852$*).

INTRACORTICAL SYNAPSE DENSITY INCREASES FOLLOWING BRIEF LID SUTURE IN WT AND CX3CR1 KO BRAINS

Populations of axons originating from the thalamus or from within the cortex itself have different baseline dynamics and reactiveness to sensory input ((De Paola et al., 2006), (Yamahachi et al., 2009)). For this reason, we hypothesized that unlabeled, corticocortical synapses of binocular cortex L4 would react differently to MD. In WT animals that had undergone 3 days of MD, we found a slight but significant *increase* in the density of putative corticocortical connections – the normalized volumetric density of unlabeled synapses increases following MD (**Fig. 2.8a**; *WT: 0.79 ± 0.02, WT+MD: 0.85 ± 0.02, $p = 0.004$*) with the same trend in KO animals (**Fig. 2.8c**; *KO: 0.73 ± 0.03, KO+MD: 0.78 ± 0.01, $p = 0.035$*). At baseline, unlike with thalamocortical synapses, the normalized volumetric density of unlabeled synapses is less in KO animals (**Fig. 2.8e**; *$p = 0.005$*).

Both WT and KO animals showed the classic phenotype of intracortical terminals being smaller than thalamocortical terminals (**Fig. 2.8f**; *WT labeled vs. WT unlabeled: $p < 0.001$; KO labeled vs. KO unlabeled: $p < 0.001$*). However, the way in which these

unlabeled presynaptic terminals react to brief lid suture is statistically different: In WT animals, intracortical terminal size is unchanged following MD (**Fig. 2.8b**; *WT: median = 0.19, WT+MD: median = 0.18, Mann-Whitney U Test: p = 0.051*), whereas in KO animals, intracortical terminals *increase* in size following MD (**Fig. 2.8d**; *KO: median = 0.19, KO+MD: median = 0.21, Mann-Whitney U Test: p < 0.001*). Brief MD has a larger effect on CX3CR1 KO intracortical circuits – they have *more* synapses, and their presynaptic terminals are *larger* – whereas in WT animals, these same circuits have a *higher* density of intracortical terminals of the *same* size (**Fig. 2.9**).

Discussion

Paolicelli et al. proposed the theory that microglia lacking CX3CR1 are rendered "blind" in the hippocampus (Paolicelli et al., 2011). We find that CX3CR1 KO microglia are capable of detecting sensory manipulations in the cortex: in the KO animal, 3 days of MD results in increased microglial lysosomal content (with no change in migration in either genotype, similar to (Hoshiko et al., 2012) in the barrel cortex). However, our data show that experience-dependent plasticity occurs normally without the fractalkine receptor, which could be due to either a lack of involvement for either CX3CR1 *or* microglia in producing OD shifts following MD. Regardless, with this form of deprivation in animals without CX3CR1, microglia are still able to rapidly detect that there is a change in the pattern of activity that results in plasticity, suggesting that CX3CR1-deficient microglia are not "blind" in the cortex of juvenile mice.

This structural data suggests that in WT animals, the different qualities of an OD shifts may be the product of changes in different circuitry. In WT animals, deprived-eye depression results from shrinkage and removal of thalamic input (Coleman et al., 2010). We find open-eye potentiation in both genotypes after 3 days of MD, which is slightly premature when compared to previous studies (Frenkel and Bear, 2004). The putative mechanism of open-eye potentiation is complementary to deprived-eye depression: after thalamic input driven by the deprived eye is reduced, the thalamic input driven by the open eye is strengthened. Our EM data suggests that, in our case in both genotypes, open-eye potentiation may be a product of increased horizontal input. Whether all instances of open-

eye potentiation, especially that which is responsible for OD plasticity in adult mice, is due to synaptic plasticity of thalamocortical or corticocortical networks is an open question. Measuring OD shifts manifested purely by thalamic synapses is possible by recording VEPs in the absence of intracortical synaptic transmission (Khibnik et al., 2010), and is certainly a promising follow-up experiment to our MD data.

Our EM data of animals with unmanipulated vision reveals a baseline difference between WT and CX3CR1 KO animals. Labeled synapses in KO brains are smaller, but denser. In ferret visual cortex, thalamocortical input and synapse density is a product of age; by adulthood, they have less thalamocortical synapses that are larger in size (Erisir and Dreusicke, 2005). This suggests that the KO cortex might be less mature than the age-matched WT cortex. The process of V1 activity-dependent refinement begins with patterned visual experience (Erisir and Harris, 2003), so it is possible that eye opening is delayed in our KO animals, which in turn would delay cortical maturation. While we have not systematically quantified eye opening in these animals, anecdotally we do not observe any difference in the onset of eye opening between the genotypes. Instead, we think our data parallels those found in the hippocampus (Paolicelli et al., 2011) and the barrel cortex (Hoshiko et al., 2012) that suggests an overall developmental delay in the brains of CX3CR1 KO mice. However, the quality of the MD shift in the KO is virtually identical to the WT, which does not support the theory that the cortex is immature. Our results are consistent with the synaptic multiplicity model of the KO hippocampus proposed by Zhan et al (Zhan et al., 2014); it's possible that the presence of numerous weak, small thalamocortical synapses prevents the formation of large, strong synapses at a lower density.

Whether or not our findings are a result of immaturity of the visual cortex, the structural differences of the synapses in CX3CR1 KO brains don't manifest in visual acuity deficits. Furthermore, VEP-assessed plasticity of the visual circuits is indistinguishable from WT animals. That the visual system as a whole can undergo experience-dependent plasticity despite significant synaptic deficits is a testament to the compensatory mechanisms inherent to the brain as a whole. It also reflects the many receptors and ligands that microglia have to detect and influence neurons (Kettenman et al., 2011). Our data shows that fractalkine signaling is not required for general microglial activation, but confers some sort of information for developmental cortical wiring.

To our knowledge, we are the first to show increased lysosomal activity of WT microglia in L4 of binocular visual cortex following brief MD. This shows that increased microglia phagocytosis at the site of binocular thalamic input is a consequence of visual deprivation. Despite only a weak dependence on the expression of CX3CR1, it remains a possibility that proper microglia function is a requirement for the expression of OD shifts. MD experiments in animals lacking components of the complement system may result in no visual cortical OD plasticity, but it will be important to rule out improperly segregated eye-inputs (as seen in the LGN) as a developmental source. Regardless, our finding adds to the increasingly convincing case that microglial behaviors are activity-dependent and coincident with synaptic plasticity.

Our results also reveal intriguing possibilities for future non-microglial-centric visual cortical synaptic plasticity experiments. As our microglial CD68 staining correlates to physiology, this assay could be used in OD plasticity generally: one would predict that protocols which do not induce OD shifts (ex: dark exposure, monocular inactivation) would also not induce increased microglial lysosomes, and the timescale of this activation would correlate with the timescale of deprived-eye depression (i.e. peaking at 3 days). Since this immunohistology can be done relatively fast, it could be a first-pass experiment in new gene or pharmacological manipulations.

The juvenile WT SRP data was very surprising: other experiments have shown a lack of SRP (as in arc KO animals; (McCurry et al., 2010)) or a decrease in the maximal magnitude (aged WT animals; Peter Finnie, Sam Cooke personal correspondence), but this is the first time we have seen a dramatic change in the rate of acquisition. That it takes a single visual presentation in juvenile mice to reach the same asymptotic potentiation that is observed following a week of exposure in the exact same adult mouse is remarkable, and pinpointing the age during which this transitions from one rate to another (between P25 and P50) could point to specific mechanisms for rapid synaptic potentiation available to the young brain that is lost during development. Our prediction is that this transition occurs during the closure of the critical period. The SRP protocol is incredibly robust and reliable with a huge dynamic range between untrained and trained stimuli, which would make it a promising method for screening drugs that could re-open the juvenile adaptability that is currently a holy grail for plasticity research.

METHODS

Animals

All procedures adhered to the guidelines of the National Institutes of Health and were approved by the Committee on Animal Care at MIT, Cambridge, MA, USA. They were housed in groups of 2-5 with food and water available *ad libitum* and maintained on a 12 hour light-dark cycle. For all experiments, CX3CR1 transgenic mice (B6.129P-Cx3cr1^{tm1Litt}/J) mice, wherein green fluorescent protein (GFP) has replaced the first coding exon of the CX3CR1 gene (Jung et al., 2000) were obtained from The Jackson Laboratory and maintained on a C57BL/6 background. All mice used were male littermates, resulting from parents heterozygous for the *CX3CR1* gene. All experiments were conducted blind to genotype and treatment.

Eyelid suture

Under isoflurane anesthesia (1.5-2%), hair surrounding the eye was removed and lid margins were trimmed. The eye was thoroughly flushed with sterile saline and antibiotic ophthalmic ointment (Vetropolycin, Pharmaderm) was applied to the eye. Using 6-0 vicryl sutures, approximately 5 stitches were placed along the extent of the trimmed lids and knots were secured with cyanoacrylate glue.

Three days post-suturing, the eye was opened by removing the tissue covering the eye, and the eye was cleaned with saline. The eye was carefully inspected for signs of damage, and any animal showing opacity or other injury was excluded. Suture integrity was inspected prior to eye opening, and animals whose eyelids were not fully sealed were excluded from further experiments.

Tissue preparation for Electron Microscopy (EM)

Perfusions: Animals were anesthetized with nembutal and transcardially perfused with Tyrode solution until vasculature was flushed clear (<2 min). This was immediately followed by 100ml of 4% PFA/0.5% glutaraldehyde in PB (EM grade; Electron Microscopy Sciences). Experimental animals were always perfused on the same day as littermate controls. Tissue was postfixed for 1–2 d at room temperature (RT).

Immunohistochemistry: Occipital lobe blocks were placed in a vibratome and cut at 60 μm. For each group of animals, yoked, littermate control tissue was always processed with experimental tissue. Sections were subsequently immersed in a 1% sodium borohydride/PB solution, followed by a series of PB rinses until borohydride solution was cleared. Free-floating sections were stored in PBS containing 0.05% NaN_3 at 4°C. VGluT2 was visualized using guinea pig anti-VGluT2 (Millipore Bioscience Research Reagents) diluted 1/5000 in PBS, pH 7.4, containing 0.9% NaCl, 1% BSA, and 0.05% NaN_3 at RT for 36–48 h. Next, sections of V1 were immersed in biotinylated anti-guinea pig IgG (Vector Laboratories) secondary antibody at 1/100 for 2 h. Sections were then incubated in ABC solution for 2 h, followed by three rinses in PBS for 3 min. Sections were then exposed to a 1% diaminobenzidine (DAB) solution in the presence of 0.003% H_2O_2 with gentle agitation for 5–8 min.

Embedding: The embedding procedure was performed blind to the history of the tissue using previously published protocols, thereby eliminating any biases in selecting regions for analysis (Erisir et al., 2001; Nahmani and Erisir, 2005). DAB-treated sections were rinsed in PB and treated with 1% osmium tetroxide in PB for 30–45 min. Osmicated sections were then treated with 4% uranyl acetate in 70% ethanol for 2 h, and they were dehydrated in a series of ethanols. Sections were then dehydrated in acetone and placed in a 1:1 acetone to resin (Epon 812; Electron Microscopy Sciences) mixture for 2 h. Next, sections were placed in full resin for 2 h, flat-embedded between two acetate sheets (Aclar; Ted Pella), and cured in a 60°C oven. Binocular V1 was delineated using a brain atlas based on C57BL/6J mice, and the region of V1 that represents the upper binocular hemifield, which served as the site for previous electrophysiological recordings (Frenkel and Bear, 2004), was identified. Tissue containing all six cortical layers was excised from the flat embed and placed in a plastic capsule, which was then filled with resin. Capsules were cured in a 60°C oven overnight or until polymerized. Embedded sections were traced using a camera lucida, capsule blocks were then trimmed down to a trapezoid that contained only layer 4, and ultrathin sections (~70 nm) were collected on 400 mesh copper grids (Ted Pella) using an ultramicrotome (Ultracut UCT; Leica). As antibody penetration can be limited to several micrometers from the surface of individual thick vibratome sections, ultrathin sections were collected at a plane that is nearly parallel to the surface, thereby maximizing the width of the tissue that contained labeled regions. Using this cutting approach, we obtained strips of

labeled tissue that were at least 50 (and up to 150) μm wide. Data collection was performed within the first 10–100 μm from the tissue–resin transition zone on ultrathin sections. Particular care was paid during ultrathin sectioning to obtain tissue "strips" that contain the tissue–resin transition zone and that span all of layer 4 dorsoventrally. Collecting sections in this manner allowed for ample sample area (~25 photographs; 20–30 μm^2 per electron micrograph) within each ultrathin section containing cortical layer 4. Moreover, the width of the labeled strip enabled us to choose optimal areas for both VGluT2 labeling and ultrastructural preservation. Although the specific dimensions of this labeled strip necessarily varied from section to section, in the rare instance wherein ultrathin sections did not adhere to the above criteria they were omitted from all of our analyses. These strips were then systematically photographed (blind to tissue history) to obtain minimally overlapping images of layer 4, regardless of label or profiles present in the sections.

Ultrathin sections were examined on a JEOL 1010 EM. Digital pictures were captured using a 16 megapixel SIA-12C (sia-cam.com) camera coupled with MaxIm DL CCD software (Diffraction Limited). Individual ultrathin sections were photographed at the tissue–resin interface, in which label is present within a 50- to 150-μm-wide strip along the dorsoventral expanse of layer 4 as described above. Images captured at 12,000× magnification yielded 20–30 μm^2 per micrograph, excluding blood vessels, myelinated axons, and somata areas.

EM image analysis and quantification: Each EM micrograph was examined using Image-Pro Plus, version 5.0, software (Media Cybernetics), at a final screen magnification of 60,000–80,000×. Profiles were identified as synaptic terminals if they met the following criteria: (1) the presence of at least three vesicles, (2) parallel alignment of presynaptic terminal membrane in apposition with that of the postsynaptic membrane ((Colonnier, 1968), (Peters et al., 1991)), and (3) a pronounced asymmetric postsynaptic density (PSD). In each digital picture, vesicle-filled profiles that displayed a synapse at the level of cross section (i.e., synaptic terminals) were identified and classified as containing VGluT2-DAB chromogen (labeled) or unlabeled. For each labeled synaptic profile, the postsynaptic target was classified as a dendritic spine or shaft. Dendritic shafts were defined principally by the presence of an organized arrangement of microtubules or at least one mitochondrion. When there were no microtubules or mitochondria present inside a profile, it was classified as a dendritic spine. Presence of a spine apparatus also aided in identifying dendritic spines.

In each micrograph, the numbers of synaptic labeled and unlabeled terminals were counted, terminal profile areas and synaptic lengths (PSD lengths) were quantified, and the effective sampling area was measured. Effective sampling area was calculated as the total area of an individual micrograph minus the area occupied by cell bodies, blood vessels, and myelinated axons, as these elements may otherwise inflate the amount of neuropil available for synaptic interaction nonuniformly across photographs. Synapses were traced by following the entire length of the postsynaptic density along the parallel membranes of the synapse. In the event that a postsynaptic density was perforated, the synapse was assumed to continue along the length of the perforation.

Because experimental manipulations can potentially introduce variations in synaptic elements that could bias the sampling procedure, the size–frequency method was used to calculate volumetric densities of labeled and unlabeled synaptic terminal profiles as previously described ($N_v = N_A / d$, where N_A is the number of terminals per square micrometer and d is the average synapse length in micrometers ((Beaulieu and Colonnier, 1985), (DeFelipe et al., 1999), (Erisir and Harris, 2003)). This quantification method allows for estimations of synaptic terminal densities and has been shown to yield a reliable measure of profile density for asymmetric synapses in cerebral cortex ((DeFelipe et al., 1999), (Erisir and Harris, 2003)). The size–frequency method is sometimes preferred over the optical dissector method because it accounts for sampling biases introduced by the fact that the sampled unit (synapse) is several times larger than the tissue section thickness (Merchan-Perez et al., 2009). Although the volumetric density method yields nearly identical results to the optical dissector method applied in the same tissue samples, the former is advantageous because it allows analysis of considerably larger areas in cortex, reducing the variation across samples ((DeFelipe et al., 1999), (Benes and Lange, 2001)). Furthermore, in immunostained ultrathin sections, as used in this study, the sampling is performed at the border of tissue and resin, which progresses in consecutive sections; this makes volumetric density a more feasible method to obtain enough data for meaningful statistical comparisons between experimental and control groups after multiple manipulations ((Erisir and Harris, 2003), (May et al., 2008)). The percentage of VGluT2-labeled synaptic terminals in layer 4 was determined as follows: $\%N_{v\ \text{labeled}} = 100 \times (N_{v\ \text{labeled}}/N_{v\ \text{all}})$. To control for variations in signal intensity, tissue obtained from experimental and control animals (yoked controls) were always processed together and all values were normalized to the means of yoked controls.

Electrode implants for visually evoked potential (VEPs)

For VEP surgeries, male mice were anesthetized with isoflurane (1.5-2%) and provided indirect heat via a disposable heating pad (Warmers HotHands; Philadelphia, PA). After cleaning and sterilization of the scalp, the skin covering the skull was removed and the skull was cleaned with 70% ethanol. A small headpost was affixed onto a skull anterior to Bregma and secured with cyanoacrylate glue (Loctite 454; Small parts Inc., Miami Lakes, FL). Small (<0.5 mm) burr holes were drilled into the skull overlying the binocular visual cortex (3.2 mm lateral of lambda and 0.5 mm anterior of the back suture) of each hemisphere. Tapered tungsten microelectrodes (75 μm in diameter, FHC; Bowdoinham, ME) were inserted and lowered 450μm below the cortical surface. A silver wire (A-M Systems; Sequim, WA) reference electrode was placed over the prefrontal cortex of the left hemisphere. All electrodes were secured in place using gel cyanoacrylate glue. Dental cement (Lang Dental Inc., Nashua, NH) was applied to cover the skull and enclose all electrodes into a stable, protective head cap. Animals were monitored postoperatively for 48 hours of recovery.

VEP recording

All VEP recordings were conducted in awake, head-restrained mice, remaining still but alert during presentation of visual stimuli. 48 hours after surgery, animals were habituated to handling and the apparatus by sitting head-fixed in front of a gray screen for two periods of 30 minutes. VEP amplitude was quantified using Plexon recording software, and the trough-peak response amplitudes were measured as described previously (Sawtell et al., 2003) and presented using custom-designed matlab software (Jeffrey P. Gavornik).

Visual stimuli

Full-field visual stimuli were presented via a VSG2/2 card (Cambridge Research System) on a computer monitor linearized by gamma correction. The screen was placed 20 cm in front of the animal, thereby occupying 92 x 66° of the visual field. Mean luminance was 27 cd/m2, with gamma-correction to ensure constant total luminance between the gray screen and patterned stimulus conditions. VEPs were elicited by phase reversing oblique (15, 45, 75, 105, 135, or 165°) bars. Visual stimuli were generated using the PsychToolbox extension (http://psychtoolbox.org).

For acuity experiments, stimuli were presented binocularly with 200 phase reversals of each stimulus at 100% contrast and spatial frequencies as noted in the text. Each day's recordings used oriented stimuli at least 30° different from any experienced previously by the individual mouse.

During SRP experiments, binocular stimuli were presented with 400 phase reversals of each stimulus at 100% contrast, with the spatial acuity and orientation denoted in the text. This was repeated identically every day for 7 days. On the seventh day, a novel orientation stimulus was presented interleaved with the trained stimulus to confirm stimulus specificity. At P58-P61, the mice were habituated again, and then experienced a second SRP protocol with a new stimulus orientation for both the trained and the novel stimuli.

During MD experiments, stimuli of 100% contrast at 0.4 cycles per degree were presented and recorded to each eye separately, with the opposing eye blocked by an opaque drape placed flush with the animal's nose. After the first recording, the lid contralateral to the recording hemisphere was sutured. Upon eye opening, animals were given 30-60 minutes of recovery from anesthesia in a light-blocked cage before being recorded with a visual stimuli of orthogonal orientation.

Labeling eye-specific projections to the LGN

Juvenile mice (P28-P30) were anesthetized with isoflurane (1.5-2%). To access the vitreous chamber for TTX and saline injections, the temporal portion of the globe was reflected anteriorly by gently pulling a 7-0 silk suture threaded through the conjunctiva and securing it to the operating surface. The conjunctiva was then trimmed using fine angled scissors to expose the sclera. A small puncture was made at the corneoscleral junction into the vitreous chamber with a fine needle. A glass micropipette with a tip diameter of 40–50 μm was attached to a Nanoject II injection system (Drummond Scientific) and inserted into the vitreous chamber at a depth of ~2 mm. Animals received 1 μL intravitreal injections of CTB conjugated to Alexa fluorophores (Thermo Fisher Scientific; Grand Island, NY) into each eye: the left eye received CTB-Alexa-647 and the right eye received CTB-Alexa-555. The eye was then rinsed with sterile eye drops and coated with an antibiotic ointment to prevent infection.

After 48 hours, animals were anesthetized with nembutal and perfused with 4% paraformaldehyde in PBS. 60 μm coronal brain slices containing the LGN were collected,

and every second slice was mounted on glass slides with fluoromount G. Samples were blinded to experimenter and 3 sections representing the middle third of the LGN were selected for each hemisphere. Z-stacks were acquired with confocal microscopy (Olympus confocal microscope) and a 20x objective lens, with a step size of 5 μm, resulting in 8-10 images per brain slice.

For analysis, background fluorescence was subtracted and normalized (0-255) using Fiji (http://fiji.sc). Grayscale images were converted into binary, and an ROI containing only the dLGN was traced. The "add images" function was used to superimpose the channels containing the 555 and 647 generated signal. With pixel counts, the area of the contralaterally labeled retinal projection, the area of the ipsilaterally labeled retinal projection, and the area containing overlap of both projections were measured.

Statistics

All data is expressed as a mean ± standard error of the mean (S.E.M.). Sigmaplot was used for parametric statistical analysis. Normality of distribution and homogeneity of variation was tested and ANOVAs were performed where appropriate. If ANOVAs yielded significance, Student-Newman-Keuls post-hoc tests with adjustment for multiple comparisons were applied for individual comparisons. Repeated measures ANOVAs were applied for all within subject comparisons. For other comparisons, unpaired ANOVAs were used. For volumetric density EM measurements, one-way ANOVAs with nested replicate measures were used. $P < 0.05$ is used as a threshold for significance for non-parametric tests. The N is an individual animal (biological replicate), except for CD68 activation per cell and thalamocortical terminal size. In these cases the N is a cell or terminal; as this data is not normally distributed, non-parametric tests (Mann-Whitney U) were performed using SPSS software. To correct for repeated comparisons, statistical significance for non-parametric tests was $p < 0.005$.

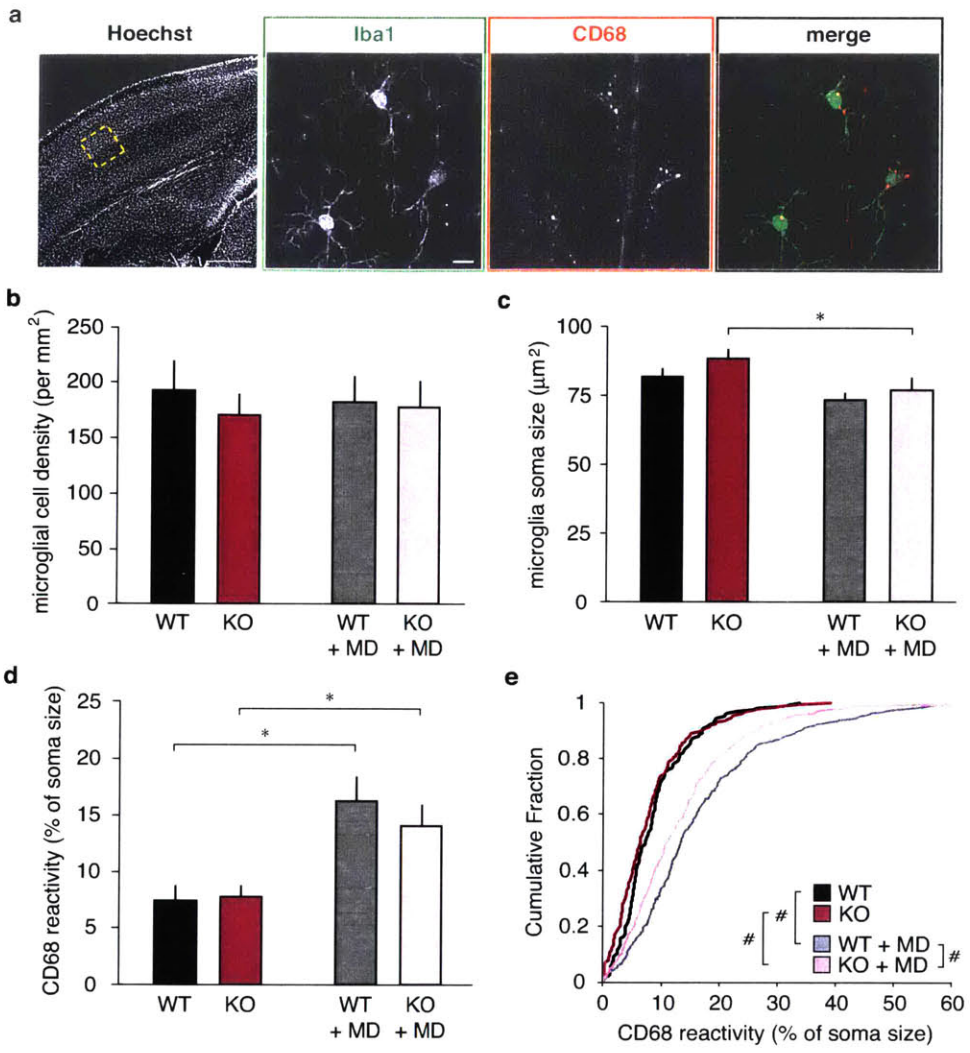

FIGURE 2.1: MICROGLIA HAVE INCREASED LYSOSOME CONTENT FOLLOWING BRIEF MD

a, Example images of microglia in L4 of binocular V1 (*nuclei labeled with Hoechst 33342*) stained with anti-Iba1 labels the entirety of microglia (*green*), and anti-CD68 labels microglial lysosomes with some staining in blood vessels (*red*). In the merged image, the CD68 puncta are specific to microglial somas (*except for blood vessels; see the faint vertical line running through the image).* All data uses the cortex contralateral to MD. **b,** The density of microglia in L4 is not different between genotypes (*ANOVA genotypes:* $p =$

0.572) or following MD (*ANOVA MD condition: $p = 0.968$*). **c,** The volume of the microglia soma (i.e. excluding including ramified processes) decreases slightly in WT animals following MD, though not significantly (*$p = 0.059$*), as well as decreasing in KO animals (*$p = 0.014$*), which may be a product of increased ramification. **d,** Per animal averages of the amount of lysosome content within microglial somas increases following MD in both genotypes (*WT: $p = 0.003$; KO: $p = 0.026$*). **e,** Cumulative distributions of individual microglial CD68 increase following MD. On this per-microglia basis, CX3CR1 KO deprived animal microglia have less lysosome reactivity when compared to WT deprived animals (*WT vs KO: $p = 0.093$; WT vs WT+MD: $p < 0.001$; KO vs KO+MD: $p < 0.001$; WT+MD vs KO+MD: $p = 0.001$*). (*Individual data points indicate per animal averages. *post-hoc tests $p > 0.05$ after two-way ANOVA; #Mann-Whitney U test $p > 0.005$; $n = 4$ WT, 6 KO animals*).

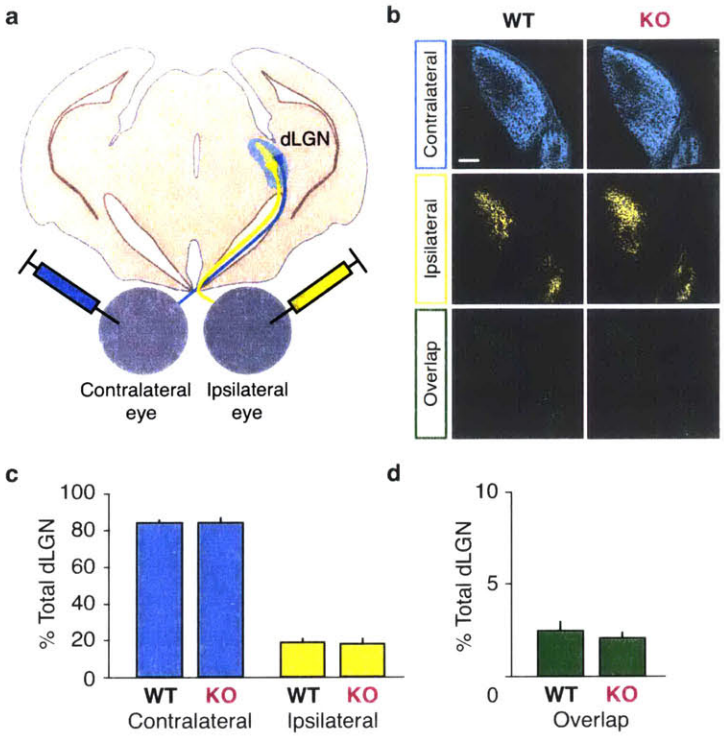

FIGURE 2.2: SEGREGATION OF OCULAR INPUT TO LGN IS NORMAL IN JUVENILE CX3CR1 KO ANIMALS

a, Schematic of eye injection experiment, where anterograde tracers (Cholera Toxin Subunit B Alexa Fluor Conjugates) are injected into each eye, labeling retinal ganglion cell projections in the dorsal Lateral Geniculate Nucleus (dLGN). **b,** Representative images of dLGN with contralateral retinal projections (*blue*), ipsilateral projections (*yellow*), and the overlapping signal of both eyes (*green*). **c,** Average of the labeled dLGN areas shows no difference in any measurement between genotypes (*contralateral: $p = 0.585$; ipsilateral: $p = 0.528$; overlap: $p = 0.482$*), **d,** and overlap between contralateral and ipsilateral projections is minimal. *($n = 6$ WT, 10 KO animals)*

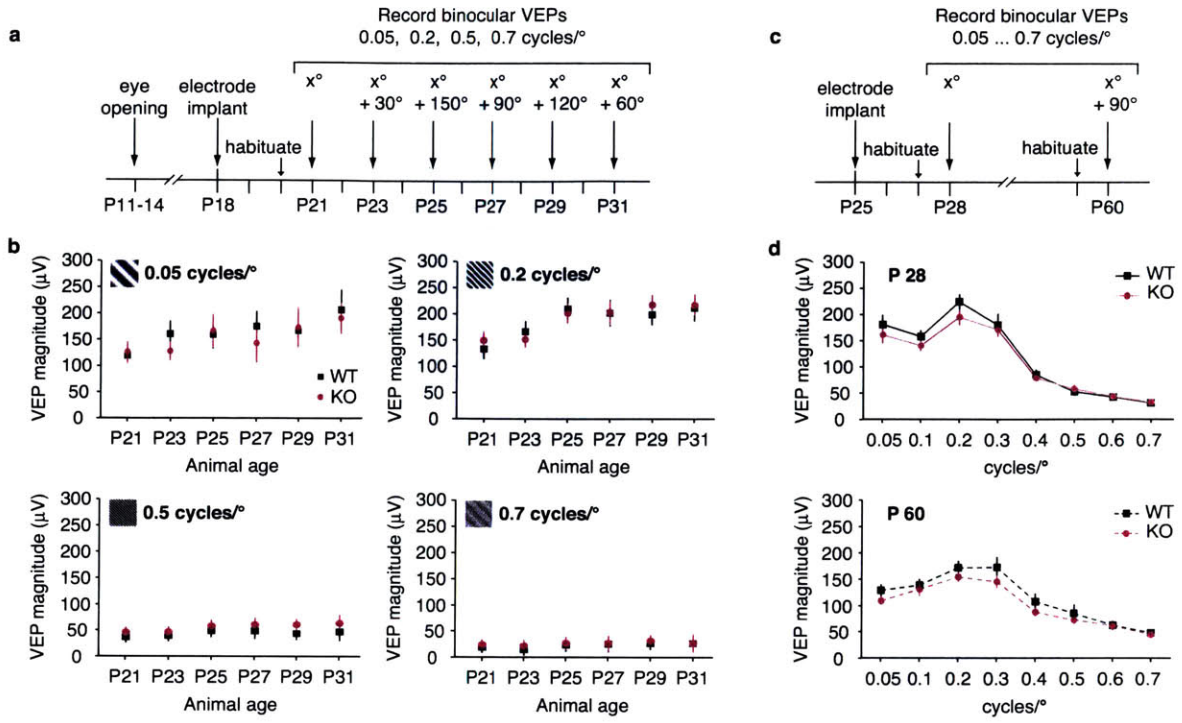

FIGURE 2.3: DEVELOPMENT OF VISUAL ACUITY AS MEASURED BY VEPS IS NORMAL IN CX3CR1 KO ANIMALS

a, Experimental timeline of juvenile visual acuity development in primary visual cortex. VEPs were recorded every-other day from P21 to P31 across 4 spatial frequencies (0.05, 0.2, 0.5, and 0.7 cycles per degree) with a uniquely oriented stimuli each day separated by 30° to prevent response potentiation (Cooke and Bear, 2010). **b,** There is no detectable difference between CX3CR1 KO (*magenta*) and WT mice (*black*) at any of the 4 spatial frequencies tested. In both genotypes, there is a gradual increase in VEP magnitude as the animal matures. (*ANOVA animal age: 0.05 cyc/degree $p < 0.001$, 0.2 cyc/degree $p < 0.001$, 0.5 cyc/degree $p = 0.141$, 0.7 cyc/degree $p = 0.043$; $n = 14$ WT, 17 KO animals*). **c,** Experimental timeline of visual acuity assessment at adulthood. Animals were implanted and VEPs recorded at 8 different spatial frequencies (0.05, 0.1, 0.2, 0.3, 0.4, 0.5, 0.6, 0.7 cyc/degree) as juveniles for comparison purposes, and then recorded again at 2 months of age. **d,** Adult VEP magnitudes (*dashed lines*) do not vary between CX3CR1 KO animals and WT animals, including difficult to detect spatial frequencies which are greater than

noise (*grey bar*) (*n = 8 WT, 7 KO animals; *post-hoc tests p < 0.05 after two-way ANOVA)*).

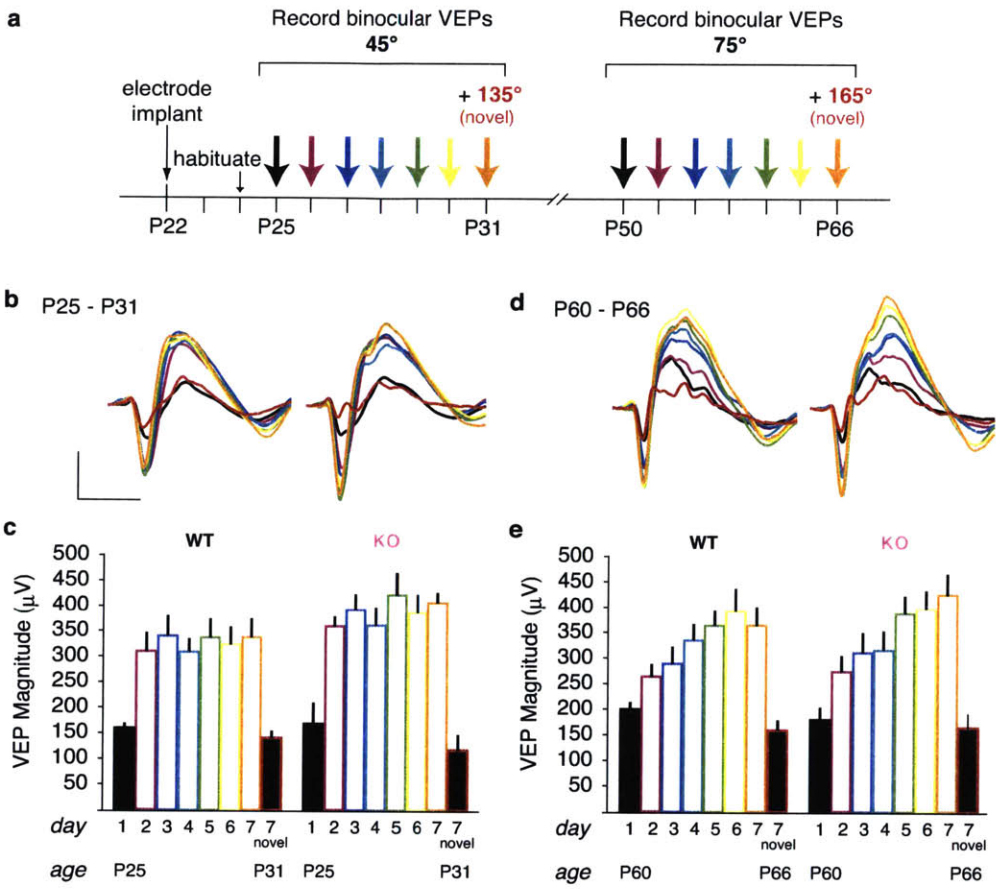

FIGURE 2.4: CX3CR1 KO MICE DEMONSTRATE NORMAL EXPERIENCE-DEPENDENT SYNAPTIC POTENTIATION FOLLOWING STIMULUS-SELECTIVE RESPONSE POTENTIATION (SRP)

a, Experimental timeline of SRP protocol. Animals were implanted at P22 and habituated to the recording apparatus 48 hours later. Over the next 7 days, binocular VEPs were recorded from awake, head-fixed animals, driven by the same stimulus with an orientation of 45°. On the final day, an additional visual stimuli with a novel orientation of 135° was interspersed with the trained 45° stimuli. A month later, this same week long protocol was repeated with adult animals and a new stimulus (75°, 165° on test day, *[red filled bars]*). **b,** Average traces showing VEPs potentiate similarly in WT and CX3CR1 KO juvenile mice (*ANOVA genotype: $p = 0.659$*). **c,** An asymptote is reached after one day, and a novel

stimuli is not potentiated (*WT day 1 [black filled bar] vs day 7 [red filled bar] novel: $p = 0.628$; KO day 1 vs day 7 novel: $p = 0.340$*), demonstrating that the increased VEP magnitude is specific to the trained stimuli (*WT day 1 vs day 7 [orange open bar]: $p < 0.001$; KO day 1 vs day 7: $p < 0.001$*). **d,** Average traces of VEPs in adult animals potentiate similarly in CX3CR1 KO and WT adult mice (*ANOVA genotype: $p = 0.778$*). **e,** VEP magnitude gradually increases across 7 days and is specific to the trained stimuli (*WT day 1 vs day 7 novel: $p = 0.074$; KO day 1 vs day 7 novel: $p = 0.538$*). (*filled bars, first day of stimulus presentation; open bars, repeated stimulus; scale bar for traces: 100mV by 100ms; WT n = 11, KO n = 9 animals; *post-hoc tests $p < 0.05$ after two-way ANOVA).*

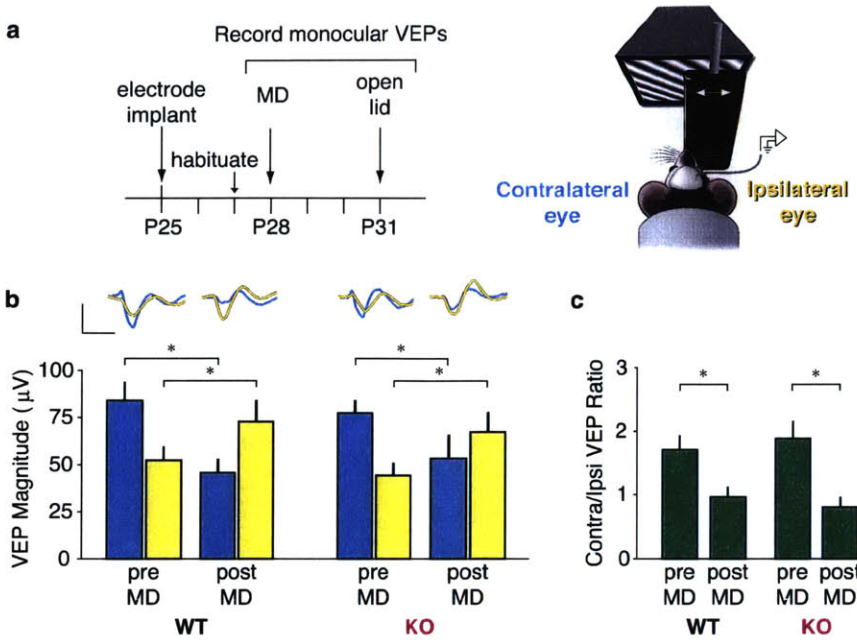

FIGURE 2.5: EFFECT OF BRIEF MD ON VEP IS UNAFFECTED IN CX3CR1 MUTANTS.

a, (*left panel*) Timeline of 3 day MD experiment and (*right panel*) cartoon of VEP recording apparatus: an awake mouse is head-restrained in front of a computer screen with a phase-reversing visual stimulus that is presented monocularly, with an occluder blocking one eye. VEPs driven by the eye contralateral to the recorded hemisphere are shown in blue and the eye ipsilateral to the recorded hemisphere are shown in yellow. **b,** After 3 days of monocular deprivation of the contralateral eye (*post-MD*), VEPs driven by the contralateral/deprived eye decrease significantly in both genotypes (*ANOVA condition: $p < 0.001$, WT pre-MD vs. WT post-MD: $p = 0.003$, KO pre-MD vs. KO post-MD: $p = 0.044$*), while VEPs driven by the ipsilateral/open eye increased significantly in both genotypes (*ANOVA condition: $p < 0.001$, WT pre-MD vs WT post-MD: $p = 0.031$, KO pre-MD vs KO post-MD: $p = 0.007$*). **c,** The ocular dominance shift can be measured through a ratio of contralateral VEP to ipsilateral VEP (*green*), shifting from approximately 2:1 to 1:1 following MD in both WT and KO animals. (*scale bar for traces: 50mV by 100ms; n = 15 WT, 15 KO animals; *post-hoc tests $p < 0.05$ after two-way ANOVA)*

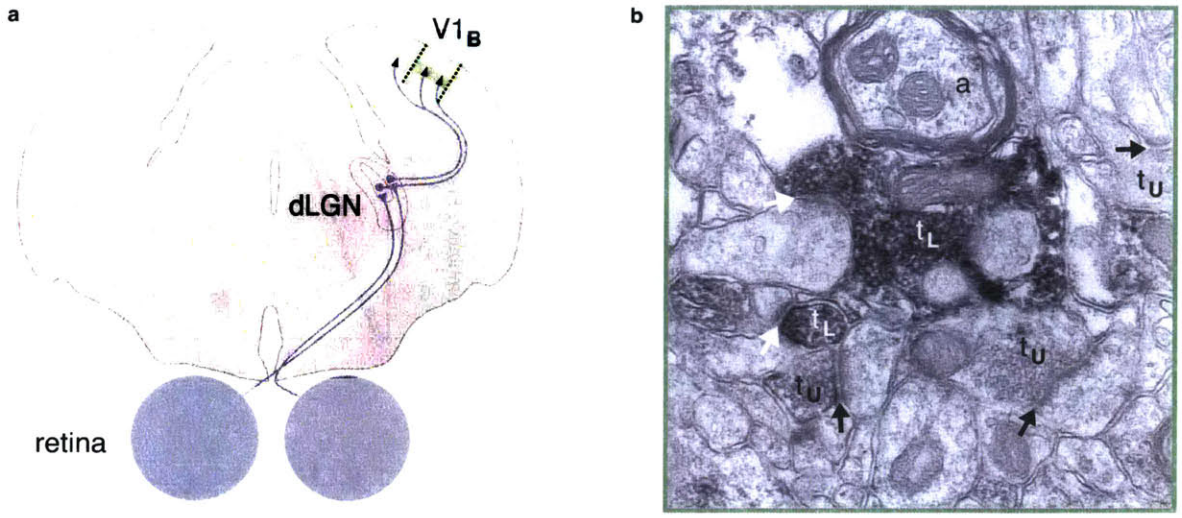

FIGURE 2.6: EM IMAGING OF THALAMOCORTICAL SYNAPSES IN L4 OF BINOCULAR VISUAL CORTEX

a, Cartoon depiction of the mouse visual system. Visual experience enters through each retina and is transmitted to the dLGN (*grey*). Thalamic axons subserving each eye converge in L4 (*green shaded rectangle*) of binocular visual cortex (*$V1_B$, green dashed lines*), the area of EM imaging, and are immunoreactive to vGluT2 staining (*black arrowheads*). **b,** Example EM image. Synapses consisting of terminals darkly stained by DAB (*white arrows, t_L*) are thalamic, while synapses with unstained terminals (*black arrows, t_U*) are intracortical. Other structures, such as cross sections of mylenated axons (*a*) are visible in the images.

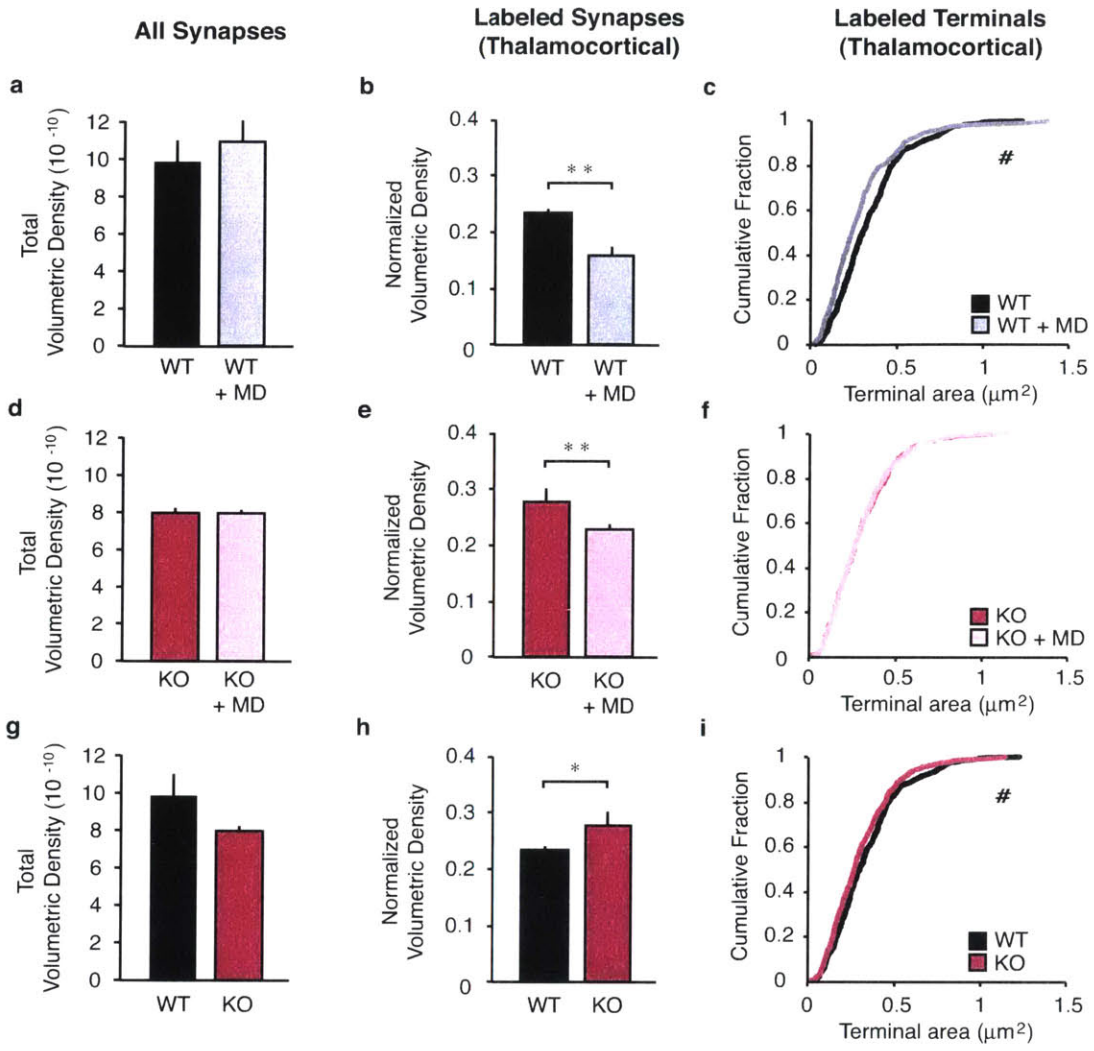

FIGURE 2.7: THALAMOCORTICAL SYNAPSES ARE LESS DENSE, SMALLER FOLLOWING BRIEF MD IN BOTH WT AND CX3CR1 KO ANIMALS

a, Total volumetric density of all synapses in WT animals is unchanged following MD ($p < 0.05$), but the **b,** normalized volumetric density of labeled synapses is significantly decreased ($p = 0.005$), **c,** as is the size of the terminals ($p < 0.001$). In KO animals, **d,** total volumetric density is unchanged after MD ($p < 0.05$) and **e,** normalized volumetric density of labeled synapses is decreased ($p = 0.003$), yet the **f,** size of labeled terminals is unaffected ($p =$

0.852). When comparing WT and KO animals without manipulated vision, **g,** KO brains have a non-statistically significant trend towards less synapses (*p < 0.05*), but when just looking at **h,** the density of labeled synapses, KO animals have a higher normalized volumetric density (*p = 0.02*) of terminals that are smaller, **i** (*p = 0.004*) *(n = 3 WT, 3 WT+MD, 3 KO, and 6 KO+MD animals; terminal n = 489 WT, 381 WT+MD, 473 KO, 845 WT+MD; *post-hoc tests p < 0.05 after ANOVA; #Mann-Whitney U test p < 0.005).*

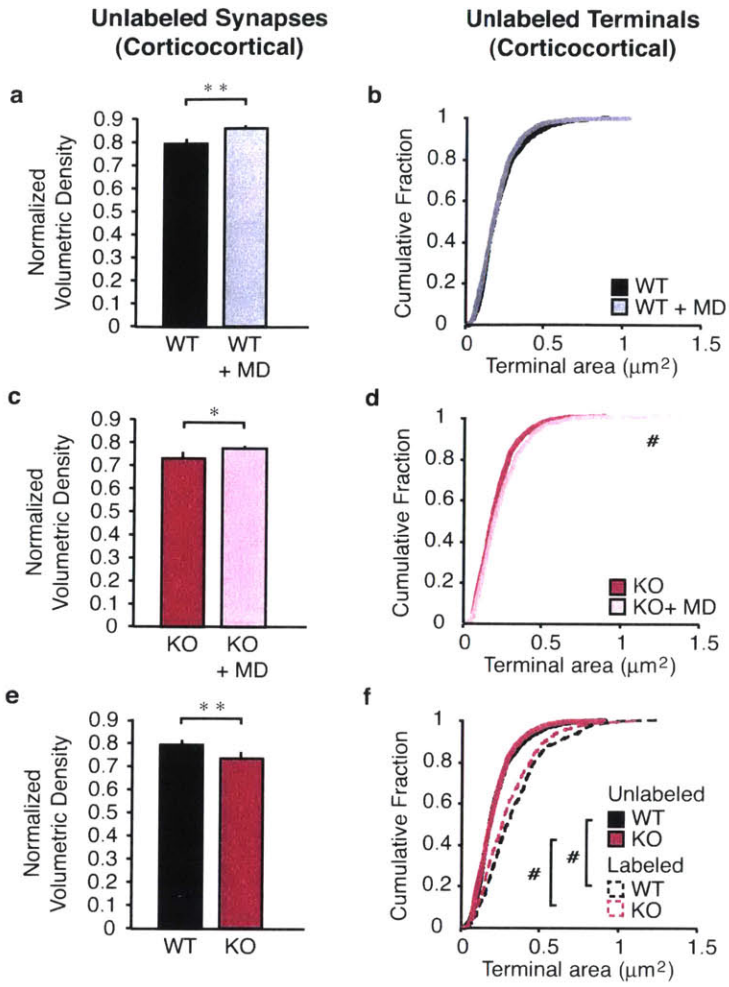

FIGURE 2.8: INTRACORTICAL SYNAPSES ARE DENSER FOLLOWING BRIEF MD IN BOTH WT AND KO ANIMALS

a, Following MD, WT brains have increased normalized volumetric densities of unlabeled synapses ($p = 0.004$) and **b,** no change in unlabeled terminal size. In KO animals, **c,** MD also causes an increase in the unlabeled synapse normalized volumetric density ($p = 0.035$) and additionally an **d,** increase in unlabeled terminal size ($p < 0.001$). **e,** There is no baseline difference in the normalized volumetric density of unlabeled synapses between WT and KO brains ($p < 0.05$). **f,** The unlabeled (*solid lines*) and labeled (*dashed lines*) populations of both genotypes are significantly different from each other (WT: $p < 0.001$; KO: $p < 0.001$) *($n = 3$ WT, 3 WT+MD, 3 KO, and 6 KO+MD animals; terminal $n = 1243$*

*WT, 1410 WT+MD, 1014 KO, 2228 WT+MD; *post-hoc tests $p < 0.05$ after ANOVA; #Mann-Whitney U test $p < 0.005$).*

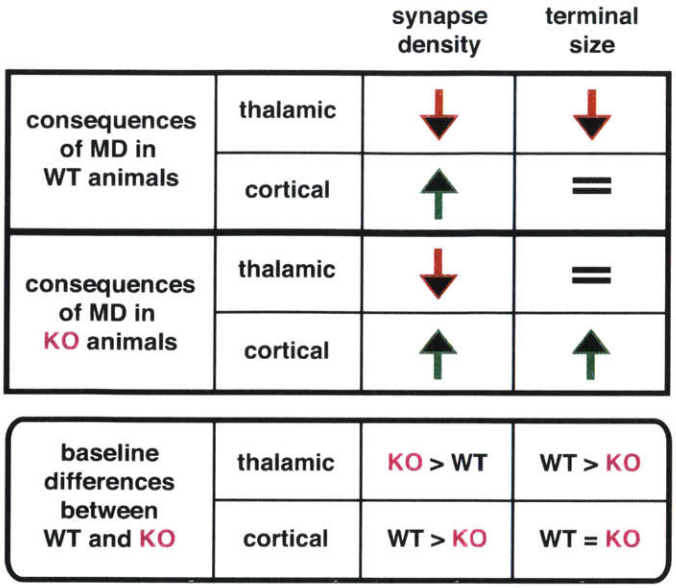

FIGURE 2.9: SUMMARY OF EM DATA

Following brief MD in WT animals, there are fewer, smaller thalamocortical synapses – resulting in a decrease of thalamic input – and an increase in corticocortical synapses – resulting in a slight increase of intracortical input. In CX3CR1 KO animals following MD, there is a decreased density of thalamocortical synapses that does not impact terminal size, and an increase in the density and size of corticocortical terminals. However, there is a basal difference between the thalamic synapses in WT and KO brains, which may be a result of delayed or reduced maturation (Erisir and Dreusicke, 2005).

acuity development - 0.05 cyc/°	P 21	P 23	P 25	P 27	P 29	P 31
WT	119 ± 15 μV	160 ± 25 μV	159 ± 27 μV	175 ± 29 μV	167 ± 29 μV	207 ± 38 μV
KO	126 ± 21 μV	127 ± 18 μV	166 ± 32 μV	142 ± 37 μV	172 ± 39 μV	190 ± 30 μV
comparsions between WT and KO	*p = 0.872*	*p = 0.424*	*p = 0.861*	*p = 0.432*	*p = 0.894*	*p = 0.691*

acuity development - 0.2 cyc/°	P 21	P 23	P 25	P 27	P 29	P 31
WT	132 ± 19 μV	165 ± 20 μV	209 ± 21 μV	201 ± 25 μV	198 ± 20 μV	210 ± 25 μV
KO	148 ± 17 μV	150 ± 15 μV	200 ± 20 μV	201 ± 23 μV	216 ± 19 μV	215 ± 19 μV
comparsions between WT and KO	*p = 0.540*	*p = 0.567*	*p = 0.747*	*p = 0.978*	*p = 0.499*	*p = 0.840*

acuity development - 0.5 cyc/°	P 21	P 23	P 25	P 27	P 29	P 31
WT	36 ± 8 μV	39 ± 7 μV	48 ± 10 μV	48 ± 8 μV	43 ± 9 μV	47 ± 13 μV
KO	45 ± 10 μV	46 ± 11 μV	57 ± 12 μV	60 ± 15 μV	60 ± 12 μV	63 ± 17 μV
comparsions between WT and KO	*p = 0.308*	*p = 0.461*	*p = 0.450*	*p = 0.166*	*p = 0.133*	*p = 0.291*

acuity development - 0.7 cyc/°	P 21	P 23	P 25	P 27	P 29	P 31
WT	19 ± 5 μV	15 ± 4 μV	23 ± 4 μV	25 ± 5 μV	26 ± 4 μV	27 ± 5 μV
KO	23 ± 4 μV	21 ± 3 μV	26 ± 4 μV	26 ± 4 μV	31 ± 7 μV	27 ± 7 μV
comparsions between WT and KO	*p = 0.412*	*p = 0.253*	*p = 0.602*	*p = 0.858*	*p = 0.421*	*p = 0.991*

SUPPLEMENTAL TABLE 2.1: SUMMARY OF VALUES AND STATISTICS OF FIGURE 2.3B

acuity curve - juvenile (p28)	0.05 cyc/°	0.1 cyc/°	0.2 cyc/°	0.3 cyc/°	0.4 cyc/°	0.5 cyc/°	0.6 cyc/°	0.7 cyc/°
WT	181 ± 18 μV	158 ± 11 μV	224 ± 14 μV	180 ± 21 μV	85 ± 10 μV	52 ± 7 μV	42 ± 5 μV	31 ± 6 μV
KO	161 ± 18 μV	140 ± 10 μV	195 ± 13 μV	171 ± 12 μV	78 ± 4 μV	58 ± 8 μV	43 ± 4 μV	32 ± 3 μV
comparsions between WT and KO	*p = 0.224*	*p = 0.282*	*p = 0.075*	*p = 0.584*	*p = 0.703*	*p = 0.759*	*p = 0.950*	*p = 0.954*

acuity curve - adult (P60)	0.05 cyc/°	0.1 cyc/°	0.2 cyc/°	0.3 cyc/°	0.4 cyc/°	0.5 cyc/°	0.6 cyc/°	0.7 cyc/°
WT	130 ± 11 μV	140 ± 11 μV	173 ± 13 μV	173 ± 20 μV	108 ± 15 μV	87 ± 17 μV	63 ± 8 μV	49 ± 6 μV
KO	110 ± 8 μV	132 ± 14 μV	155 ± 10 μV	146 ± 12 μV	89 ± 8 μV	73 ± 8 μV	61 ± 7 μV	45 ± 5 μV
comparsions between WT and KO	*p = 0.204*	*p = 0.617*	*p = 0.265*	*p = 0.084*	*p = 0.211*	*p = 0.388*	*p = 0.933*	*p = 0.828*

SUPPLEMENTAL TABLE 2.12: SUMMARY OF VALUES AND STATISTICS OF FIGURE 2.3D

SRP - juvenile (P25 - P31)	day 1	day 2	day 3	day 4	day 5	day 6	day 7	day 7 - novel
WT	153 ± 10 μV	302 ± 31 μV	335 ± 36 μV	316 ± 25 μV	335 ± 34 μV	317 ± 31 μV	342 ± 35 μV	141 ± 12 μV
KO	148 ± 25 μV	307 ± 39 μV	324 ± 42 μV	342 ± 34 μV	396 ± 41 μV	358 ± 35 μV	377 ± 29 μV	123 ± 21 μV
comparsions between WT and KO	p = 0.912	p = 0.914	p = 0.791	p = 0.562	p = 0.174	p = 0.356	p = 0.356	p = 0.427
p values of adjacent days, WT	day 1 vs. day 7 novel p = 0.628	day 1 vs. day 2 p < 0.001	day 2 vs. day 3 p = 0.660	day 3 vs. day 4 p = 0.859	day 4 vs. day 5 p = 0.728	day 5 vs. day 6 p = 0.462	day 6 vs. day 7 p = 0.731	day 7 vs. day 7 novel p < 0.001
p values of adjacent days, KO	day 1 vs. day 7 novel p = 0.628	day 1 vs. day 2 p < 0.001	day 2 vs. day 3 p = 0.546	day 3 vs. day 4 p = 0.495	day 4 vs. day 5 p = 0.187	day 5 vs. day 6 p = 0.335	day 6 vs. day 7 p = 0.472	day 7 vs. day 7 novel p < 0.001

SRP - adult (P50 - P66)	day 1	day 2	day 3	day 4	day 5	day 6	day 7	day 7 - novel
WT	200 ± 14 μV	263 ± 25 μV	289 ± 33 μV	335 ± 32 μV	364 ± 30 μV	392 ± 46 μV	364 ± 37 μV	159 ± 20 μV
KO	180 ± 25 μV	274 ± 31 μV	311 ± 39 μV	316 ± 37 μV	388 ± 35 μV	397 ± 36 μV	425 ± 41 μV	164 ± 28 μV
comparsions between WT and KO	p = 0.671	p = 0.822	p = 0.639	p = 0.684	p = 0.611	p = 0.911	p = 0.199	p = 0.912
p values of adjacent days, WT	day 1 vs. day 7 novel p = 0.074	day 1 vs. day 2 p = 0.005	day 2 vs. day 3 p = 0.256	day 3 vs. day 4 p = 0.042	day 4 vs. day 5 p = 0.420	day 5 vs. day 6 p = 0.220	day 6 vs. day 7 p = 0.432	day 7 vs. day 7 novel p < 0.001
p values of adjacent days, KO	day 1 vs. day 7 novel p = 0.538	day 1 vs. day 2 p < 0.001	day 2 vs. day 3 p = 0.138	day 3 vs. day 4 p = 0.838	day 4 vs. day 5 p = 0.004	day 5 vs. day 6 p = 0.713	day 6 vs. day 7 p = 0.432	day 7 vs. day 7 novel p < 0.001

SUPPLEMENTAL TABLE 2.3: SUMMARY OF VALUES AND STATISTICS OF FIGURE 2.4C, 2.4D

CHAPTER III

Structural plasticity mechanisms of ocular dominance shifts in the primary visual cortex

---

Experimental techniques in this chapter were developed in collaboration with Jason E. Coleman

ABSTRACT

Axon remodeling has been long implicated in experience-dependent plasticity. Recent studies have shown that synapse elimination can occur very rapidly after only 3 days of monocular deprivation (MD). In order to assess whether axon branch removal or retraction underlies this rapid structural modification, we used lentiviral vectors to label eye-specific thalamocortical axon arbors that project to the binocular region of primary visual cortex of the mouse. Using *in vivo* 2 photon microscopy, individual axon tips were tracked before and after 3 days of monocular deprivation (MD) in the presence or absence of AM251, an endocannabinoid receptor antagonist which has previously been shown to block layer 2/3 ocular dominance plasticity *in vivo* and layer 2/3 LTD *ex vivo.* We did not detect significant axonal retractions following MD in vehicle or AM251 treated animals. Therefore we performed *in vivo* electrophysiology to determine if these animals were of an age in which 3 days of MD typically results in robust deprived eye depression. We found that the visually evoked potential (VEP) in cortex contralateral to the eye undergoing MD only decreased slightly. This suggests that without a strong OD shift after MD, there is not a readily observable structural shift. We believe our lack of detected structural plasticity is a consequence of the limitations of our preparation, as the MD begins at P38-P40, an age at which animals may not exhibit the same time course or mechanism of synaptic weakening expressed in younger animals.

INTRODUCTION

Experience-dependent plasticity and the underlying synaptic modifications has been one of the most interesting and important topics in neuroscience (See Chapter 1). Monocular deprivation (MD), during which vision through one eye is degraded, results in a persistent shift in the relative responsiveness of cortical neurons away from the deprived eye and towards the non-deprived eye ((Hooks and Chen, 2007), (Smith et al., 2009)). This OD shift has been shown across many species ((Hubel et al., 1977), (Fagiolini et al., 1994), (Gordon and Stryker, 1996)) and its induction is most robust during early development (Sawtell et al., 2003). In mouse V1, the OD shift occurs through a stereotyped sequence of physiological plasticity that can be divided into two mechanisms: starting immediately after MD, the closed eye becomes less capable of driving large numbers of cortical neurons ((Wiesel and Hubel, 1963), (Gordon and Stryker, 1996)) and is termed deprived-eye depression; subsequently, the open eye responses increase and is termed "open-eye potentiation" ((Frenkel and Bear, 2004), (Mrsic-Flogel et al., 2007)).

While it is clear that deprived-eye depression is a consequence of MD, it is less clear what synaptic changes are responsible for decrease in cortical responsiveness to the closed eye. Electrophysiological recordings provide strong evidence for weakening of the deprived-eye inputs ((Singer, 1977), (Tsumoto and Suda, 1978), (Mitzdorf and Singer, 1980)), and these changes measured after MD share many common molecular hallmarks of LTD, including a shared dependence on NMDAR activation ((Bear, 1996), (Malenka and Bear, 2004)). Furthermore, both LTD *ex vivo* and MD *in vivo* share similar biochemical changes in the phosphorylation state of AMPARs ((Malenka and Bear, 2004), (Heynen et al., 2003)) as well as a dependence on AMPAR internalization ((Yoon et al., 2009)). The finding that MD *in vivo* occludes induction of LTD *ex vivo* ((Crozier et al., 2007)) is a particularly convincing argument that LTD mechanisms play an important role in the physiology of MD.

While the electrophysiological mechanisms are detectable immediately after MD, there are slower anatomical correlates. The size of afferent cortical inputs can be measured with injections of transsynaptic eye tracers, and in mammals with ocular dominance columns, the column size reflects the extent of geniculocortical arbors subserving that eye. MD results in a decrease of columnar size for those being fed by afferents of the deprived eye and an increase in area for the nondeprived eye ((Hubel and Wiesel, 1968), (LeVay et al.,

1980), (Shatz and Stryker, 1978)). This result was reiterated by reconstruction of geniculocortical axons in the kitten after MD: afferents serving the deprived eye had shorter arbors and were less complex ((Friedlander et al., 1991), (Antonini and Stryker, 1993)). The Antonini and Stryker study had started with the field's supposition that "synapses become physiologically ineffective before the branches on which they sit are withdrawn", but to their surprise, axon retractions in kittens were seen after short periods of deprivation (4-7 days), paralleling the physiological timeline of MD and suggesting that structural modifications contribute to the functional consequences of MD ((Antonini and Stryker, 1993), (Antonini and Stryker, 1996)).

Mice, which lack ocular dominance columns and have intermingling of cells with varying degrees of eye dominance within binocular V1, also show less axon volume from thalamocortical neurons subserving the deprived eye after long periods (17-44 days) of MD begun before P19 (Antonini et al., 1999). These MD periods are weeks longer than the physiological asymptote is reached in mice at 3 days of MD ((Frenkel and Bear, 2004)). Recent quantitative immuno-electron microscopy (EM) points towards an even faster structural effect of MD; the density and size of thalamocortical synapses in layer 4 decreases after just 3 days of MD (Coleman et al., 2010). Though this assay did not allow for determination of whether a given synapse served the deprived or nondeprived eye, it provides exciting evidence that anatomical synaptic remodeling of thalamocortical inputs occurs very rapidly following MD in the mouse visual cortex, mirroring what has been shown physiologically.

The studies discussed thus far are very convincing that substantial structural rearrangements accompany functional OD shifts, but they are all limited by the fact that they are static, postmortem glimpses into thalamocortical projections. The recent popularity of two-photon microscopy when used with stable expression of fluorescent proteins (as occurring in transgenic mice or via viral vectors) provides a way to longitudinally track axons within the intact brain of a living animal ((Svoboda et al., 1997), (Holtmaat et al., 2009), (Holtmaat and Svoboda, 2009)). It also allows us to identify particularly rapid changes in cortical circuitry of individual axons with temporal and spatial precision at the resolution of single terminal arbors.

Two-photon microscopy of the intact brain has yielded some understanding of axon growth and retraction during normal experience and after experimental manipulation.

During cortical development, axons can gain or lose tens of microns an hour (Portera-Cailliau et al., 2005). Horizontal projections have been successfully labeled and tracked in monkeys raised with normal vision (Stettler et al., 2006) and following retinal lesions (Yamahachi et al., 2009), demonstrating comparative axonal stability and motility, respectively. Over 9 months of imaging putative thalamocortical axons in normally raised adult mice, most axonal length persists, yet the axon tips are dynamic, elongating and retracting in a random walk fashion (De Paola et al., 2006). Boutons contained within these axons have their own dynamics: approximately 20% of putative thalamic terminals are gained or lost over months in the mouse (De Paola et al., 2006), and 7% of intracortical terminals are gained or lost over a week in the monkey (Stettler et al., 2006).

Two-photon microscopy affords a powerful technology for combining our understanding of how the functional OD shift occurs as a result of MD with structural plasticity correlates. To address this, we developed a lentiviral vector-based strategy for labeling axons of the relay cells in the dLGN that receive retinal input from the deprived eye and project to V1. We were able to track these stable, specifically labeled thalamocortical axon arbors, to detect axonal plasticity occurring immediately following deprivation specifically in the population of arbors receiving input from the deprived eye. By developing a technique that provided insight into rapid structural plasticity, our aim was to connect LTD mechanisms characterized in slice and *in vivo* to their correlates in cortical axonal remodeling. Ultimately, our goal was to determine the sequence of events that not only drive the OD shift observed following MD, but also allow the brain to learn and adapt to the environment

RESULTS

EYE-SPECIFIC LABELING OF THALAMOCORTICAL AXONS WITH LGN VIRAL INJECTION

Unlike higher-order mammals, mice lack a columnar organization within V1, with thalamic inputs relaying information from each eye intermingling in the binocular area of visual cortex (Mrsic-Flogel et al., 2007) (**Fig. 1.1**). What is an advantage for *in vivo*

electrophysiological studies is a hurdle for structural studies: the ocular dominance shift after MD occurs in opposing forms depending on which eye is driving the inputs, therefore requiring open-eye projections (which gain territory) and closed-eye projections (which lose territory) to be analyzed separately.

In order to specifically label axons from the eye that was sutured closed, a lentiviral injection was made into a small area of dorsal lateral geniculate nucleus (dLGN; **Fig. 3.1b**) at coordinates that restricted membrane-bound GFP expression to the portion that receives input from the contralateral eye (**Fig. 3.1e**). This labeling procedure was optimized to achieve relatively sparse labeling of the geniculate projections in V1, such that individual axons were both resolvable and trackable across time and distance. The GFP-labeled axons are clearly visible in layer 1, and dense collaterals of the same arbors are seen in layer 4 (**Fig. 3.1c**). However, due to the imaging depth limitations of the 2-photon microscope, we were unable to track axons deeper than approximately 300*mm* (depending on the quality of infection and clarity of the cranial window) beneath the pial surface. As a result, we focused our efforts on tracking layer 1 axonal branches. These afferents contact apical dendritic arbors within the layer to influence the activity of cortical neurons, even though they are outside of the primary input layer. Our results demonstrate that we are able to experimentally isolate geniculocortical axons subserving the contralateral (deprived) eye.

STRUCTURAL PLASTICITY OF THALAMOCORTICAL AXONS SUBSERVING THE DEPRIVED EYE DURING CANNABINOID BLOCKADE

There is strong evidence that MD leads to LTD of synaptic transmission in the visual cortex, including that MD *in vivo* induces LTD and occludes cortical LTD induction *ex vivo* ((Heynen et al., 2003), (Crozier et al., 2007)). The molecular mechanisms of LTD vary according to cortical layer (Daw et al., 2004): layer 4 requires clathrin-dependent AMPAR endocytosis, while layer 3 requires signaling through cannabinoid receptors ((Crozier et al., 2007), (Liu et al., 2008)) (**Fig. 3.2**). Both types of LTD are reduced *in vivo* after brief MD (Crozier et al., 2007). The question remains as to how these distinct, layer-specific molecular mechanisms underlying synaptic depression contribute to structural remodeling of geniculocortical axons after MD.

As a step towards determining rapid structural plasticity resulting from endonnabinoid signaling in layer 2/3, we pharmacologically blocked endocannabinoid signaling by systemic delivery of the CB1 receptor antagonist AM251 during lid suture, which has been shown to block OD plasticity in superficial cortical layers ((Liu et al., 2008), (Crozier et al., 2007)) (**Fig. 3.3a**). We then followed axon branch tips before and after MD in the presence or absence of endocannabinoid signaling to determine the subsequent structural dynamics (**Fig. 3.3a**). We observed no significant retraction in the AM251-administered group (**Fig. 3.3c**; *AM251 day 0 = -0.54μm net change in axon length; AM251 day 3 = -1.42μm net change in axon length; n = 155 branch tips in 4 animals*). However, we also did not detect any significant retraction in the vehicle-administered group (**Fig 3.3c**; *vehicle day 0 = -0.12 net change in axon length, vehicle day 3 = -0.66μm net change in axon length; n = 260 branch tips in 5 animals*). When separating our data into axon retractions and axon extensions, we did not detect a significant difference in axon loss or growth between vehicle treated or drug treated animals (**Fig 3.3d**; *vehicle retraction = 2.12μm, n = 139; AM251 retraction = 2.23μm, n = 85; vehicle extension = 1.67μm, n = 108, AM251 extension = 1.02μm, n = 58*), though we do see a trend towards retractions over extensions in both groups (*total retractions: n = 224; total extensions: n = 166*).

WEAK OD SHIFT OBSERVED AFTER 3 DAYS OF MD IN P40-P43 ANIMALS

It has long been theorized that functional rearrangement of the cortex is largely possible during a specific age range termed the "critical period". Hubel and Wiesel's early work in cats showed that induction of the OD shift is most robust early in postnatal development and virtually absent in adulthood (Hubel and Wiesel, 1970). In mice, the ability of MD to drive an OD shift in visual cortical neurons declines with age ((Gordon and Stryker, 1996), (Huang et al., 1999) (Sawtell et al., 2003), (Hofer et al., 2006a)), and that which occurs in adults is mechanistically distinct from juvenile animals. The adult OD shift occurs after longer deprivation periods (5 days and greater) and is comprised almost entirely of strengthening of open-eye inputs without weakening of those from the deprived-eye ((Frenkel and Bear, 2004), (Sato and Stryker, 2008)). In juvenile animals, an OD shift in response to brief (3-4 day) MD is still restricted to a critical period occurring around P28,

although the termination of susceptibility varies slightly per laboratory (<P36 for (Gordon and Stryker, 1996); <P40 (Sawtell et al., 2003); <P42 for (Huang et al., 1999)).

The timeline for our axon imaging is restricted by technical limitations, and prevents lid suture from occurring at the height of juvenile OD plasticity. Our MDs are performed at the approximate end of the critical period and window for deprived-eye depression induction. It is therefore crucial to ensure that our structural plasticity measurements occur when brief MD can induce an OD shift. Therefore we wanted to verify that mice of this age show an OD shift physiologically. Field recording electrodes were chronically implanted in layer 4 of the binocular zone of primary visual cortex. Baseline VEPs were measured at P40 (**Fig. 3.4a**; *contralateral eye VEP – blue; ipsilateral eye VEP – yellow*) and the eyelid of the eye contralateral to the experimental hemisphere was sutured closed. After three days of MD, the sutured eye was opened, the animal was allowed to recover from anesthesia, and VEPs were again recorded. We assessed ocular dominance plasticity by determining the ratio of contralateral to ipsilateral eye responses (**Fig. 3.4b**; *C/I ratio - green*), which in unmanipulated mice is approximately 2.5:1, and decreases after MD to become approximately 1:1. Our results show that P40 animals do show a C:I ratio shift, although not to the extent where both eyes are shifted to be equal (**Fig. 3.4b**; *pre-MD = 2.63; post-MD = 1.90; $p = 0.034$; $n = 8$*). Upon closer examination of the responses, we found that in mice of this age, there was a moderate depression in the contralateral (deprived) eye response (**Fig. 3.4a**; *pre-MD =132.84mV; post-MD = 107.47mV; $p = 0.083$*) and a slight, but non-significant increase in the ipsilateral (open) eye response (**Fig. 3.4a**; *pre-MD = 51.60mV; post-MD = 66.61mV; $p = 0.281$*). These data suggest that the mice used for structural imaging are capable of an OD shift, but this age might be on the edge of the mouse critical period for deprived-eye depression. Our lack of a structural phenotype is in line with this physiology data: an MD that does not strongly drive a physiological OD shift does not strongly drive a structural change.

Discussion

Our data show that at P40, after a 3-day period of MD, only a slight deprived eye depression is observable and therefore may lack immediately observable structural remodeling. Based

on the data presented, it is not conclusive how axons receiving input from the deprived eye would behave during deprivation at the height of deprived eye depression, and it is a topic worthy of further study. For immediate investigation, data using mice that were not injected with either drug or vehicle during the MD period should be thoroughly analyzed. Although preliminary results do not show any significant retraction in mice undergoing MD verses those that have not (**Fig. 3.3**), it will be important to confirm that the lack of axon retraction is not a product of animal handling or a side effect of vehicle treatment, which contains detergents for solubility.

There are many suggestions that can be gleaned from these data for future studies looking at axon retraction: First, interleaved electrophysiology data should be obtained concurrently with 2-photon data in order to measure the shift in synaptic strength. Because the time point chosen is not at the peak of the visual critical period, the induced effect of MD might have a lesser effect on synaptic weakening, and subsequently a lesser effect on structural remodeling. The data presented above suggest that without a strong immediate OD shift, there is not a measurable immediate thalamic axon withdrawal in superficial cortical layers.

Secondly, because the structural phenotype is expected to follow the physiological phenotype, all efforts should be made to perform MD and imaging as close to the height of the critical period as possible (P25-P30). Due to limitations on weaning age, the surgery cannot be performed any earlier than P18; due to viral expression time and surgical recovery, axons cannot be stably imaged until two weeks post-surgery. This leaves animals to begin imaging at age P32. The current imaging timeline (**Fig. 3.1a**) begins with optical intrinsic imaging to map the binocular zone, placing the mice at P33 for the first day of 2-photon imaging. Two baseline images are acquired before the lid suture is performed. This results in the earliest possible MD occurring from P36 to P39, though with technical difficulties (additional time for viral expression, surgical recovery, window clarity; a second day of optical intrinsic imaging) it often is performed as late as P40 to P43.

Based on the lack of phenotype shown here, we advise the following modified timeline (**Fig. 3.5**): 2-photon imaging will begin immediately after expression and window clarity is stable (P32). This will require the area of binocular visual cortex to be estimated initially, and then confirmed after 2-photon imaging is completed to determine which data will be included or excluded. The current timeline includes two imaging sessions pre-MD in

order to exclude axons that are dynamic at baseline. As the experiment can be agnostic to whether the axons were initially motile or not and should contain the proper control of animals with unmanipulated vision, I do not believe that this is worth the additional 3 days to delay MD. Instead, MD should be performed immediately after the first imaging session, placing the period of deprivation well within the sensitive period (P32 to P35). I also believe it would be better to accept some attrition in the experimental animals and not proceed with animals that are unready to be imaged by P32. Animals that require additional days of recovery could be imaged and then analyzed separately, as they may no longer be in the same period of development by the time the MD has completed.

As the up-front preparation and imaging of animals is already in place, I would suggest adding a second post-MD imaging session. As an animal ages, longer periods of MD are required to induce the same shift seen after shorter MDs in younger animals ((LeVay et al., 1980), (Sawtell et al., 2003)). This raises the possibility that lid closures performed later in life may require more time to produce the same anatomical changes generated by lid closures performed earlier in life. By adding an additional time point 5-7 days after MD, it is possible we can capture the structural remodeling occurring in a time frame reflective of the published physiology ((Sawtell et al., 2003), (Frenkel and Bear, 2004)). However, older animal OD shifts are characterized more by an increase in open-eye signals, which may not be reflected in the thalamocortical axons serving the deprived eye. Regardless, it will still be informative to track these axons to see how they behave during a period of time not known for deprived-eye depression. The prediction would be that there would be little ongoing retraction of axons serving the deprived eye between 3 to 7 days of MD.

There is a final drawback inherent in this method: only axons projecting to layer 1 are trackable. While the axons imaged are collaterals of the same axons that project more extensively to layer 4, it is an assumption that geniculate inputs behave similarly regardless of layer and that effects seen in one layer are reflective of other layers. However, there is heterogeneity in thalamic cells, with different populations projecting to different layers (Rubio-Garrido et al., 2009) and it is possible they have plastic qualities and may behave differently. Also, it has been demonstrated that different layers of cat visual cortex have different critical periods for responsiveness to monocular deprivation ((LeVay et al., 1980), (Daw et al., 2004), (Trachtenberg et al., 2000)), although layer 1 is omitted in each of these studies. Another study virally labeling LGN inputs to monocular V1 has found that the

projections to layer 6 are very different from those to layer 4 in synaptic properties despite being from the same pool of labeled neurons; furthermore, the authors found that MD only produced an effect on the layer 4 projecting collaterals (Wang et al., 2013). A recent study has shown unique tuning properties and sensitivities between the thalamic input to superficial cortex in layer 1 and deeper input to layer 2/3 and 4 (Sun et al., 2016). These data call into question the assumption that what occurs to thalamocortical axons in layer 1 will be a proxy for what occurs at layer 4.

Ideally, technical limitations could be overcome and imaging could occur on layer 4 directly. Accessing deeper cortical layers, including layer 4, is not easily addressed by cranial window 2-photon microscopy due to the optical scatter of the cortex limiting image generation. Specially built microscopes with adaptive optics must be utilized to resolve structures as fine as axons in deeper layers (Sun et al., 2016). Without that, however, a way to align the structural events of layer 4 to layer 1 would be to repeat the quantitative EM experiments using layer 1 to determine if there is an equivalent decrease in thalamocortical synapse density and terminal size following brief periods of MD.

METHODS

Cranial window surgery

Cranial window surgeries were performed on the left hemispheres of P18 animals essentially as described by Mostany (Mostany and Portera-Cailliau, 2008). Mice were injected with carprofen (5 mg/kg) and dexamethasone (.2mg/kg) subcutaneously prior to anesthesia with isoflurane (4% initially, 1.5% maintenance). Surgeries were performed with mild indirect heat provided by a disposable heating pad.

After cleansing and sterilization of the scalp, the skin covering the skull was removed. The skull was cleaned with 70% ethanol and dried with compressed air before affixing a small head post anterior to Bregma, and a second head post just above the ear on the right hemisphere to be used during intrinsic imaging. After adjusting the animal's head to lie in the stereotaxic plane, a mark was made on the skull at 1.7 mm posterior from Bregma and 3.3 mm lateral from the midline suture. The animal's head was rotated 30 degrees in the rostro-caudal plane, and a glass injection pipette filled with EGFP-expressing lentivirus was

positioned directly over the marked injection site. A 3 mm circle of skull flush with the back skull suture was thinned with a dental drill, taking extreme care to not pierce the dura. The circle was delicately removed by gentle rocking of forceps pierced into the edge of the craniotomy.

Once the brain is exposed, the glass pipette was lowered 2.6 mm below the surface of the brain into the dLGN. The virus was infused using 5, 14 nL pulses every 15 seconds, before raising the pipette to 2.45 mm below the brain surface and administering 5 more injections, and raising the pipette again to 2.3 mm below the brain surface for a final 5 injections. The pipette was left in place for 10 minutes and then slowly removed. A custom made 4 mm glass coverslip (Number 1 thickness, Thermo Fisher Scientific) was placed directly on the dura and anchored to the skull using high-viscosity cyanoacrylate glue. Once the coverslip was in place, glue was applied around the diameter to create an airtight seal. Bone cement (Palacos-R, Zimmer Biomet, Warsaw IN) was applied, completely covering the glue and the skull surrounding the window. The remaining exposed areas of skull were covered with dental cement (Ortho-Jet, Lang Dental, Wheeling IL). Animals were given subcutaneous injections of Lactated Ringer's solution (0.3 cc) and allowed to recover under a heat lamp. The animals were singly housed, and initially provided with wet food due to their young age. They were maintained on an oral suspension of sulfamethoxazole (1 mg/mL) and trimethoprim (0.2 mg/mL) in their drinking water to aide in the clarity of the imaging window.

AM251 preparation and administration

AM251 (Tocris Bioscience, Avonmouth UK) was dissolved in sterile distilled water (12.5 mg/mL) and stored at -20°C. Immediately prior to injection, it was diluted in 10% Tween 80 (Sigma-Aldrich, St. Louis MO), 20% DMSO, and water to yield a solution of 1.25 mg/mL. Animals were weighed and given intraperitoneal injections of either AM251 (5mg/kg) or vehicle, coded blind to the experimenter. The first dose was administered one hour prior to MD, followed by every 24 hours subsequent until the final imaging session was complete.

Optical intrinsic signal imaging

The binocular region of V1 in each of the experimental animals was functionally

mapped using optical imaging of intrinsic signals as described previously ((Cang et al., 2005); (Kalatsky and Stryker, 2003)) (**Fig. 3.6**). Two weeks after cranial window surgery, animals were anesthetized initially with 2% isoflurane. Animals were restrained using the lateral headpost and indirect heat was provided. The animal's heart rate was monitored via 28 gauge electrodes inserted subcutaneously behind the front limbs flanking the ribcage. Isoflurane was lowered to approximately 1.2% until 8-10 heartbeats a second was achieved.

The animal was adjusted such that the cranial window was level with the imaging system, and an opaque curtain was attached to the front headpost, isolating the cranial window and imaging objective from the light of the visual stimulus. A high-refresh-rate LCD monitor was positioned 25 cm in front of the animal. The visual stimulus consisted of a thin, white, horizontal bar (73 degrees wide by 2 degrees high) on a gray background at 50% contrast, drifting upwards with a period of 12 seconds. The cranial window was evenly illuminated with fiber optic 610 nm red light at maximum brightness. A 2x objective was focused on the dura, and a picture of the blood vessels was taken to be used as a map for all future imaging. The objective's focus was lowered to 600*mm* beneath the dura, and an ROI was selected to include the most posterior portions of the window while excluding any saturated pixels. Images were continuously obtained using the LongDaq Imager 3000/C system (Optical Imaging Inc., New York City NY) for 40 blocks of 24 seconds. In order to determine the visual areas responding to the ipsilateral (right) eye only, the contralateral (left) eye was occluded by drape and recorded in addition to binocular visual stimulation.

For all data analysis, images were spatially binned into 4 x 4 pixels. The cortical intrinsic signal was obtained by extracting the Fourier component of light-reflectance changes that matched the stimulation frequency (12 s^{-1}). The response magnitudes in these maps are fractional changes in reflectance, and a threshold of 30% of peak response amplitude was applied to the response magnitude map in order to define the border of response region. The binocular zone of V1 was defined as the area stimulated by both ipsilateral-eye (right eye) visual stimulation and binocular visual stimulation (**Fig. 3.6c**).

Two-photon imaging

Approximately 15 to 18 days post surgery, the animals were anesthetized with isoflurane (1.5-2%), restrained using the front headpost, and adjusted such that the cranial window was evenly horizontal. Animals were then imaged using a Prairie Technologies

Ultima two-photon laser scanning microscope (Prairie Technology, Sioux Falls, SD) fitted with a Chameleon Ti:Sapphire laser light source (Coherent, Salem NH) at a wavelength of 930 nm. Areas for imaging were targeted based upon the binocular zone of V1, as defined by the intrinsic imaging analysis, and identified using blood vessel landmarks (**Fig. 3.6c**). A 20X water-immersion lens (N.A. 0.95) was initially focused on the most superficial mGFP-labeled axons, and the location of the deepest resolvable axons was identified (approximately 300 μm beneath the brain surface, depending on the clarity of the window and the quality of the viral label). Z-stacks were acquired at 2.5X zoom (512 x 512 pixels, resulting in a pixel scale of 0.45 x 0.45 μm) with a step-size of 1.0 μm starting at the surface. Laser power was increased incrementally, ranging from 20-60 mW at the objective, by the acquisition software (Prairie View) at increasing cortical depths. 2-7 different regions were imaged per animal, resulting in an imaging session lasting for 1-2 hours.

Image analysis

All analyses were performed blind to condition and animal. Branch measurements were performed using previously published methods and criteria (Holtmaat et al., 2009). Axon branch tips were identified by scanning through the first baseline image and confirmed in the second baseline image, and defined as being greater than 4μm long. The branch tip was identified in the third (post-manipulation) image, and an easily identifiable hallmark on the axon was marked across all images. The axon was traced from the common point to the branch tip across the Z-stack on each imaging day using the "simple neurite tracer" plug-in for Fiji image processing software (http://fiji.sc). For presentation purposes, axon segment paths were isolated and the z-stack was projected to result in a single image. In most cases, a second, independent researcher confirmed branch tip identification. When sorting data with a focus on motility, non-zero length changes were categorized as "retractions" when the difference between day 0 and day 3 was a negative value, and "extensions" when the difference was a positive value.

Histology of imaged animals

To confirm the location of the viral injection post-hoc, after imaging was completed, mice were anesthetized with isoflurane (1.5-2%) and the eye ipsilateral to the imaged hemisphere (the right eye) received intravitreal injections of CTB conjugated to an Alexa-

555 (Thermo Fisher, Grand Island, NY). In addition, a small hole was drilled in the glass coverslip using a diamond bit (1/12" bit, Patterson Dental, St. Paul MN) fitted to a high-speed micro drill (Fine Science Tools, Foster City CA). Using the vasculature map as a locational guide, the imaged areas of V1 were labeled by lowering a glass pipette loaded with CTB-Alexa-647 450 μm beneath the cortical surface and 50 nL was injected. The coverslip hole was sealed with glue, and the animal was left for 2-5 days to allow thorough labeling.

Animals were then euthanized with nembutal and perfused with 4% paraformaldehyde. 100 μm thick coronal serial sections containing the dLGN were cut on a vibratome and mounted on glass slides with fluormount G. Slices were imaged using confocal microscopy (Olympus confocal microscope, Tokyo Japan) with the FITC setting (viral GFP expression), Alexa 555 setting (ipsilateral eye projections), and Alexa 647 setting (retrogradely labeled cell bodies of imaged area). Only animals that had clear viral GFP labeling in the dLGN and lacked labeling in the dorsal portion of the lateral posterior nucleus (which also projects to binocular V1) were included in analysis. It was also confirmed that the CTB-647 labeling of the imaged area retrogradely labeled cell bodies located in the medial portion of dLGN, demonstrating that the areas imaged were indeed binocular V1. A second independent researcher confirmed all histological analysis.

Eyelid suture

Monocular eyelid sutures were performed as previously described ((Coleman et al., 2009), (Frenkel and Bear, 2004)). Under isoflurane anesthesia (1.5-2%), hair surrounding the eye was removed and lid margins were trimmed. The eye was thoroughly flushed with sterile saline and antibiotic ophthalmic ointment was applied to the eye. Using 6-0 vicryl sutures, approximately 5 stitches were placed along the extent of the trimmed lids and knots were secured with cyanoacrylate glue. Suture integrity was inspected prior to imaging sessions, and animals whose eyelids were not fully sealed were excluded from further experiments.

Electrode implants for visually evoked potential (VEPs)

For VEP surgeries, P25 male mice were anesthetized with isoflurane (1.5-2%) and provided indirect heat via a disposable heating pad. After cleaning and sterilization of the scalp, the skin covering the skull was removed and the skull was cleaned with 70% ethanol.

A small headpost was affixed onto a skull anterior to Bregma and secured with cyanoacrylate glue. Small (<0.5 mm) burr holes were drilled into the skull overlying the binocular visual cortex (3.2 mm lateral of lambda and 0.5 mm anterior of the posterior suture of each hemisphere. Tapered tungsten microelectrodes (75 μm in diameter, FHC) were inserted and lowered 450μm below the cortical surface. A silver wire (A-M Systems) reference electrode was placed over the prefrontal cortex of the left hemisphere. All electrodes were secured in place using gel cyanoacrylate glue. Dental cement was applied to cover the skull and enclose all electrodes into a stable, protective head cap.

VEP recording

All VEP recordings were conducted in awake, head-restrained mice, remaining still but alert during presentation of visual stimuli. 24 hours after surgery, animals were habituated to the apparatus by sitting head-fixed in front of a gray screen for two periods of 30 minutes. VEP amplitude was quantified using Plexon recording software (Dallas TX), and the trough-peak response amplitudes were measured and plotted using custom-designed matlab software.

Visual stimuli

Full-field visual stimuli were presented via a VSG2/2 card (Cambridge Research System, Rochester, Kent UK) on a computer monitor linearized by gamma correction. The screen was placed 20 cm in front of the animal, thereby occupying 92 x 66° of the visual field. Mean luminance determined by a photodiode placed in front of the computer screen was 27 cd/m^2. VEPs were elicited by phase reversing (0.5 Hz) oblique (15, 45, 75, 105, 135, or 165°) bars. During MD experiments, stimuli were presented and recorded to each eye separately, with the opposing eye blocked by an opaque drape placed flush with the animal's nose. Each eye was presented stimuli at 100% contrast and 0.05 cycles per degree for 300 phase reversals. After the first recording period, the eyelid contralateral to the recording hemisphere was sutured as previously described. 3 days post-suturing, the eye was opened by removing the tissue covering the sutured eye, and the eye was cleaned with saline. The eye was carefully inspected for signs of damage, and any animal showing opacity or other injury was excluded. Suture integrity was inspected prior to eye opening, and animals whose eyelids were not fully sealed were excluded from further experiments.

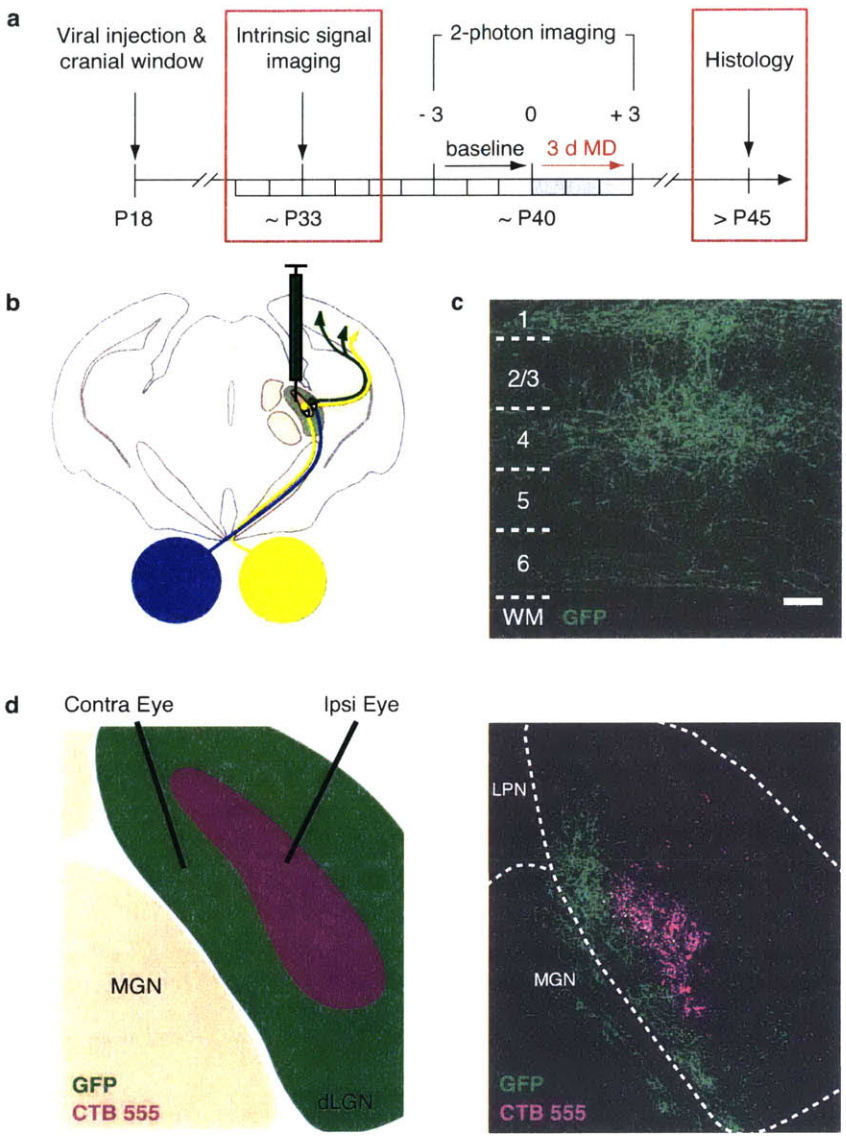

FIGURE 3.1: LENTIVIRAL LABELING OF EYE-SPECIFIC THALAMOCORTICAL AXONS

a, Experimental design of axon imaging experiments. **b,** Schematic of the mouse visual system showing targeting of viral injection to the contralateral input portion of the dLGN. **c,** Example confocal image reveals labeling of thalamocortical axons predominantly projecting to layer 4 and layer 1 of the binocular visual cortex. **d,** After experiments were complete, the ipsilateral eye was injected with an anterograde tracer (*CTB-555*) to label the ipsilateral

input to the LGN (*purple*), and confocal image stacks were assessed to ensure no overlap between labeled cells (*green*) and ipsilateral eye label (*purple*).

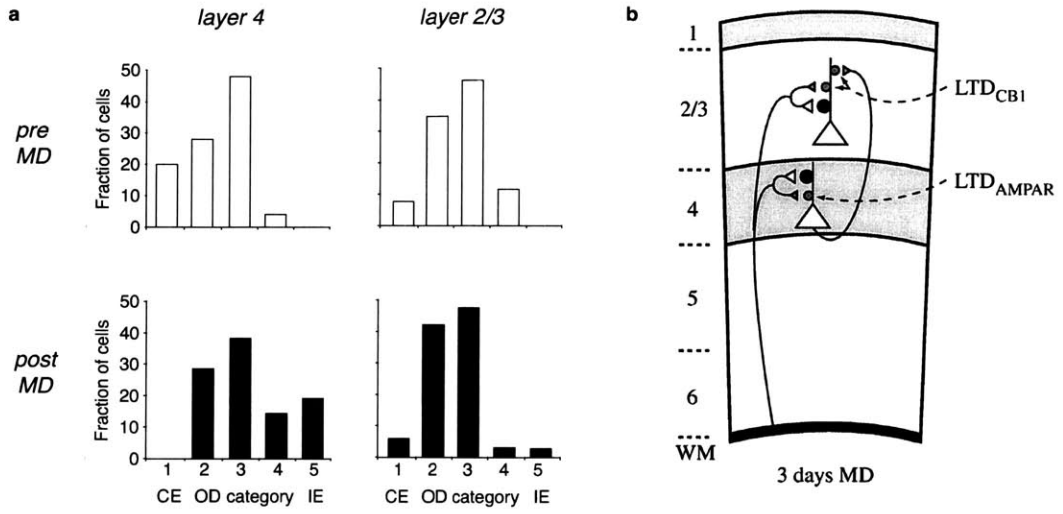

adapted from Liu et al., 2008

adapted from Smith et al., 2009

FIGURE 3.2: MECHANISMS OF DEPRIVED-EYE DEPRESSION VARY ACROSS CORTICAL LAYERS

a, OD histograms of single unit recordings mice that had been treated with AM251, an endocannabinoid antagonist, of layer 4 and layer 2/3 before and after MD. Blocking endocannabinoid signaling blocks OD shifts specifically within layer 2/3 after lid suture (Liu et al., 2008). **b,** Three days of MD produces depression of deprived-eye responses in both layers 2/3 and 4 through distinct mechanisms. In layer 3, LTD and deprived-eye depression requires endocannabinoid signaling, whereas in layer 4 they require AMPAR endocytosis (Smith et al., 2009).

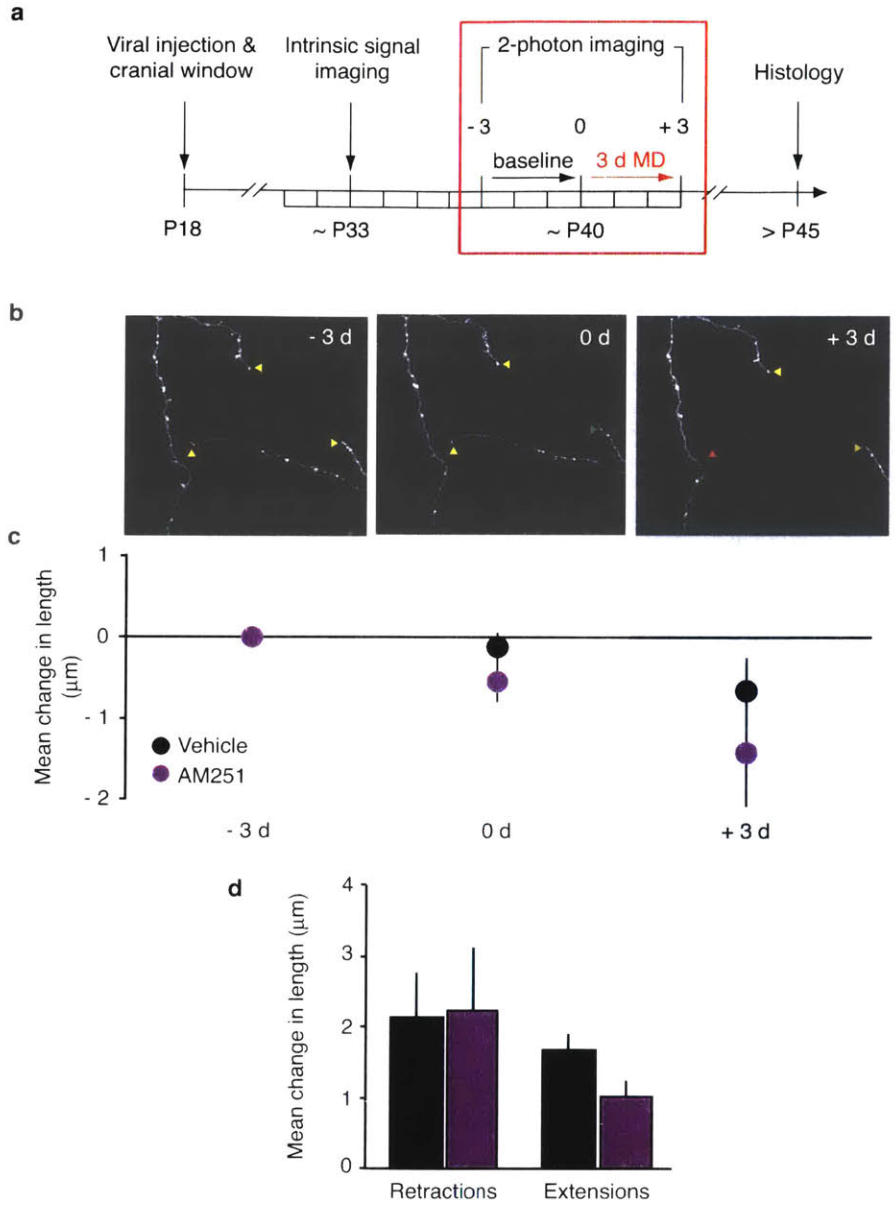

FIGURE 3.3: STRUCTURAL PLASTICITY OF THALAMOCORTICAL AXONS AFTER MD

a, Experimental design. **b,** Representative images of thalamocortical axons traced from tips (*arrowheads*) and projected through the z-stack. Over the course of imaging, some axons tips do not change (*yellow*), while others extend (*green*) or retract (*red*). **c,** Average branch

tip dynamics before and after MD in the presence of AM251 (*purple*) or vehicle (*black*). **d,** Summary of average branch tip retractions and extensions show a weak trend in both groups towards retractions over extensions.

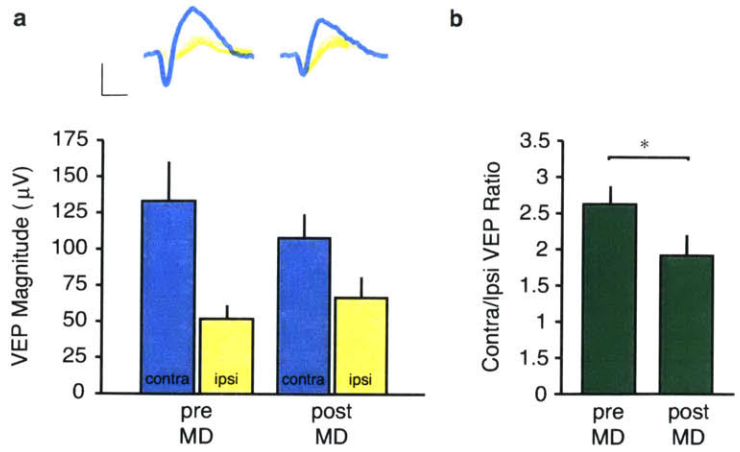

FIGURE 3.4: OCULAR DOMINANCE PLASTICITY IS MILD IN P40 MICE

a, Average traces of VEPs driven by the contralateral/deprived eye (*blue*) and ipsilateral/open eye (*yellow*) with group averages before and after MD. The contralateral/deprived VEP decreases slightly in response to lid suture ($p = 0.08$) and a slight, but non-significant increase in the ipsilateral/open eye response ($p = 0.28$). **b,** The ocular dominance shift can be measured through a ratio of contralateral to ipsilateral responses, and shows a statistically significant decrease following MD ($p = 0.03$). (*scale bar for traces: 50mV by 50ms; n = 8 animals; *post-hoc tests p < 0.05 after ANOVA)*

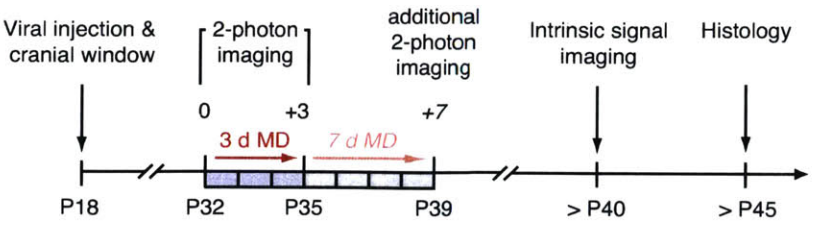

FIGURE 3.5: PROPOSED EXPERIMENTAL TIMELINE OPTIMIZED FOR MD DURING CRITICAL PERIOD

In an effort to ensure measurements occur when V1 is most plastic, a modified timeline is proposed where only one baseline 2-photon image is taken once the viral expression and window clarity is stable (P32) and the lid suture immediately follows, resulting in a second timepoint for a 3 day MD at P35. As OD dynamics change as the mouse ages and deprivation continues, an additional timepoint to compare 7 days of MD (P39) is suggested. Once axon imaging has been completed, the binocular visual cortex is mapped with optical intrinsic signal imaging and lastly the animal undergoes histological processing to confirm the location of the viral injection.

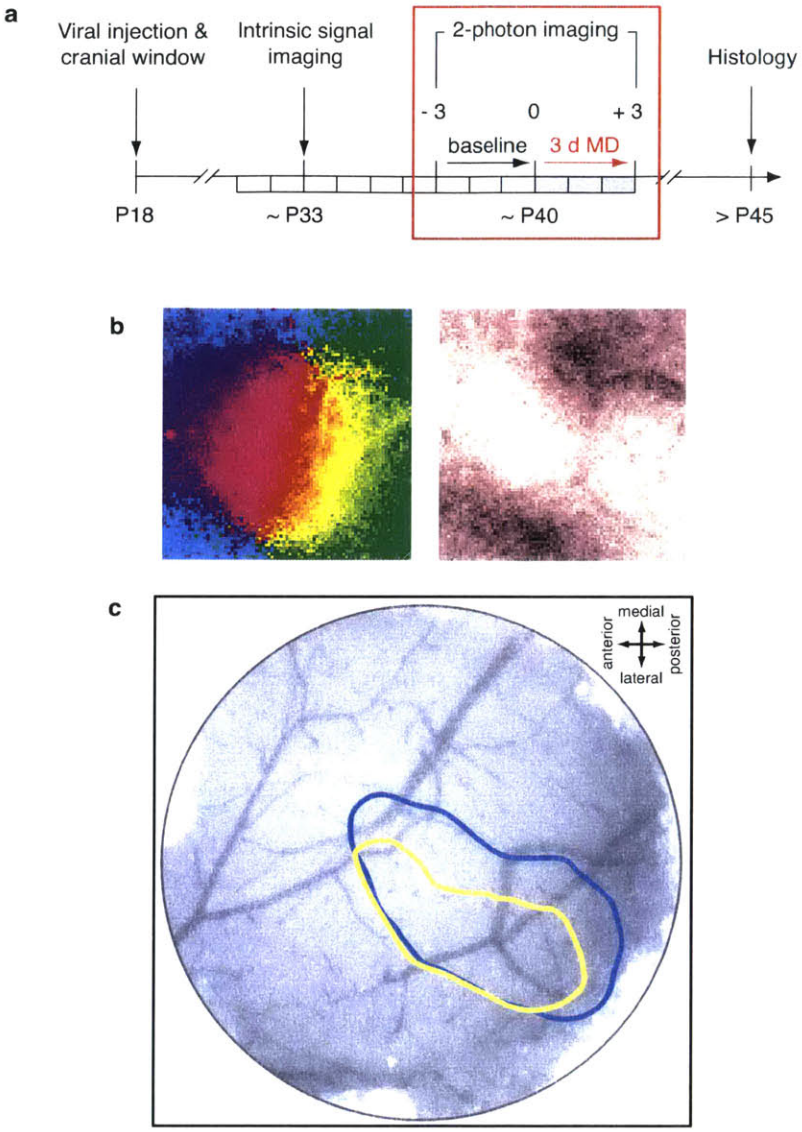

FIGURE 3.6: INTRINSIC IMAGING REVEALS BINOCULAR VISUAL CORTEX

a, Experimental design. **b,** Representative images of the retinotopic map (*left panel*) and magnitude map (*right panel*) derived from optical intrinsic imaging. **c,** Signal from each eye separately (*contralateral eye: blue line; ipsilateral eye: yellow line*) are overlaid to define the area of binocular visual cortex to designate a map for 2-photon imaging.

CHAPTER IV

CPG15 is implicated in mediating proper spine dynamics and protein synthesis

---

Experiments in this chapter were done under the direction of Elly Nedivi

ABSTRACT

There is evidence to suggest that CPG15 may have a role in regulating basal levels of dendritic spine dynamics. However, using mature hippocampal neuron culture to assess this has been inconclusive, and should be abandoned. A protocol for purifying heterologously-produced CPG15 was scaled such that high yields can be produced quickly and cleanly, but it did not result in the development of a CPG15-specific antibody from a mouse model that does not down regulate self-antigens. Promising data shows that CPG15 may be a potent inducer of protein synthesis, which may provide a mechanism for the synapse and learning phenotypes detected in the cpg15 KO mouse.

INTRODUCTION

The theoretical basis for connecting activity to learning and memory largely began with the Hebbian theory, positing that neurons which are activated at the same time have their connections strengthened (Hebb, 1949). This coincident activity results in rapid changes in the electrophysiology of brain circuits, followed by remodeling of structure. Recent imaging techniques have provided new insights into the small-scale refinements that connect these physiological changes to anatomical changes, and points to adult circuits which show cellular changes occurring on the order of days ((Trachtenberg et al., 2002), (Lendvai et al., 2000)).

Because of their distinct morphology, dendritic spines – protrusions that house excitatory postsynaptic molecular machinery (Harris and Kater, 1994) – have been a popular focus of time-lapse imaging studies. Serial EM reconstruction of dendritic spines imaged *in vivo* demonstrates that spine sprouting and retraction are associated with synapse formation and elimination ((Trachtenberg et al., 2002); ((Knott et al., 2006), (Svoboda and Yasuda, 2006), (Arellano et al., 2007)), making spines a useful correlate of excitatory synapse dynamics. During development, spines show a high degree of motility that declines with age (Zuo et al., 2005) and is biased towards spine loss (Grutzendler et al., 2002). By adulthood, spine number is balanced between formation and elimination ((Xu et al., 2009), (Hofer et al., 2009)).

Spine dynamics are continually influenced by experience-dependent shifts in activity. Two-photon imaging of primary sensory areas reveals that neurons in brain regions receiving both deprived and spared sensory experience show the greatest spine dynamics ((Wilbrecht et al., 2010), (Hofer et al., 2009)). Motor learning also drives enhanced spine plasticity ((Xu et al., 2009), (Yang and Zhou, 2009)), as does fear conditioning and extinction (Lai et al., 2012). Dendritic arbor and spine stability deficits are seen in many psychiatric illnesses (Lin and Koleske, 2010), including schizophrenia (Kalus et al., 2000), depression (Stockmeier et al., 2004), Alzheimer's (Terry et al., 1991), mental retardation (Purpura, 1974), and autism ((He and Portera-Cailliau, 2013; Purpura, 1974)); they are thought to contribute to the disease pathology resulting from, or as a result of, altered synaptic connectivity and plasticity (Koleske, 2013).

It is interesting – and important – to note that static views of dendrites do not necessarily reflect these findings. Spine density in adult mice is largely constant, as spine

addition and subtraction is balanced in the adult mouse brain (Chow et al., 2009). Changes in the rates of spine dynamics are sometimes followed by an opposing shift in dynamics that results in a total spine density that is ultimately equal to baseline levels ((Xu et al., 2009), (Yang and Zhou, 2009)). For this reason, overall spine density may not be an accurate reflection of network function, and may be a source for inconsistent findings across groups (He and Portera-Cailliau, 2013).

The molecular players that control spine stability are only beginning to be understood. Activity-regulated genes play a critical role in adaptive circuit refinement as a mechanistic link between activity and synaptic modification. A member of the immediate early gene family, *cpg15* was discovered in a screen for novel genes which were upregulated in the hippocampus after seizure induction (Nedivi et al., 1993). *cpg15* expression is responsive to environmental stimuli and is coincident with activity-dependent plasticity during development ((Nedivi et al., 1996), (Corriveau et al., 1999), (Lee and Nedivi, 2002), (Harwell et al., 2005)). Despite CPG15's role in promoting progenitor survival during cortical neurogensis (Putz et al., 2005), *cpg15* knockout animals (cpg KO) are viable and lack obvious abnormalities (Fujino et al., 2011). cpg15 KO mice show deficits in fear conditioning; yet after increased training, are able to retain and retrieve the memory weeks later (Fujino et al., 2011). The lack of CPG15 also results in delayed thalamic arbor elaboration (Fujino et al., 2011), which complements data showing overexpression enhances axon growth (Javaherian and Cline, 2005). Electron microscopy (EM) performed on cpg15 KO hippocampi of mice at 2 and 9 months revealed a lack of age-dependent synaptic remodeling seen in littermate WT animals (Fujino et al., 2011) and also documented by other groups ((Rakic et al., 1986), (Markus et al., 1987)). Therefore we hypothesized that CPG15 could play a role in the selective stabilization of synapses as a molecular mechanism of Hebbian plasticity, and may affect the formation and stabilization of spine synapses.

RESULTS

SPINE DYNAMICS IN CPG15 KO PRIMARY NEURON CULTURE

Spine dynamics as assessed by imaging are correlated with synapse dynamics assessed by EM ((Trachtenberg et al., 2002), (Knott et al., 2006)). As depletion of CPG15 decreases synapse density and remodeling, we imaged primary dissociated hippocampal neurons to measure if spine dynamics were also affected by loss of CPG15. We cultured neurons from WT and cpg15 KO embryos and virally labeled a small, random population of cultured neurons to stably express eGFP. We waited until neurons matured, forming mushroom type spines and we were able to image the same neuron twice at 3-day intervals (**Fig. 4.1**).

Preliminary data (using 2005 B27 supplement; see Methods section for detailed discussion) measuring the stability of spines between 32 DIV to 35 DIV reveals a balance between lost (*9.1%*) and gained (*7.8%*) spines in WT neurons (*black bars*, **Fig. 4.2a**). cpg15 KO neurons show this same balance, but have significantly more pruned (*13.2%, p = .010*) and newly formed (*14.0%, p = .001*) spines, and a complementary reduction in stable spines (*86.8%*) as compared to WT (*90.9%, p = .010*) (*red bars*, **Fig. 4.2a**). These results suggest that CPG15 does not affect the absolute spine density, but does have a role in regulating spine dynamics.

However, in order to perform further experiments characterizing how CPG15 specifically modulates spine stability, this phenotype must be consistently replicable. Shortly after these initial data were collected, it became exceedingly rare for neuron cultures to survive, let alone maintain their health, past 30 DIV. During the course of weekly culturing sessions over six months, we were able to collect images of only half the number of healthy neurons (*n = 11-14 per genotype*) as the initial dataset. The number of lost and gained spines was no longer balanced in either WT (*11.6% lost verses 8.4% gained*) or KO cells (*13.7% lost verses 9.5% gained*), with a shift towards losing spines (**Fig. 4.2b**). The portion of stable WT spines was slightly lower than the previous dataset (*88.4%*), while the portion of stable KO spines is approximately the same (*86.3%*) (**Fig. 4.2b**). While the trend of less stable spines in cpg15 neurons remains, the margin of difference between the two went from significant but small (*4.1%*) to even smaller (*2.1%*).

As 1) such a small dynamic range came at such a high cost of resources and time, and 2) the increase across genotypes of lost spines implies that the neurons might have begun their initial stages of health decline and 3) having neurons survive until 30 DIV and later became a rarity, we adjusted our protocol to improve the overall health of our cultures. The largest change came with the addition of 5% heat-inactivated FBS into the initial growth media, which was removed and replaced with non-serum containing media 24 hours after plating (**Fig. 4.2c, 4.2d**). In these cultures, we replaced glutamine with GlutaMAX and did not replace any of the media after the 1 DIV change to serum-free. We found that this protocol yielded cultures that were much healthier than the protocol using post-2005 B27 alone, and they were often viable after 30 DIV, although rarely past 38 DIV. However, although we were unable to directly compare conditions, neurons cultured using the previous protocol and 2005 B27 were often healthy up to 40 DIV and later.

Measuring spine stability in neurons cultured with serum (*n = 12-13*) from 32 to 35 DIV did not continue the trends of the earlier data (**Fig. 4.2c**). Both WT and cpg15 KO spines were more stable (*93.7% and 95.7%, respectively*) than neurons cultured without serum. The balance between gained (*7.3%*) and lost (*7.3%*) spines was equal for WT cells, but shifted towards gained spines (*9.6%*) over lost spines (*4.3%*) in cpg15 KO neurons (**Fig. 4.2c**).

In an effort to reconcile the different spine dynamics seen in culturing with versus without the addition of serum, we collected data from serum-grown neurons at an earlier time point (**Fig. 4.2d**). We made this transition, in part, based upon the observation that 1 DIV serum neurons extend their neurites earlier and farther than neurons cultured at the same time and plated without serum. Over the first week of growth, serum-grown neurons are qualitatively more similar to non-serum-grown neurons 1-3 days older. We believe that the many factors contained in the serum that help culture viability could also accelerate development, including synaptic plasticity. Our data from 24-27 DIV neurons is more compatible with our original data, with the percentage of WT stable spines (*94.6%*) exceeding cpg15 KO stable spines (*92.8%*). While both genotypes demonstrate a shift towards adding spines rather than losing them, cpg15 KO neurons gain (*10.3%*) and lose (*7.3%*) more spines than WT neurons (*8.1% and 5.4%*) (**Fig. 4.2d**), but with a much smaller margin of difference than neurons cultured without serum and original B27 (**Fig. 4.2a, 4.2d**).

Ultimately, we cannot draw strong conclusions from these data. There is a trend towards cpg15 KO leading to decreased spine stability, but the margin is small and it varies highly based upon culturing conditions. Furthermore, it is possible that the addition of serum to the growth media has an effect on spine dynamics, but we believe this is likely attributable to overall health of the culture and not specific to synaptic plasticity.

SYNAPTIC LOCALIZATION OF CPG15

cpg15 expression is induced in response to changes in activity ((Nedivi et al., 1996), (Harwell et al., 2005)), and enhances the maturation and growth of dendritic and axonal arbors ((Nedivi et al., 1998), (Cantallops et al., 2000)). Despite the evidence that cpg15 expression is synaptogenic and has pre and postsynaptic effects, the location of the protein in neurons is unclear. Without the ability to spatially track CPG15 over periods of synaptic development and in response to activity, a clear mechanism of action remains elusive. Repeated attempts to generate a specific monoclonal or polyclonal antibody against CPG15 have been largely unsuccessful, both by commercial organizations and individual labs. In order to address the direct effects of CPG15 activity, we sought to develop tools to identify the location of expression and action within the synapse.

Attempt to generate an anti-CPG15 antibody

The amino acid sequence of CPG15 is highly conserved across mammals, with 100% identity of the mature protein between mouse and human. We believe a primary reason for the previous failures to generate a suitable CPG15 antibody that is appropriate for immunohistochemistry is a problem of immune tolerance: the mammalian immune system minimizes response to self-antigens (Sakaguchi et al., 2008). An injection of a protein which is highly similar to one produced by the animal would not be immunogenic, and does not yield antibodies. Improper functioning of immune tolerance results in autoimmune disease. We chose to exploit this deregulation by using a murine model of systemic lupus erythematosus, the New Zealand Black/White mouse, which produces autoantibodies ((Shirai and Mellors, 1971), (Talal and Steinberg, 1974), (Kono and Theofilopoulos, 2006)). These mice have been successfully used for generating antibodies against proteins where

traditional antibody production techniques have failed ((Reimer et al., 1987), (Dobersen et al., 1985), (Jacquemart et al., 1988), (Hurpin et al., 1992), (Zhou et al., 2009)).

The first step begins with a highly pure form of CPG15 to be injected along with adjuvants into mice to induce the production of antibodies against CPG15. The protocol to generate a robust immune response recommends multiple injections of 50mg of protein in each mouse, with a minimum of two mice used. This was an immediate concern, as the largest previous purification attempt within the lab had yielded an order of magnitude less protein than required. The main contributor to this low yield was that immunoprecipitations from typically cultured HEK cells, which had been stably transfected to express CPG15 with a Flag Tag (**Fig. 4.3a**) were contaminated by proteins found in the growth media serum, which also bound to the flag antibody during immunoprecipitations. For this reason, the HEK cell media was replaced by serum-free media (Excell293, Sigma), drastically decreasing HEK cell viability and hindering our efforts for large-scale preparations. We found that cell viability could be significantly improved by efforts to increase cell adherence; in particular, coating the plating surface with gelatin resulted in rates of cell attachment in the serum-free media that were comparable to cells grown in serum-containing media. This yielded approximately 50mg per mL of a CPG15 sample free of contaminants (**Fig. 4.3b**) aside from the flag peptide, which is required for protein elusion (*not seen on the gel due to its 1 kDa size*).

In order to test the immunized mouse blood serum for a CPG15-specific antibody, we needed a method of enrichment for endogenously produced CPG15. Once we were successful in scaling up the purification process, we began to develop a protocol for identifying endogenous CPG15. Our first attempt used differential centrifugation to separate brain homogenate into different components (**Fig. 4.4a**), and the separation of Akt and GluR2 into soluble and pellet fractions, respectively, confirmed our technique (**Fig 4.4b**). However, we were not able to identify CPG15 (*green bands*) in any of the samples using a previously generated CPG15 antibody, used only for Western Blots and in very limited supply, which did produce a band against the purified, HEK cell produced CPG15 (**Fig. 4.4c**). Because the CPG15 protein has a GPI anchor and is often integrated into the membrane, we next isolated the membrane-bound and soluble fractions of dissected hippocampal and cortical tissue (**Fig. 4.4d**). Our efforts did not yield bands positive for CPG15 (*green bands*, **Fig. 4.4f**) in either the membrane (*hydrophobic; confirmed with the*

presence of GluR2, **Fig. 4.4e**) or cytosolic (*hydrophilic; confirmed with the presence of Akt,* **Fig. 4.4e**) fractions.

Although we failed to identify a technique for enriching CPG15 from the brain, we were still able to test the NZB/W blood serum against HEK purified CPG15 (**Fig. 4.5c**). A successfully generated polyclonal antibody should, at minimum, be specific against the identical antigen injected. We were unable to identify a CPG15 band using blood serum provided from two NZB/W mice after two sequential injections of flag-tagged CPG15 (**Fig. 4.5c**). As the health status of the mice precluded further injections and we had a complete absence of evidence to support that any of the bleeds contained a CPG15-specific antibody, we aborted this line of antibody development and did not proceed to monoclonal production.

Flag-tagged protein cannot be used for localization in cell culture

Without a sufficiently specific anti-CPG15 antibody, we investigated an alternate route for examining the synaptic localization and trafficking patterns of CPG15 using a flag tagged sequence. Similar to that which was transfected into HEK cells and purified as detailed above, the mature version of the protein has a flag-tag on its C-terminus (**Fig. 4-3a**). We could then use the anti-flag antibody as an indirect way of tracking the location of CPG15. We generated lentivirus with a construct that contained this flag-tagged cpg15 gene under the ubiquitin promoter, followed by an IRES cassette and a copy of the GFP gene. This results in infected cells that express flag-tagged CPG15 and are easily identifiable by the presence of GFP (**Fig. 4.6a, left panel**). By infecting neurons cultured from CPG15 KO animals, we would be able to compare neurons that express CPG15 (GFP positive) cultured with cells that do not (GFP negative). While the ubiquitin promoter removes the activity-regulated component of the endogenous cpg15 gene and constitutively produces flag-tagged CPG15, it would still be possible to localize and track how the soluble form of the protein functions downstream of secretion.

We found this virus to infect and express well in cultured hippocampal neurons (**Fig. 4.6a, left panel**). However, proper controls revealed that the anti-flag staining was not specific to the flag-CPG15 (**Fig. 4.6a, right panel and 4.6b**); we found punctate staining even on coverslips that were not infected at all and that was qualitatively identical to those cultures that had been infected (**Fig. 4.6b**). In hindsight, this is not surprising when

considered along with our HEK purification protocol: the anti-flag antibody binds strongly to a protein found in serum, and our neuron protocol requires serum during plating.

CPG15 HAS EFFECTS ON BASAL PROTEIN SYNTHESIS IN HIPPOCAMPAL NEURONS

The formation of new memories requires proper protein synthesis: new protein translation is essential during the brief time immediately following training ((Flexner et al., 1963), (Kelleher et al., 2004), (Costa-Mattioli et al., 2005)). Early experiments performed in rodents showed that injection of protein synthesis inhibitors during the acquisition of contextual fear conditioning (Nader et al., 2000) or spatial learning tasks (Lattal and Abel, 2001) block the formation of memory. Yet, once learned, memory is not disrupted by inhibition of protein synthesis ((Flexner et al., 1963), (Davis and Squire, 1984)). Similar results are seen in acute slice preparations from hippocampus, where memory is modeled as the long-term potentiation of synaptic strength (LTP): application of protein synthesis inhibitors during LTP induction blocks sustained potentiation, however, the same treatment is ineffective when applied after LTP is established ((Montarolo et al., 1986), (Frey et al., 1988)). Interestingly, cpg15 KO mice exhibit almost a complete lack of single-trial fear conditioning in both tone and context paradigms, yet are capable of maintaining fear memories with repeated training (Fujino et al., 2011). This suggests a deficit in memory formation and not memory retention, and led us to investigate the effect of CPG15 on protein synthesis.

We began by measuring the levels of protein synthesis in acute dorsal hippocampal slices prepared from WT and cpg15 KO littermate animals incubated with 10 microCi/mL 35S-methioninecysteine mix according to established protocols (Osterweil et al., 2010), measuring new protein synthesis in the absence of transcription (**Fig. 4.7**). Our results reveal a decrease in the basal protein synthesis detected in CPG15 KO slices when compared to WT slices (85.4% incorporation of WT incorporation) (**Fig. 4.7a**). To further probe this relationship, we measured protein synthesis in WT dissociated hippocampal neuron cultures incubated with purified CPG15. We found that CPG15 application caused a dramatic increase in protein translation in a dose-dependent fashion (**Fig. 4.7b**; 10 nM CPG15 = 141.9% incorporation vs vehicle, 20 nM CPG15 = 244.8% incorporation vs vehicle). This suggests that CPG15 can induce protein synthesis independent of

transcription, and that cpg15 KO animals may have a deficit in the basal levels of protein translation.

DISCUSSION

DATA FROM CULTURED CPG15KO NEURONS INCONCLUSIVE AS TO ALTERED BASAL DYNAMICS

Stefanie Kaech and Gary Banker wrote, "Choosing to work with primary neuronal cultures means accepting the fact that there will be some bad culture days" (Kaech and Banker, 2006), and our experience with neuron culture has been predominantly frustrating with only rare "good days". Our efforts have yielded a protocol that can overcome the limitations of the current form of B27 by adding serum to the neurons during plating, increasing the viability and health of our cultures. However, studying equivalents to adult synaptic plasticity within cultures has proven to be a time-consuming process fraught with difficultly and frequent to collapse, and we believe that makes it, at best, an unreliable model for these kinds of studies. The culture system continues to be a great resource for many studies of neural development, especially those in the early days *in vitro*, but its limitations should not be dismissed. Other models should be considered wherever possible, especially those that keep the laminar organization and spatial segregation typical of the cortex and hippocampus intact and preserve the developmental trajectory found *in vivo*.

The hypothesis remains that cpg15 acts as a sort of "Hebbian selector", identifying which spines should be stabilized and kept and which should be removed. Moving forward, I would suggest testing this hypothesis using other systems. It would be very informative to use an *in vivo* model wherein massive reorganization of circuits is required, and the responsiveness – or lack of responsiveness – of cpg15 KO animals could be compared to WT. For example, in the two months following a retinal lesion in WT mice, the deafferented area of the visual cortex demonstrates an almost complete replacement of dendritic spines, coincident with functional recovery (Keck et al., 2008). Based upon our hypothesis, we would expect circuits lacking cpg15 to be deficient in this experience-driven rewiring and would lack the ability to recover responsiveness to other portions of the visual field. As this

retinal scotoma technique uses a physiologically relevant paradigm to turnover 91% of spines in WT mice, it should be much more informative than the slim margins of the 5-10% spine turnover in WT neuron cultures reported by others (Akbik et al., 2013) and delineated here. *In vivo* studies can also correlate structural plasticity with functional recovery, avoiding accusations of epiphenomena that marginalize *ex vivo, ex situ* neuron culture results.

CPG15 LOCALIZATION

Our efforts to generate brain homogenate fractions enriched for CPG15 were mixed: differential centrifugation and membrane extraction yielded clear fractions but none that were positive for CPG15 in Western Blot (**Fig. 4.4**). Although the membrane isolation technique has been reported to be successful for CPG15 enrichment, it is complicated by conflicting reports as to whether CPG15 should be identified in the membrane or cytosolic fraction ((Putz et al., 2005), (Fujino et al., 2011)).

For future attempts to generate a CPG15-specific antibody, I would suggest using the protein purification protocol we developed, as it generated large quantities of pure protein quickly and consistently. When considering the animal used for immunization, I would suggest using the CPG15 KO animals themselves, as their immune systems will be naive to the CPG15 protein and should thus produce antibodies against it. This technique has been successful in generating antibodies against highly conserved proteins ((Declerck et al., 1995), (Nguyen et al., 2006)). Previous unsuccessful attempts by the lab have utilized permutations of purified protein, bacterial inclusion bodies, conjugated peptides, and crosslinked peptides in mice, rabbit, and chickens. The CPG15 antibody used in Western Blots - at a concentration 100-fold higher than most antibodies need to detect a signal – resulted from a rabbit immunized with bacterial inclusion bodies; yet 7 other attempts in rabbits and one attempt in mice were unsuccessful. Though the insights into CPG15 that would be possible with a sufficiently specific antibody are endless, the number of failed attempts within our lab alone does not inspire confidence that a slightly modified attempt will be any more successful.

We believe that the best way around this lack of CPG15 is still using a peptide tag. The flag-tag has proven to be unsuitable for use in serum-grown cells, even those that were

at any point grown in serum-containing media (which has an interesting secondary implication: serum elements remain in the culture even weeks after serum has been subtracted from the medium, which is the case in our neuron culture protocol). However, many different short, easily cloned, inert peptide tags remain, including HA, His, and Myc tags. Once one is demonstrated to not have non-specific binding in cultured neurons, many questions, including whether CPG15 acts pre or postsynaptically, and whether it is capable of binding to itself *ex vivo*, can be answered quickly and definitively.

CPG15 AS A POTENT PROTEIN SYNTHESIS INDUCER

Lasting, stable changes in synaptic strength require the production of new proteins ((Abraham and Williams, 2003), (Lynch et al., 2004), (Pittenger and Kandel, 2003), (Kauderer and Kandel, 2000), (Manahan-Vaughan et al., 2000), (Sajikumar and Frey, 2003)). Identifying and understanding the mechanisms by which protein synthesis regulates and influence synaptic transmission in the brain is an important area of study for both basic and translational research (Bear et al., 2004). Our metabolic labeling results reveal exciting possibilities for CPG15's function in synaptic plasticity. Our data suggests that CPG15 activates the production of new proteins, and CPG15 KO animals may have decreased protein synthesis. This finding could provide a source for the learning deficit seen during fear conditioning (Fujino et al., 2011) wherein CPG15-induced protein synthesis is required for rapid learning but other mechanisms compensate for repeated training, and could also be a mechanism for how CPG15 might act as a Hebbian selector. Once these results are repeated, there are many experiments that can be performed to pinpoint where CPG15 acts in the production of new proteins. First, generating synaptoneurosomes from CPG15 KO brain tissue and WT brain tissue with application of purified CPG15 can assess synapse-specific protein synthesis. Next, pharmacological drugs can be applied to CPG15 KO samples to determine if inducible protein synthesis is affected or if it is a basal protein synthesis deficit. Another important advantage to this assay is it provides a robust phenotype to identify the CPG15 receptor: purified CPG15 can be applied to neurons after pharmacological blockade of classes of receptors, or samples lacking a putative receptor.

METHODS

Dissociated neuron culture

The possibility of observing neurons *in vitro* was realized over a century ago (Harrison, 1910). Dissociated neurons grown as a monolayer circumvent much of the difficulty in visualizing and manipulating the same cells *in vivo*, and, because they are mitotically committed at the time of dissection (Fletcher and Banker, 1989), they retain the bulk of their genetic properties and develop similarly in a dish as they would in situ. These advantages have led neuron cultures to be a standard model across neuroscience subfields ((Banker and Goslin, 1991), (Kaech and Banker, 2006)), including synaptogenesis and synaptic plasticity (Craig et al., 2006). Growing neurons outside of their native environment does have its limitations: the investigator is obligated to recreate the environment of the brain for both scientific fidelity and the health of the neurons. Even with tightly controlled protocols for growth and vigilant maintenance, cultures surviving for longer than 30 DIV are rare ((Banker and Goslin, 1991), (Porter et al., 1997), (Brewer, 1997)). This presents dissociated neuron culture as a great substrate for studying growth and development, but not ideal for investigations of adult neural functioning.

There are many factors that can positively and negatively influence the viability of neuron cultures. Somewhat surprisingly, the perceived importance of each factor varies among laboratories, even those within the same institutes. In an effort to establish a consistent, repeatable protocol to produce mouse hippocampal and cortical neurons viable beyond initial synapse formation, and biologically equivalent to juvenile and adult synaptic plasticity, we methodically tested many elements of the culturing process.

Culture health was assessed differently at each developmental stage: one day after plating, healthy cultures had few floating dead cells and many strongly adhered phase-bright cells ("Stage 1" according to (Kaech and Banker, 2006)). Through the few days of culturing, the majority of cells should have multiple phase-bright processes ("Stage 2"), which, by 4 DIV extend for tens of μm and are often branched ("Stage 3"). Healthy cultures over a week *in vitro* should be an even monolayer with highly branched dendrites approximately 1 μm wide, and axons that form a continuous web across the surface (**Fig. 4.8, top panel**). By 10-14 DIV, dendritic spines should be apparent at high resolutions as thin filopodia, which should transition into large, mushroom-type spines by 18-21 DIV and beyond. For

imaging purposes, healthy cultures aged 21-40 DIV are characterized by: phase-bright cell bodies; smooth, even dendrites and axons with clear borders; and few detached cells in the media and dead cellular debris on the surface.

Cultures decline in health by initially showing unevenness in the structure of the dendritic branches and less clear borders of spines; dead or dying cells and their debris can also be seen floating in the media or still adhered to the surface, and subsequently there is a progressive decrease in cell density (**Fig. 4.8**). Unhealthy cultures develop large, distinct axonal varicosities that speckle the surface of the coverslip and dendrites that lack spines and atrophied tertiary and secondary branches. Another major sign of decreased viability that can happen as cultures age is the fasciculation of projections, leaving clumps of cell bodies and bare patches of growth surface to which axons and dendrites are unable to adhere. Especially when looking at morphology of GFP-filled cells at high magnifications (40-100x) over 3 days, we found that the early signs of culture sickness (i.e. uneven dendritic backbones, slight blebbing of any cells, unclear membrane borders) almost always looked markedly worse (**Fig. 4.9c and 4.9d**; i.e. increased blebbing, collapse of tertiary dendrites, complete cell death) by the second imaging time point. For this reason, any cultures that showed initial signs of sickness were not used for data collection (**Fig. 4.8**). Importantly, we would recommend vigilance for any researcher interpreting data from older cultures as they may not reflect healthy cellular function and, instead, may be in the early stages of degradation and death.

Tissue dissociation: We used mouse embryos aged 16.5 days, with the day of plug discovery considered half a day after fertilization. Deviating from this age group resulted in a much lower quality of cultures. E15.5 hippocampi were less defined and thus harder to dissect, and the resulting neurons were less robust and had decreased viability after plating. E17.5 tissue was more viable, but the brain meninges were more established and harder to remove. These older neurons survived plating relatively well, but had increased glial growth over time.

In order to produce littermate-matched cultures of both WT and KO neurons, embryos harvested from heterozygous dams were dissected and processed for culturing separately. This significantly increases the time from dissection to plating, and results in decreased viability. Initial experiments found that performing the dissection and dissociation on 4 embryos at a time, approximately doubling the experiment time had the

tissue been pooled into one sample, resulted in healthier cultures. To ensure age-matched samples, initially two completely separate rounds of dissection, dissociation, and plating were performed. We tried various strategies in an effort to decrease experimenter time and mouse usage. We found that the most important factor related to culture viability was minimizing the amount of time the tissue incubated both at the digestion step and in DNase-containing dissociation media (before and after triteration). As we found that initially dissected tissue can incubate in ice-cold HBSS for 1 hour without affecting viability, our final protocol involved consecutive dissection of up to 8 embryos from one dam; all subsequent steps were performed with two groups of 4 embryonic tissue. The protocol steps were interleaved, such that each step was performed to completion on each group before proceeding to the next, and in such a way that tissue only sat in HBSS and never any other media (i.e. digestion, dissociation, or plating).

Papain has been reported to be less toxic to embryonic tissue in comparison to trypsin, as it leaves the surface proteins intact (Brewer, 1997). Our tests did not show a difference in viability before plating as assessed with Trypan Blue or after plating.

Growth substrate: One of the most crucial elements for the survival of dissociated neurons is the surface on which they grow. We found plastic to be significantly better than glass for neural attachment, but for imaging purposes, this is not feasible. Glass coverslips provide an optically clear surface, but only those acquired from a German manufacturer (Schott Desag) will allow for proper cell attachment. Before use, coverslips must be cleaned and sterilized; we found two methods that worked well. Glass coverslips can be baked at 200°C for 4 hours and then stored in dry, sterile conditions. Coverslips can also be acid-washed in pure nitric acid and shaken, but this is a lengthy process requiring many water washes over days (1 – 10 days), followed by autoclaving and storage in sterile water before use. However, we found acid washing to be preferable, as baked coverslips were brittle, causing them to chip or crack while being handled with sharp forceps.

It is extremely important for plastic and glass surfaces to be coated with substrates that are permissible to neuronal attachment (Letourneau, 1975). Pre-coated glass coverslips are available, although we did not find a difference between those purchased and our method except in price, and for our experiments the expense of pre-coated coverslips was not feasible. Poly-lysine, a polymer of the basic amino acid which alters the surface charge of the coverslip, is a necessary component of the coating solution, but which isomer works

best depends on the experimenter. Many experimenters have found a significant improvement with poly-L-lysine over poly-D-lysine (Asha Bhakar, personal communication, (Brewer et al., 1993)), presumably because the L-isomer can be broken down by proteases released from the cells. However, we found poly-L-lysine to be indistinguishable from poly-D-lysine in our cultures and, in addition to whether they were dissolved in borate buffer or water, we did not detect a difference in initial attachment, survival, or fasciculation. The addition of laminin, a glycoprotein component of basement membranes *in vivo* (Kleinman et al., 1981) to the coating solution helped adhesion and survival length greatly, but with certain media conditions discussed below, encouraged glial overgrowth to the extent that the glia overtake the culture after 2-3 weeks. Incubation in the coating media should occur in light protected environments with gentile shaking. After no less than 12 hours (up to a week), the coverslips must be washed with sterile water, as leftover laminin and lysine can be toxic. Some laboratories use five washings or washings occurring over 3 days, but we found three washings over three hours to be as effective as any more extensive protocol.

A final and important method we discovered was to allow the coated coverslips to incubate in the plating media for 2-3 hours in the CO2 buffered 37° incubator. Enough media, formulated as described below (5% heat-inactivated FBS, 2% B27, .5mM GlutaMAX in Neurobasal), was added to fully submerge the coverslip and then removed immediately before plating the cells. We believe this allowed the serum and B27 to saturate the plating substrate, facilitating both attachment and long-term health.

Media formulations: The development of defined artificial media provides a controlled, replicable growth environment ((Bottenstein et al., 1979), (Romijn et al., 1984), (Brewer et al., 1993)), although neurons do not survive as well in an incubator as they do in within the brain. Glutamine, an essential precursor for protein synthesis, is a necessary media addition, but it is unstable in solution (Tritsch and Moore, 1962)) As glutamine is metabolized, ammonia accumulates in the media and is toxic to cells (Schneider et al., 1996). Replacing a portion of the media on a weekly basis mitigates some of this toxicity, but we found using GlutaMAX, a stabilized version of glutamine which does not degrade into ammonia and slowly releases glutamine over time for use by the cultured cells (Christie and Butler, 1994), to be preferable to glutamine. With GlutaMAX, we found that media changes (replacing half of the cultured media with fresh media) negatively impacted the health of the neurons. Even replacing smaller fractions of the media resulted in less healthy

looking cells than those wells that had been untouched. Although 2mM GlutaMAX is recommended, our tests demonstrated .5mM to result in marginally healthier neurons.

We also found the addition of serum during plating results in huge improvements of culture quality. Despite the fact that serum is of variable composition, we did not find a significant difference between company of origin or production lot. Concentrations of 5% to 10% of heat-inactivated FBS lead to higher attachment and more developed cells one day after plating with more neurite outgrowth. However, it is crucial that the media is changed to new media without serum 12-24 hours after plating; if the neurons remain in serum, their viability decreases sharply after 4-7 days. Here it is important to note that serum and GlutaMAX in addition to laminin in the coating solution results in replication of glia to the extent that they overtake the neuron culture within a few weeks; omitting or replacing any of the three components (serum, GlutaMAX, or laminin) is enough to keep the glia replication at bay, and we found that leaving out laminin and keeping serum and GlutaMAX brought about the best neural survival.

A final, crucial component of the culture media is the addition of the supplement B27. Originally formulated to reduce the variability resulting from undefined serum, it improved neuron survival in culture and quickly became the standard for primary dissociated cultures ((Brewer et al., 1993), (Brewer, 1995)). We found that much of the difficulty in culturing long-term hippocampal neurons correlated with a change of production lot number used. After testing 15 different lots, at varying concentration, over 4 years, none was found to produce neurons as healthy as a lot purchased in late 2005. Despite contacting the manufacturer, we could not resolve this change in quality, and suffered a sharp decrease in plating survival and ultimate viability. With post-2005 B27 lots, we achieved cultures that maintained their health until 15-21 DIV at best, whereas the 2005 B27 lot was able to support cultures 36-42 DIV regularly. The addition of serum to the plating protocol resulted in an additional week of viability, allowing the neurons to survive up to an extra week as with B27 alone, until 22-28 DIV (**Fig. 4.2**), but was still significantly less healthy in appearance and viability than the cultures performed in 2005 or earlier. Frustrations with B27 have since been reported by numerous other labs ((Chen et al., 2008), (Roth et al., 2010), (van der Valk et al., 2010), (Schluter et al., 2006), (Tsui and Malenka, 2006)). Preliminary experiments using a published alternative supplement, NS21 (Chen et

al., 2008), did not improve culturing conditions over those with B27 and serum, but extensive testing was not performed.

Lentivirus production

Lentivirus inducing EGFP expression was made essentially as described in Lois ((Lois et al., 2002)). HEK293T cells were grown on gelatinized 15-cm tissue culture dishes in standard HEK media (10% FBS, 100U-mg pen-strep in DMEM). Once 90% confluence was reached, the HEK medium in each plate was removed such that only 7.5mL remained. A solution of 7.5mL of Optimem (Thermo Fisher, Pittsburgh PA) containing 150 μL Lipofectamine 2000 (Thermo Fisher, Pittsburgh PA) and the following plasmids prepared using Qiagen maxiprep kits (Qiagen, Germany): 20 μg delta 8.9, 15 μg VSVg, and 25 μg FUGW (containing a HIV-1 flap sequence, human ubiquitin promoter, EGFP, and woodchuck hepatitis virus posttranscription regulatory element). After 20 minutes of incubation, the solution is added dropwise to cover the plate. The transfection medium was replaced after 5 hours with 12mL of fresh HEK medium. 24-30 hours post-transfection, the medium was collected and fresh medium added to the transfected cells. The medium was collected and replaced two more times, at approximately 48 and 72 hours post-transfection, after which the cells were discarded. Medium harvested on day 1 and day 3 were then combined. The two batches of supernatant (day 1&3, and day 2) were filtered separately through a 0.45 μm Durapore vacuum flask filter (Thermo Fisher, Pittsburgh PA) and stored on ice.

In order to concentrate the virus to yield high titers, the day 1&3 batch was added to Amicon-15 100 MWCO filters (EMD Millipore, Billerica MA) and centrifuged at 4,000 x g for 20 minutes at 4°C. The flow-through is discarded, and the filters are spun again with a PBS wash. The remaining retentate was added to the day 2 viral supernatant. The virus was then spun in a 4°C Sorvall ultracentrifuge (Thermo Fisher, Pittsburgh PA) at 25,000 rpm for 1.5 hours. The supernatant was discarded, and the pellet allowed to dry. The viral pellet was resuspended in PBS overnight, split into aliquots and stored at -80°C until ready for use.

Titering was determined via serial dilutions infecting HEK293T cells, fixed with 4% PFA two days post-infection, and generally achieved a concentration on the order of 1×10^7 pfu/μL. For infecting dissociated neuron cultures, at 12 days in vitro (12 DIV), the EGFP

lentivirus was diluted in feeding medium to a concentration of 1 pfu/10 cells for sparse labeling to optimally image dendrites.

Time lapse imaging of dendritic spine dynamics

At an age when the neurons have developed mature, mushroom spines, coverslips were removed from the incubator for no more than 20 minutes and transferred to a glass-bottom dish containing warmed (37°C) microinjection buffer (10mM HEPES pH 7.4, 135 mM NaCl, 5mM KCl, 2mM $MgCl^2$, 15mM glucose). Neurons expressing EGFP were selected based upon brightness and presence of spines and not overall morphology; 2^{nd} and 3^{rd} order branches were targeted. Dendrites were imaged with an Olympus FluoView 300 laser-scanning confocal microscope and FluoView 500 acquisition software (Olympus, Tokyo Japan). A Helium-Neon green laser was used with the FITC setting: excitation 460-500 nm, emission 510-560 nm. A 20x image containing the whole cell was taken for identification purposes. A z-stack consisting of a total depth of 4μm (9 0.5 mm slices) was acquired with a 60x water immersion objective at 5x zoom of a dendritic branch point to maximize dendritic segments and help target later. After the imaging of approximately 4 neurons, coverslips were returned to their original wells and media and placed back into the incubator. Three days later, the same coverslips were again placed into glass-bottom dishes containing microinjection buffer. Using various neuronal landmarks, the originally imaged dendritic branches will be reimaged as previously described.

The z-stacks of dendritic segments from these time lapse imaging sessions were collapsed into one maximum intensity Z-projection, blinded, and analyzed by eye. Protrusions extending further than 0.2 μm were considered spines. The first and second imaging sessions were compared to determine whether each spine has persisted or disappeared, and for the appearance of new spines.

Immunocytochemistry of cultured neurons

After a two minute wash in PBS, neurons were fixed by submersion in 4% paraformaldehyde in PBS for 15 minutes at room temperature. Three washes of PBS were performed, followed by adding 0.3% Triton-X for 5 minutes. Each coverslip was then incubated in blocking solution (5% normal goat serum in PBS) for 30 minutes. Primary antibodies were incubated with gentle rocking at 4°C overnight, the coverslips were washed

with PBS, and second antibodies (Alexa conjugated to the appropriate fluorophore at 1:500) were incubated at room temperature for an hour. After three more PBS washes, the coverslips were mounted onto slides with Fluoromount G and sealed with clear nail polish.

Images of immunocytochemistry of cultured neurons were acquired with an epi-fluorescence microscope using a 10x/NA 0.3 objective lens (Nikon, Tokyo Japan).

Purification of heterologously expressed CPG15

For CPG15 expression, HEK293T cells were generated such that a Flag tag was inserted after the signal peptide sequence of CPG15. These stabley-transfected HEK293T cells were grown in .2% gelatin-coated 15cm culture dishes containing serum-containing medium (10% calf serum, 50 U penicillin, 50 μg streptomycin, 4 mM L-glutamate in Dulbecco's Modified Eagles medium (Thermo Fisher, Pittsburgh PA). At 80% confluence, the cells were washed gently with PBS, and the serum containing medium was replaced with serum-free medium (110mM $CaCl^2$, 50 U penicillin, 50 μg streptomycin, 6 mM L-glutamine in EX-CELL 293 HEK Serum-Free Medium [Sigma]). After 48-72 hours of incubation, the medium was harvested and centrifuged (3,000 rpm, 15 min at 4°C) to remove any cell debris, and a volume of 1 to 100 1M Tris pH 7.5 was added to balance the acidity.

Beads consisting of anti-Flag coupled to agarose (EZview Red ANTI-FLAG M2 Affinity Gel [Sigma-Aldrich, St. Louis MO]) were prepared by washing five times with cold PBS and then pelleted by centrifugation (4,000 rpm for 7 minutes). At this point, the glycerol should be fully removed, and the beads were resuspended into a slurry of 50% beads, 50% PBS by volume.

120μL of the bead slurry was added per 50mL of medium and rotated at 4°C. After 12-24 hours, the beads were pelleted by centrifugation (4,000 rpm for 10 minutes at 4°C) and washed five times with PBS over three hours. The resulting beads were transferred into siliconized epindorf tubes, and all liquid was removed. 3x Flag peptide (Sigma-Aldrich, St. Louis MO) was added at two times the volume of the beads used. After rotating at 4°C for one hour, the beads were pelleted (2,000 rpm for 5 minutes) and discarded. The remaining supernatant contained eluted flag-tagged CPG15 protein.

Final protein concentration was determined by boiling the eluted protein with loading buffer for 5 minutes. After running on a 12.5% polyacrylamide gel next to defined protein standards (trypsin inhibitor) of approximately the same molecular weight as CPG15,

a silver stain was performed. The gel was washed in water two times, before fixed with 30% ethanol and 10% acetic acid for 15 minutes two times. The fix solution is drained and replaced with 10% ethanol for 5 minutes two times, followed by two water washes. 50μL of SilverSNAP Sensitizer (Pierce Biotechnology, Rockford IL) in 25 mL water is added to the gel for one minute, before washing in water twice. The gel is then incubated in 500uL of SilverSNAP Enhancer in 25mL SilverSNAP Stain for 30 minutes, followed by two washes of water. 500μL of SilverSNAP Enhancer in 25mL SilverSNAP Developer is added to the gel for 2-3 minutes. When optimal band intensity is achieved, the gel is washed immediately with 5% acetic acid for 10 minutes. The gel was then scanned, and bands were quantified using ImageJ software (http://imagej.nih.gov/ij*)*. The quantity of CPG15 protein in each band was extrapolated from the protein standard curve.

Enrichment of brain CPG15

Adult (approximately P60) WT and cpg15 KO male littermate mice were individually euthanized with CO^2, and their brains removed. Hippocampi and cortices were dissected out and put on ice. Each tissue was put in a glass Dounce homogenizer containing cold homogenization buffer (320 mM sucrose, 1mM DTT, 1mM EGTA, 1mM EDTA, 40mM HEPES-KOH pH 7.4, and Complete Mini protease inhibitors) manually homogenized 10x with a loose pestle, followed by 10x with a tight pestle until no tissue chunks remained.

The protein content of all samples were measured using the BCA Protein Assay Kit (Pierce Biotechnology, Rockford IL), and the concentrations were adjusted as needed. Proper separation was confirmed by loading 40μg of each sample and immunoblotting for GluR2 (1:1000, anti-mouse [Chemicon]) and Akt (1:1000, anti-rabbit [Cell Signaling]).

Differential centrifugation: Samples were pelleted via centrifugation (2,000 rpm for 10 minutes) and the pellet (P1) was isolated from the supernatant (S1). The S1 fraction, minus a 50uL sample, was centrifuged for 10 minutes at 12,000 rpm at 4°C, resulting in a pellet (P2) and supernatant (S2). The S2 fraction, again minus a 50uL sample, was spun in a 4°C ultracentrifuge for one hour at 48,000 rpm, resulting in the final pellet (P3) and supernatant (P3) fractions. The P1 fraction was discarded, and the P2 and P3 fractions were resuspended in homogenization buffer.

Hydrophobic/hydrophilic isolation: Hydrophobic and hydrophilic brain fractions were isolated using a Mem-PER extraction kit (Pierce Biotechnology, Rockford IL). The samples were pelleted via centrifugation (3,500 rpm for 5 minutes at 4°C), and the supernatant discarded. The pellet was resuspended by pipetting in Reagent A and occasionally vortexed for 10 minutes. Reagents B and C were added, and the samples were placed on ice for 30 minutes. The supernatant was isolated after centrifuging (11,100 rpm for 3 minutes at 4°C) and the pellet discarded. Samples were incubated in a 37°C water bath for 20 minutes. After centrifuging (10,000 x g for 2 minutes at 25°C), the sample resolved into two layers. The fractions were carefully separated, resulting in a hydrophilic fraction (top layer) and a hydrophobic (bottom layer) fraction of each sample. The presence of CPG15 protein was determined by immunoblotting with anti-Flag (1:1000, anti-mouse [Sigma]) and anti-CPG15 (1:100, anti-rabbit; generated by Tad Fujino) antibodies.

Detection of CPG15 antibody

CPG15 purified from HEK cells, the antigen injected into the rabbits to generate the antibody, were boiled in Laemmli sample buffer, and resolved with an adjacent rainbow ladder on a 12.5% SDS polyacrylamide gel. Immunoblotting was performed on membranes cut to the smallest possible size in order to conserve the provided blood serum. Membranes were incubated with 1:100 blood serum as well as anti-Flag (1:1000) as a positive control overnight at 4°C.

For Odyssey imaging (LI-COR Biosciences, Lincoln NE), blots were blocked for one hour at room temperature in Odyssey Block buffer, followed by incubation for an hour at room temperature with fluorophore-conjugated secondary antibodies: IRDye 800 (1:5000, anti-mouse [Rockland]) and Alexa 680 (1:5000, anti-rabbit [Invitrogen]). After 3 10 minute 1% TWEEN20 in TBS washes, the membranes were dried and imaged with the Odyssey imaging system. For ECL visualization, HRP-conjugated secondary antibodies (GE Healthcare, Chicago IL) were used and developed with ECL plus (GE Healthcare, Chicago IL) before being exposed to film.

Metabolic labeling

For brain slice experiments, juvenile (P25-30) male WT mice were given an overdose of Nembutal, and the hippocampus was rapidly dissecting into ice-cold ACSF (in mM: 124

NaCl, 3 KCl, 1.25 NaH2PO4, 26 $NaHCO^3$, 10 dextrose, 1 $MgCl^2$, and 2 $CaCl^2$, saturated with 95% O^2 and 5% CO^2). 500mm thick slices were prepared using a Stoelting Tissue Slicer and transferred into 32.5°C ACSF within 5 minutes. Slices were incubated undisturbed for 4 hours to allow for recovery of protein synthesis (Sajikumar et al., 2005). 25μM actD was then added to the recovery chamber for 30 minutes to inhibit transcription. Slices were incubated in 10 μCi/mL 35S-Met/Cys (express protein labeling mix, PerkinElmer) plus purified CPG15 or vehicle for 5 minutes, then transferred to fresh ACSF with 10 μCi/mL 35S-Met/Cys for another 25 minutes. Slices were homogenized in ice-cold homogenization buffer (10mM HEPES pH 7.4, 2mM EDTA, 2mM EGTA, 1% Triton X-100, protease inhibitors [cocktail III, EMD Biosciences], and phosphatase inhibitors [cocktails I and II, EMD Biosciences]).

For neuron culture experiments, WT, het, and KO neuron coverslips were incubated in the tissue culture incubator in neuron feeding medium with 25 μM actD for 30 minutes, followed by a 30 minute incubation in feeding medium with 10 μCi/mL 35S-Met/Cys. The coverslips were washed with cold PBS, then shaken at 4°C in homogenization buffer for 10 minutes.

To precipitate radiolabeled proteins, all samples were then incubated in trichloroacetic acid (TCA) to a final concentration of 10% TCA for 10 minutes on ice. Samples were then centrifuged at 21,000 x g for 10 minutes. The resulting pellet was washed with water and resuspended in 1 N NaOH. After adjustment to a neutral pH with HCl, aliquots of each sample were taken in triplicate and added to scintillation cocktail (HiSafe II, PerkinElmer) and read with a scintillation counter. Another aliquot of each sample was used to assay protein concentration (Bio-Rad).

Averaged triplicate cpm values were divided by protein concentrations, resulting in cpm per mg protein. To control for daily variation in incorporation rate, the values obtained on each day were normalized to the 35S-Met/Cys ACSF used for incubation as well as the average incorporation of all slices analyzed in that experiment, as described by Lipton and Raley-Susman (Lipton and Raley-Susman, 1999).

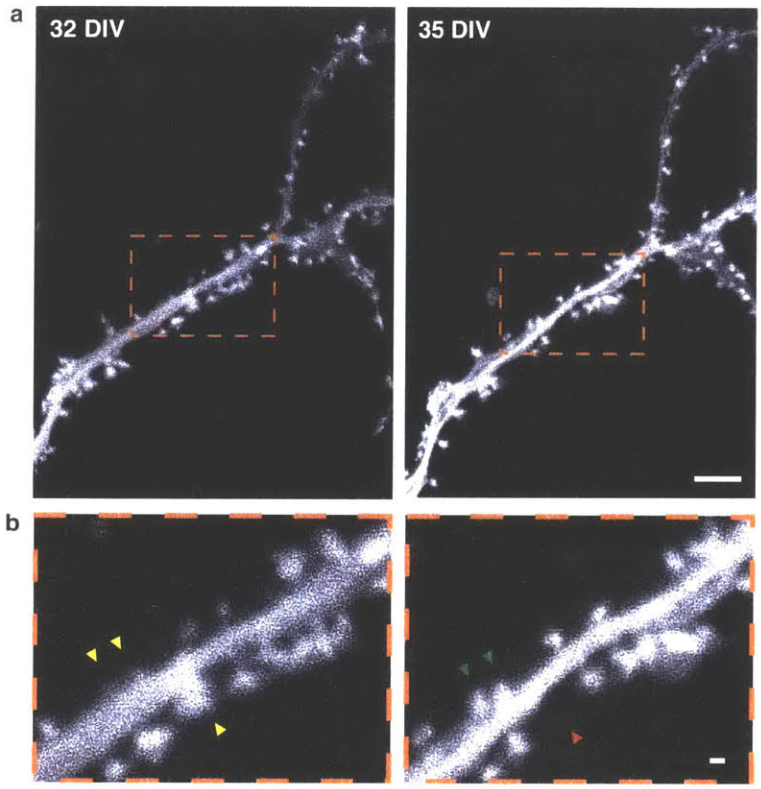

FIGURE 4.1: REPEATED IMAGING OF MATURE DENDRITIC SPINES IN DISSOCIATED NEURON CULTURE

Representative confocal imaging of cultured hippocampal neuron dendrite infected with GFP-expressing lentivirus at **a,** 32 DIV and 35 DIV. **b,** The region in the rectangle is enlarged in lower panel indicating new spines (*green arrow heads*) and lost spines (*red arrowhead*).

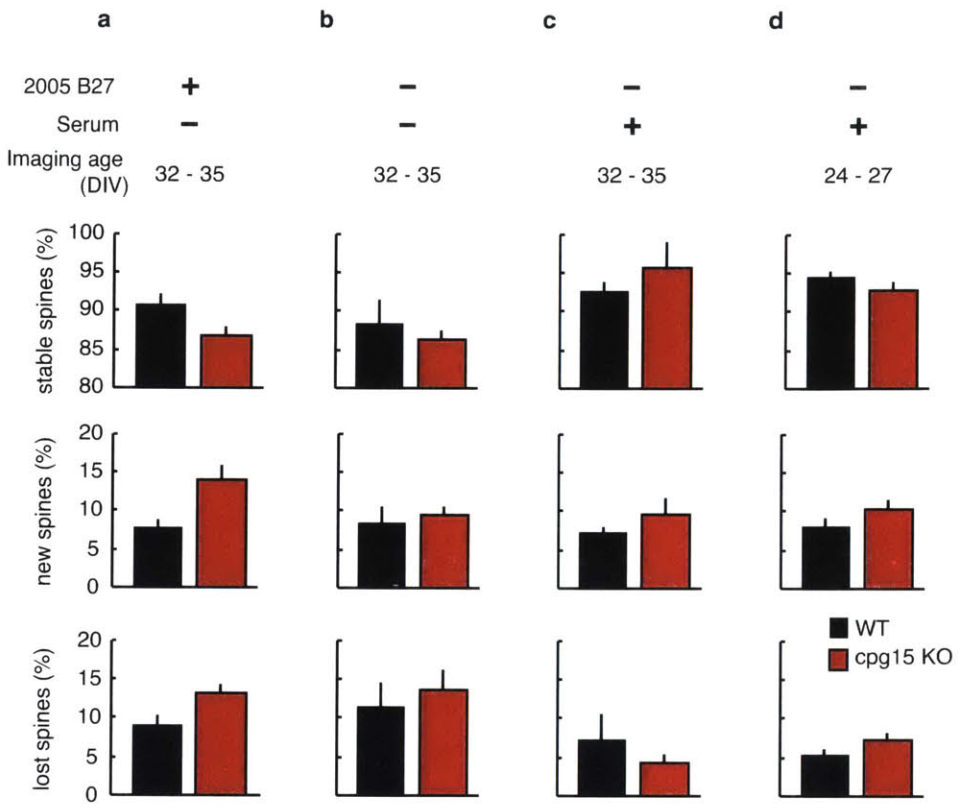

FIGURE 4.2: BASAL SPINE DYNAMICS IN CPG15 KO AND WT DISSOCIATED NEURON CULTURE

Averaged rates of spine stability (*top panels*), spine gain (*middle panels*), and spine loss (*bottom panels*) across many culturing conditions in cpg15 KO (*red*) and WT (*black*) primary cultured neurons. **a,** Neuron cultures in B27 lot from 2005 without serum (*n = 22-25 neurons per group*) show increased dynamics in KO neurons. **b**, Cultures from post-2005 B27 lot plus serum (*n = 11-14*) show no difference between the genotypes in spine behavior. **c,** Cultures from post-2005 B27 lot plus serum (*n = 12-13*), show opposite findings of our original data, which may be a product of serum inducing heightened maturity. **d,** cultures from post-2005 B27 lot plus serum at 24 – 27 DIV (*n = 22-27*) repeated the initial finding wherein KO animals had less spine stability, but with a small margin separating them from WT.

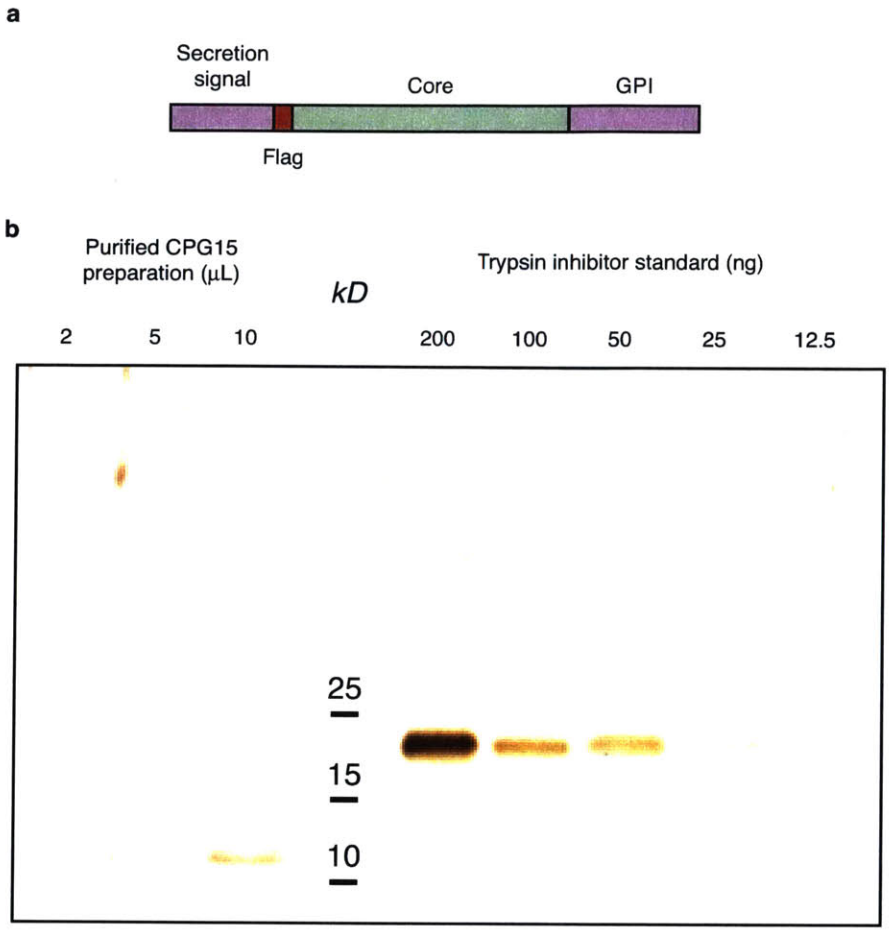

FIGURE 4.3: CPG15 PURIFICATION FROM HEK CELLS

a, Schematic of protein construct expressed by HEK cells. Harvested CPG15 consists of a 12.5 kDa protein consisting of the protein core (*green*) and flag signal (*red*). **b,** Silver stained SDS-page gel showing dilutions of harvested protein (*left*) demonstrating the purity of the preparation run next to a protein standard (*right*) for quantification purposes. Protein sizes are indicated (kD).

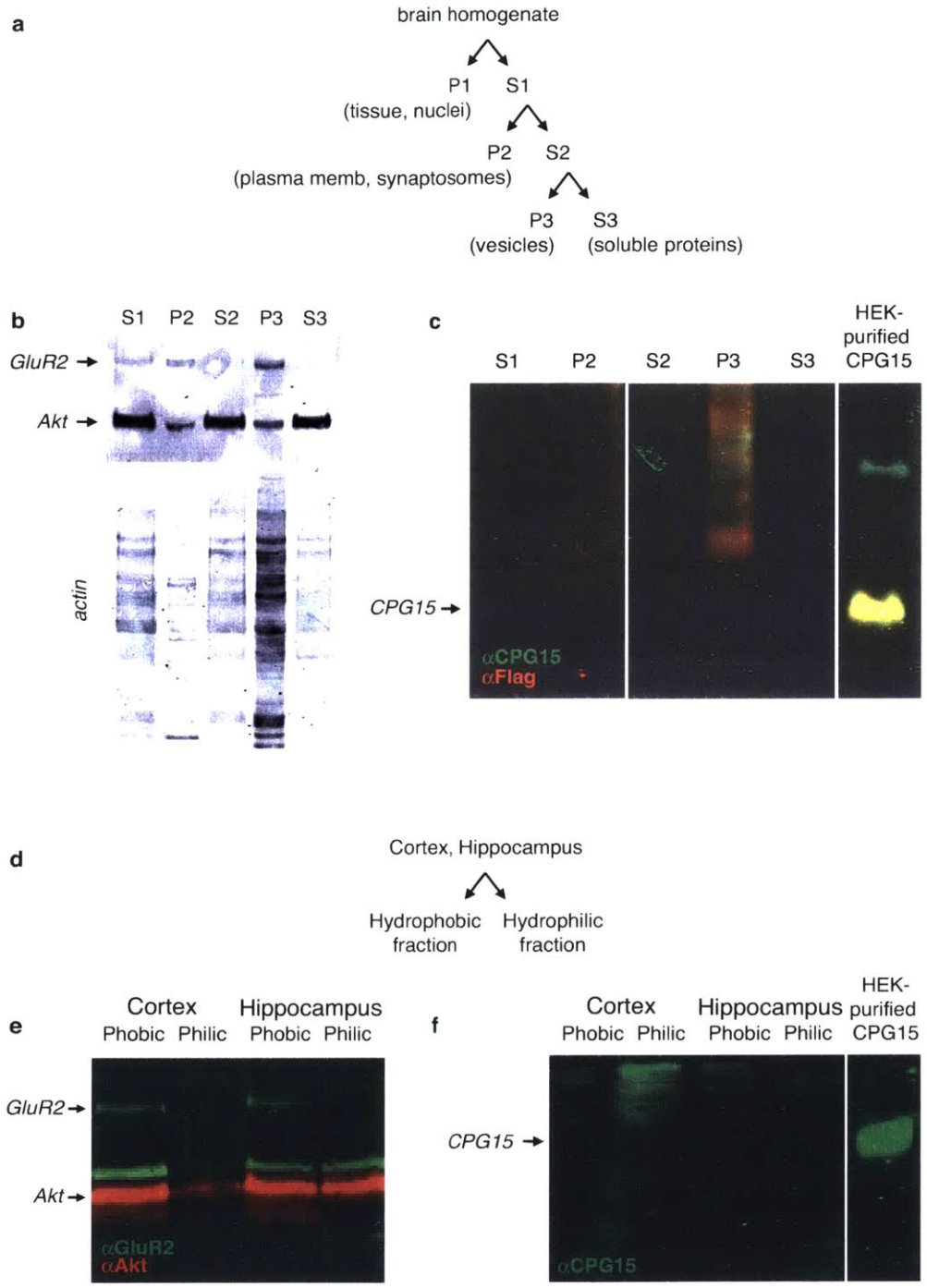

FIGURE 4.4: UNSUCCESSFUL ENRICHMENT FOR BRAIN CPG15 BY DIFFERENTIAL CENTRIFUGATION AND FRACTIONATION

a, Schematic of differential centrifugation steps and the corresponding fractions (P1 = pellet 1, S1 = soluble 1, etc). **b,** Centrifugation was successful at isolating different brain fractions, shown by the presence of GluR2 largely in the pellet fractions and Akt enriched in the soluble fractions. The lower panel shows actin is found in all of the fractions, and is a reflection of overall protein concentration. **c,** The same samples shown in **b** do not show a CPG15-positive band (*green*). A positive control of flag-tagged CPG15 purified from HEK cells shows CPG15 detection as well as flag (*red*) antibody staining. **d,** Schematic of cortex and hippocampus fractionation into hydrophobic and hydrophilic fraction. **e,** The fractionation was largely successful, shown by the enrichment of GluR2 (*green*) in the hydrophobic fractions and Akt (*red*) across all fractions. **f,** None of the same samples show a 12.5 kDa CPG15-positive band (*green*), except for the positive control of HEK purified CPG15. *(All samples in individual panels were run on the same gel and immunoblotted on the same membrane; lanes were reordered for presentation purposes.)*

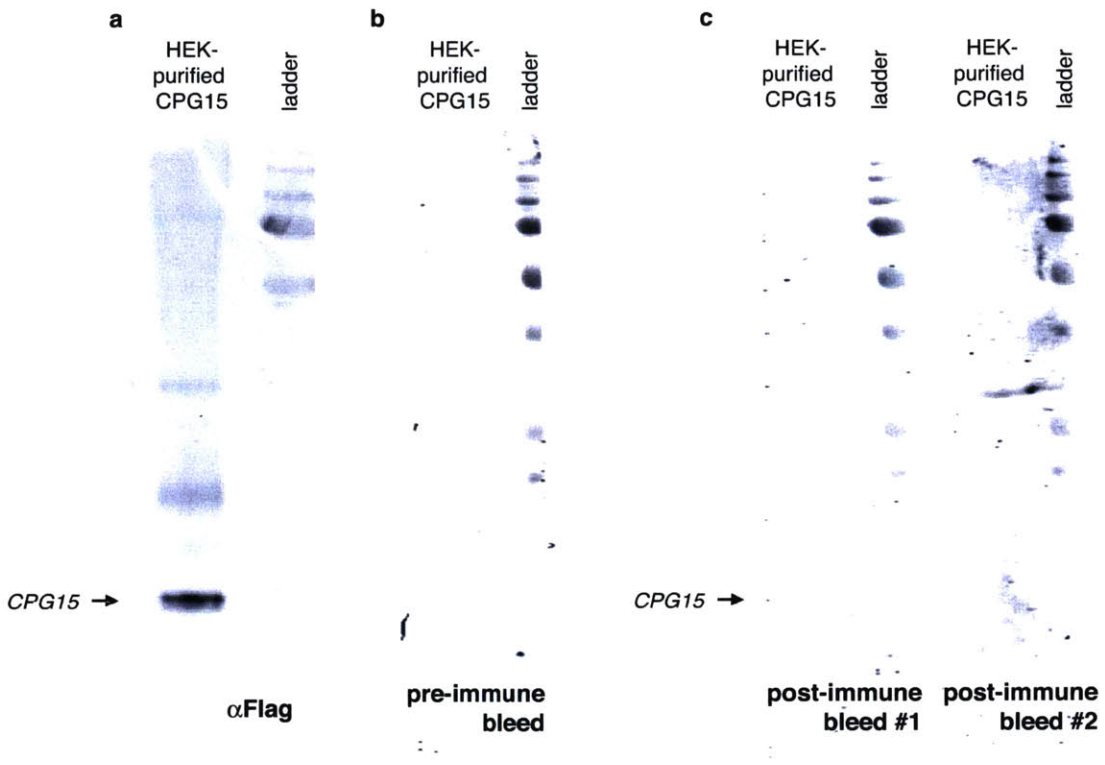

FIGURE 4.5: IMMUNIZING NEW ZEALAND BLACK/WHITE MICE DID NOT RESULT IN A CPG15 ANTIBODY

Multiple lanes of flag-CPG15 was run next to a protein ladder on the same gel; the blotted proteins were cut into strips containing one lane of CPG15 and half a lane of protein marker (in an effort to maximize the small amount of bleed provided) **a,** The flag antibody shows a 12.5 kDa CPG15 band. **b,** The bleed of the mouse prior to immunization does not show any reactivity to CPG15, as predicted. **c,** Following immunization, bleeds from either animal did not detect the presence of CPG15.

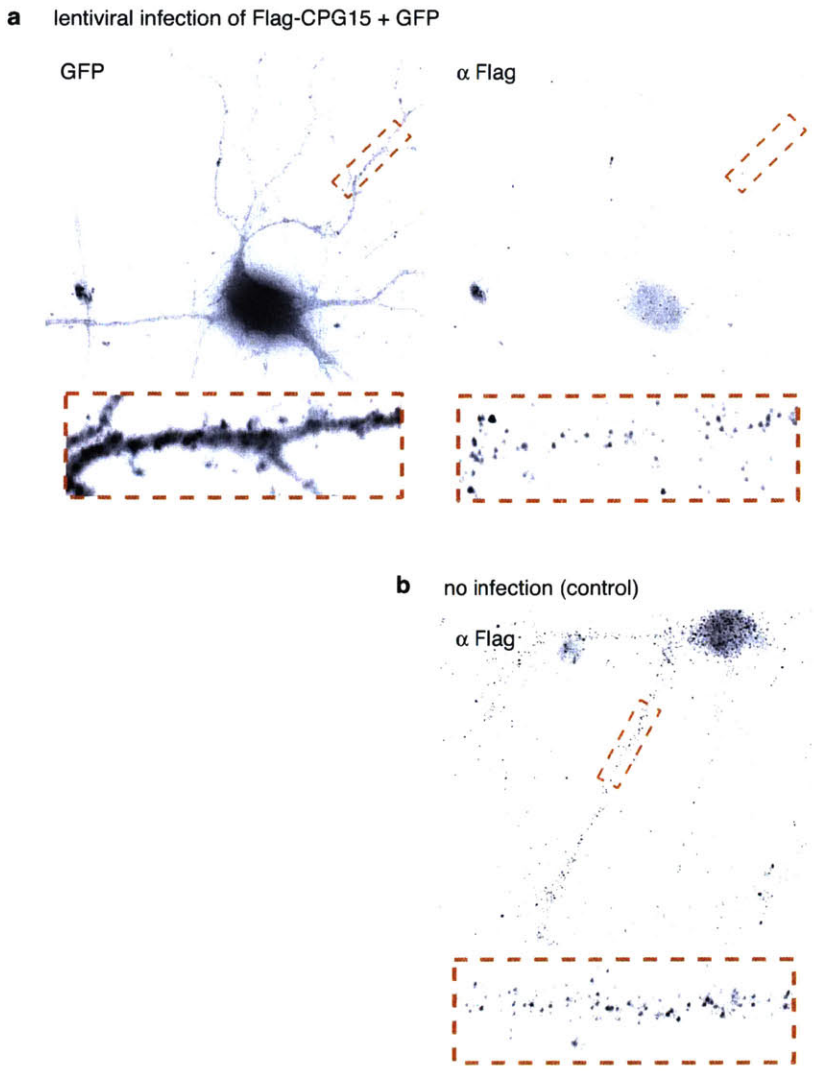

FIGURE 4.6: FLAG ANTIBODY HAS NON-SPECIFIC BINDING IN CULTURED NEURONS

a, Epifluorescence images of neurons (*orange boxes indicate zoomed dendrites. below*) infected to express Flag-CPG15 and GFP separated by an IRES cassette show GFP signal filling the neuron (*left*) and punctate Flag immunoreactivity – indirectly a measure of CPG15 expression signal (*right*). **b,** However, control coverslips of neurons not infected by any virus show non-specific Flag reactivity that appears punctate and is indistinguishable from injected neurons.

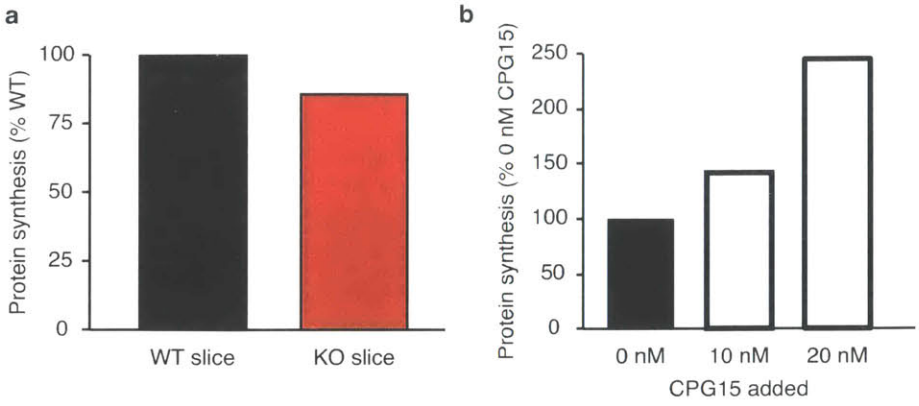

FIGURE 4.7: METABOLIC LABELING REVEALS REDUCTION OF BASAL PROTEIN SYNTHESIS IN CPG15 KO NEURONS

a, Differences in the levels of protein synthesis exist between WT and cpg15 KO genotypes in the ventral hippocampus. **b,** Purified CPG15 increases protein synthesis when added to cultured WT neurons in a dose-dependent fashion.

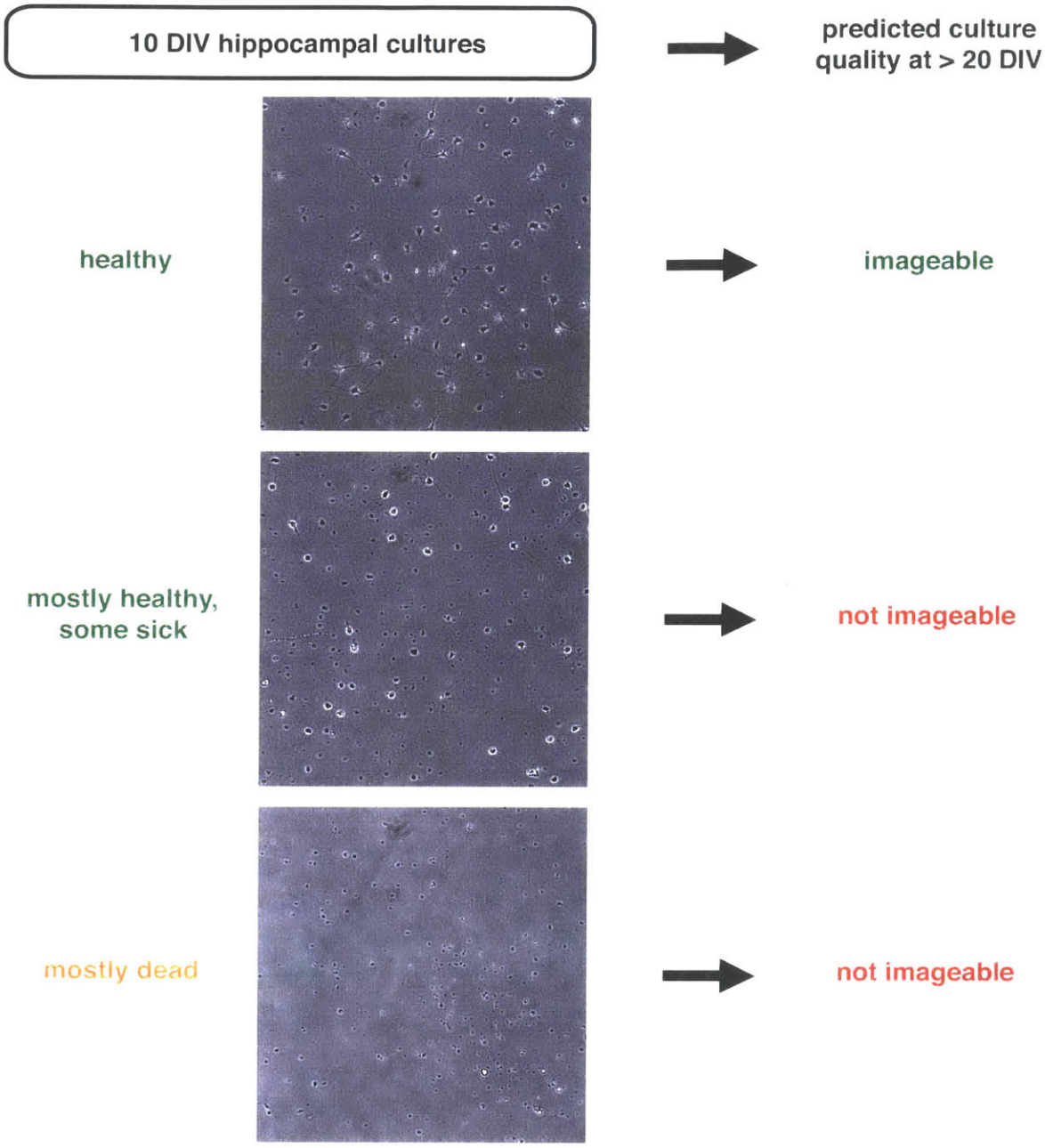

FIGURE 4.8: CULTURE HEALTH VARIES EARLY IN DEVELOPMENT

Representative images of 10 DIV hippocampal neuron cultures. A healthy culture that will usually result in healthy neurons past 20 DIV is characterized by the predominance of phase bright cell bodies with process outgrowth (*top*). An unhealthy culture will have some phase

bright cells, but a lot of debris from dead or dying cells (*middle*); this culture will not be imageable. A dead cell culture, with no evidence of adhered cells or processes (*bottom*).

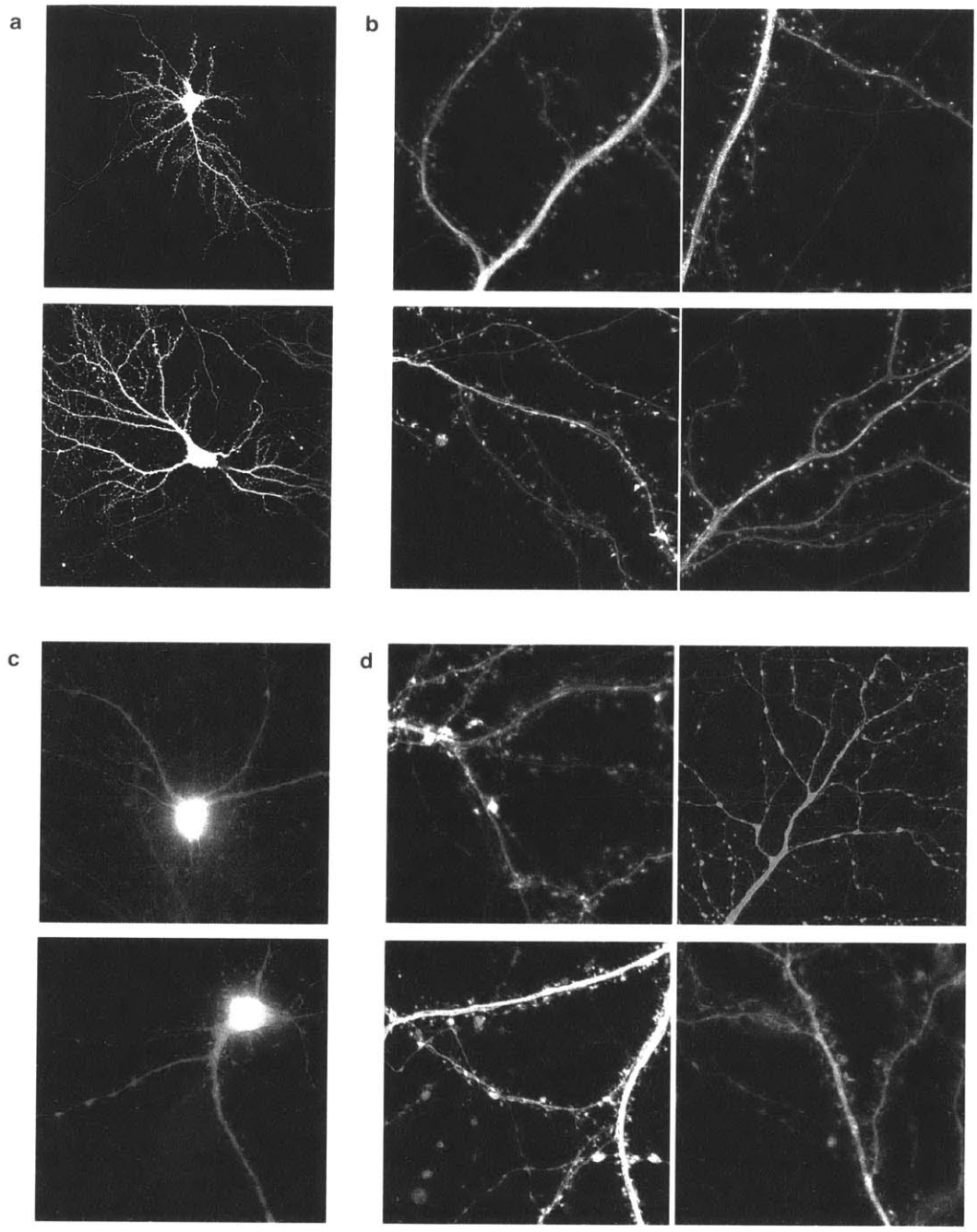

FIGURE 4.9: CULTURED NEURONS ARE OFTEN ALIVE BUT UNHEALTHY AT OLDER AGES.

a, Representative images of healthy neurons at 28 DIV cultured in serum. Dendrites are smooth and evenly labeled. **b,** Enlarged images of dendritic branches showing clear mushroom-type spines. **c,** Representative images of unhealthy neurons at 28 DIV. Dendrites are often dimmer than the cell body and are less arborized when compared to healthy cultures. **d,** Enlarged images of dendritic branches, which were not included in data presented in **Fig. 4.2**. Images excluded in quantiative analysis showed blebbing and uneven dendrites. Often, one section of a dendritic branch would have clearly defined spines, but a branch on the same dendritic arbor would be unhealthy or damaged.

CHAPTER V

Implications and future directions

The Impact of Fractalkine on Visual Cortical Development and Plasticity

While microglia are an exciting prospect in modulating experience dependent plasticity, there is more discussion than there is experimental findings. The goal of my research was to directly test the importance of microglia in experience-dependent plasticity using a manipulation that has been well characterized to drive weakening of specific neural circuits. One focus of my efforts was to investigate the relevance of the fractalkine signaling axis in normal visual cortical development. My results indicate that the visual system develops correctly in the absence of the fractalkine receptor, both at the thalamic level and the functional output of the primary visual cortex. This does not mean that fractalkine is not *involved* in the development of the visual system, just that it is not *required.* Microglia are exceptionally transcriptionally flexible, and so it is very possible that alternative mechanisms have engaged to compensate for the lack of fractalkine detection. Furthermore, although my experiments tracked visual acuity to the age limits of my experimental protocols, I cannot state that I have exhausted all developmental time points; it remains a possibility that there were delays in dLGN segregation prior to P28 or delays in early visual acuity development prior to P21. The former can be easily addressed by repeating the dLGN segregation assay, while the latter requires either an acute technique to assay acuity such as optical intrinsic imaging or a non-surgical behavioral assay that can be used on pre-weaned mice. Another way to address this issue could be to use EM: as my data reveals differences in the terminal size of thalamic input between juvenile WT and CX3CR1 KO, this experiment could be performed on mice after eye opening and before our acuity data was obtained (i.e. P10 – P20). These EM experiments are time- and labor-intensive and may not provide data that is worth the efforts required, especially without functional correlates such as VEPs or behavior.

My primary goal was to investigate the impact of CX3CR1 KO on visual cortical plasticity and the data consistently showed that the fractalkine receptor is not required for either SRP or OD plasticity following brief MD. The one impact that fractalkine receptor KO produced in my experience-dependent plasticity data is on pre-synaptic terminal size following brief MD where thalamocortical terminal size is unaffected by brief MD in the KO animals, although this deficit is not reflected in the VEP measurements. During normal

visual development, fractalkine signal may be acting in concert with other neuron-to-microglia signals, or – as addressed earlier – there may be compensatory mechanisms which were engaged following the loss of CX3CR1. Though a role of fractalkine in visual cortical experience-dependent plasticity cannot be ruled out via the data presented, the lack of data from numerous avenues of investigation (i.e. EM synaptic ultrastructure, microglia morphology, or *in vivo* electrophysiology) suggests that further experimentation on the fractalkine receptor in this kind of synaptic plasticity may yield limited returns.

If further pursuit of the fractalkine signaling axis is desired, a complementary way to probe its role in OD plasticity could utilize $CX3CL^{1105delta}$ animals (Kim et al., 2011). These mice constitutively express soluble fractalkine and would be predicted to show similar phenotypes to CX3CR1 KOs, as each synapse will lack the specific membrane tag that WT fractalkine confers.

Unanswered Questions in the Requirement for Microglia in OD Plasticity

There are still many avenues of investigation to determine whether or not microglia are required for synaptic plasticity in the fully developed brain. Prior to my work, there was general evidence to build on:

1. Many immune-related genes are required for proper synaptic plasticity and are implicated in disease states, and these genes are often expressed by microglia ((Corriveau et al., 1998), (Adelson et al., 2012), (Kettenmann et al., 2011))
2. Microglia are required for activity-dependent wiring of the dLGN during development as they phagocytose presynaptic components from less active synapses ((Stevens et al., 2007), (Schafer et al., 2012))
3. Microglia directly contact synapses, and changes in activity via sensory or pharmacological manipulation are reflected in changes of microglial behavior within the cortex ((Wake et al., 2009), (Schafer et al., 2012), (Tremblay et al., 2010))

The data described in Chapter 2 wherein WT microglia show increased lysosome activity following MD adds to the third category, and suggests that MD remains a potential paradigm for further study of microglia in experience-dependent plasticity.

In order to implicate microglia directly in the synaptic weakening that characterizes brief MD in juvenile mice, one would like to detect thalamocortical debris originating from the deprived eye within microglia. The ultimate goal would be to catch them in the act of phagocytosing thalamocortical axons subserving the deprived eye. I believe this is eminently possible based on combining methods discussed in Chapters 1 and 2: we have a protocol which specifically labels deprived thalamic axons (**Fig. 3.1**) which could be combined with a microglial label, via either endogenous expression (mouse lines expressing Iba1-GFP or CX3CR1 heterozygotes) or immunohistochemistry (post-fixation antibodies against Iba1). Confocal microscopy could be done on binocular layer 4 following brief MD of the microglia (Iba1), the microglial lysosomes (CD68), and the deprived eye axons (lentiviral GFP) with three-dimensional reconstruction to determine the level of overlap between the channels. As the spatial resolution of confocal microscopy is approximately 200 nm, it will be possible to conclude whether the GFP signal is contained within the microglia; in order to definitively conclude that the GFP is contained within lysosomes, STED microscopy can be used to reduce the size of the point-spread function to increase the imaging resolution by an order of magnitude (20 nm).

Also, the deprived eye axons and their relationship to microglia can be tracked dynamically with 2-photon microscopy and settings to perform dual-color imaging of GFP and DsRed (Kawano et al., 2008). A modified lentivirus constructed to express DsRed in place of GFP can be targeted to the deprived eye shell of dLGN in transgenic mice expressing labeled microglia (i.e. Iba1-GFP or CX3CR1 heterozygotes; though we have found that complete KO of CX3CR1 has little impact on plasticity, it should not be ignored that these microglia have half the CX3CR1 expression and this should be considered when interpreting the findings). I would advise daily imaging for 7 days following lid suture; although we would predict most microglia phagocytosis to occur between 1 and 3 days – concurrent with the VEP assessed deprived-eye depression time course – the timeline during which microglia might remove synapses, or clean up the synaptic debris, after deprivation is an interesting, unique question. As daily imaging will not allow tracking of individual microglia because they are so dynamic, time-lapse imaging at the peak of phagocytosis will provide a different view of microglial behavior after MD. Much like the basic structural remodeling following MD, how axons within superficial cortical layers behave in relation to

layer 4 will be important to define both in terms of interpreting the results and as a novel finding.

There are parallel quantitative EM studies that could be performed, either with specifically labeled deprived eye axons (it's worth noting that the method described in Chapter 3 only labels a small subset of axons), or all thalamocortical axons. Microglia and thalamocortical axons can be both labeled with immunogold and DAB, respectively, to determine if microglia contain labeled axons following deprivation. A technical concern would be to make sure fixation occurs before the phagocytosed axons are digested beyond detection: it is unclear how long it takes for vGluT2 to be digested within lysosomes to the degree where its antibody will no longer recognize it, whereas GFP is particularly resistant to lysosomal proteases (Katayama et al., 2008).

An additional obvious direction would be to repeat these MD experiments using mouse lines that lack microglia entirely. The PU.1$^{-/-}$ mouse line lacks microglia, but they also lack circulating monocytes and macrophages, which requires very controlled, pathogen-free environments making experimentation difficult ((Tondravi et al., 1997), (Grathwohl et al., 2009)). Similar KO lines lacking colony-stimulating factor 1 (CSF1) or its receptor, CSF1R, which are expressed by myeloid cells, also result in the lack of microglia ((Erblich et al., 2011), (Ginhoux et al., 2010)). However, the peripheral side effects of PU.1, CSF1, or CSF1R KO result in early-life lethality without bone marrow transplants ((Grathwohl et al., 2009), (Ginhoux et al., 2010)), and thus make juvenile and adult plasticity experiments on these mice infeasible.

Spatially and temporarily restricting deletion of microglia in mice is possible via other transgenic lines. CD11b-HSVTK mice express the herpes simplex virus thymidine kinase under control of the CD11b promoter, resulting in HSVTK expression solely in monocytic cells, which includes microglia (Heppner et al., 2005). When these animals are treated with ganciclovir, an antiviral drug, microglia are paralyzed. After one week of intraventricular treatment, half of the population of microglia are reduced, and following another week of treatment, they are depleted almost entirely (Grathwohl et al., 2009). A similar technique uses CD11b-DTR mice where myeloid cells express the diphtheria toxin receptor; injection of diphtheria induces microglia toxicity (Ueno et al., 2013). Using either of these two lines with highly specific injections that spare the periphery before electrophysiology studies begins may have promise. However, similar to the experimental

timelines discussed in Chapter 3, there may be insurmountable technical limitations related to age as no surgical interventions can begin before the animal is weaned (P18 at the absolute earliest). A better option may be administration of the CSF1R pharmacological inhibitor PLX3397 in mouse chow, which reduces the microglia population by half after only 3 days of treatment (Elmore et al., 2014). Complete microglial loss is possible after 21 days of treatment (Elmore et al., 2014), but that would require PLX3397 to be transferred by nursing dams which is currently undetermined, and microglia ablation would begin even before eye-opening and may disrupt dLGN segregation.

Recently, mouse lines have been developed wherein microglia contain *cre* expression that is either constitutively expressed ($Cx3cr1^{cre}$) or inducible with tamoxifen treatment ($Cx3cr1^{creER}$) (Yona et al., 2013). There is particular flexibility in the tamoxifen inducible line: similar to the animals described earlier, $Cx3cr1^{creER}$ mice could be crossed with lines that have floxed PU.1, CSF1, or CSF1R genes to have both temporal and cell-specific control of the KO of these genes to prevent lethality. Or, like the CD11b-DTR line, genes could be turned on if a flox-stop-flox cassette precedes them. This ability to control the onset of genetic manipulation is an important element to consider when studying experience-dependent plasticity in microglia. It has been well established that genetic knockouts that impact microglia often impact the formation of the visual circuit. While developmental wiring deficits are interesting in their own right, they complicate any plasticity that occurs in juvenile and adult animals, as they may be less the result of acute manipulation and more a consequence of an incorrectly wired visual system.

Remodeling Intracortical and Thalamocortical connectivity Following Experience-Dependent Plasticity

Ocular dominance shifts following MD result in clear, well-documented structural changes in afferents conveying information from the deprived eye, both in terms of excitatory synaptic strength and structural changes (reviewed in (Smith et al., 2009)). It has been shown that long periods of MD result in axonal remodeling of the thalamocortical inputs to the cortex ((LeVay et al., 1980), (Shatz and Stryker, 1978)). It is also clear that OD shifts measured electrophysiologically saturate after a brief 3 day period of MD (Frenkel and

Bear, 2004); our studies of brief MD on anatomical remodeling of thalamocortical axons from the deprived eye is currently inconclusive (see Chapter 3), leaving the locus of these rapid changes still unclear.

In adult animals, OD shifts following MD are qualitatively different than that observed in juvenile animals: it is driven solely by potentiation of responses to the non-deprived eye. MD in adult mice drives formation of new dendritic spines (Hofer et al., 2009), but complementary presynaptic input plasticity remains undefined. The source of this reorganization is likely to be cortical, as the dLGN afferents lack reorganization (Eysel, 1982). Studies in cats and mice following functional plasticity after retinal lesion have repeatedly shown that cortical reorganization is driven by strengthening of existing synapses and axonal sprouting of horizontal intracortical afferents ((Darian-Smith and Gilbert, 1994), (Obata et al., 1999), (Calford et al., 2003)). In the data presented in Chapter 2, 3 days of MD yields significant amounts of electrophysiological open-eye potentiation. This same period of MD on age-matched animals drives increased synapse density of intracortical synapses, and, as that is the only increase in synaptic drive found by quantitative EM, may be the source the non-deprived eye potentiation of VEPs. These results raise the possibility that rapid open-eye potentiation may initially be a product of horizontal axon potentiation and elaboration. Long periods of MD might later induce thalamocortical input strengthening, complementary to that observed in the thalamocortical input weakening driving deprived-eye depression.

We can test the role of thalamocortical inputs on open eye potentiation using an experimental design that eliminates intracortical activity while preserving a measurable thalamocortical response: a cocktail of muscimol, a $GABA_A$ receptor agonist that silences spiking of cortical neurons with strong inhibition, and SCH5091, a $GABA_B$ receptor antagonist that preserves synaptic transmission by preventing muscimol-induced nonspecific activation of presynaptic $GABA_B$ receptors ((Liu et al., 2007), (Khibnik et al., 2010)). This muscimol+ cocktail leaves feed-forward monosynaptic responses intact, and has been used to demonstrate that OD shifts resulting from brief MD can be expressed purely through modification of thalamocortical synaptic transmission (Khibnik et al., 2010).

OD shifts resulting from open-eye potentiation after extended lengths (7 days) of MD in juvenile and adult animals can be determined in the absence of intracortical transmission after muscimol+ infusion. This experiment can conclusively address whether

the increased drive from stimulating the non-deprived eye occurs similarly to the increased drive from the spared retina following lesion, namely intracortical potentation. This result will have interesting implications on our conceptions of what molecular mechanisms drive critical periods. As it has already been shown that deprived-eye depression is largely restricted to these critical periods, if my prediction is correct and most open-eye potentiation results from horizontal connectivity, it could point specifically to fast plasticity of thalamocortical input being lost in adulthood.

Furthermore, expression of stimulus selectivity following 7 days of SRP in adult animals is abolished after infusion of muscimol+ (Cooke and Bear, 2014), pointing to involvement of intracortical plasticity in the expression, if not induction, of this form of visual potentiation. Our SRP results show a very different time course of SRP induction in juvenile animals than that seen when these very same animals are adults. There are two obvious mechanistic explanations for this age-dependent change: 1) the same intracortical circuits are potentiated during the critical period which are potentiated in adulthood but this potentiation occurs at a much faster rate, or 2) a unique rapid mechanism exists during the critical period which is lost in adulthood. For the second possibility, this mechanism may be inherent to thalamocortical axons, which can be easily tested during blockage of intracortical connections. After only one day of SRP in ~P28 animals, the ratio of VEP responses from the trained stimuli to the novel stimuli can be measured before and after local infusion of muscimol+. Unlike during adult SRP, I would hypothesize that the stimulus-selective potentiation will still exist in only thalamocortical VEPs. The testing of adult SRP shown by Cooke et al., only measured stimulus-selective *expression* and not stimulus-selective *induction* in the absence of intracortical transmission (Cooke and Bear, 2014). This raises the possibility that the initial few days of training that drives weak SRP engages thalamocortical input that is consolidated in intracortical inputs over the week of training. In parallel to the one-day SRP experiment, the impact of muscimol+ infusion after one day of training in the adult – which induces significant SRP, though much less than after a full week of training – can be measured to determine if the initial stages of adult SRP induction engages thalamocortical plasticity.

The muscimol+ cocktail can also be used to further clarify our microglia data. First, we can locally infuse this cocktail after 3 days of MD in CX3CR1 KO animals to measure whether our OD shift – which is qualitatively similar to WT animals as measured by VEPs –

is driven solely or partially by the intracortical circuit plasticity that we detected with quantitative EM. Also, in our hands, WT animals with 3 days of lid suture express open-eye potentiation of VEPs. Because this treatment universally lowers VEP magnitudes ((Khibnik et al., 2010), (Cooke and Bear, 2014)), the OD shift cannot be broken down into deprived-eye depression or open-eye potentiation, as they will both be reduced; only the contralateral to ipsilateral ratio is informative, but I would predict less of a shift in the absence of intracortical transmission.

Concluding Remarks

Ocular dominance plasticity has served as a sensitive assay for determining the consequences of visual deprivation on the synapses of the visual cortex. Functional shifts in ocular dominance can be driven by temporarily closing the eyelid of one eye early in development in mice and other species, which models the human condition of amblyopia. Amblyopia in humans arises from a functional mismatch between the two eyes early in life due to a variety of perturbations (such as cataracts, astigmatism, or strabismus), and leads to visual cortex re-wiring that favors processing of inputs subserving the non-amblyopic, dominant eye. Even when the affected eye is repaired to perfect condition, the connectivity between the eye and visual cortex cannot be readily restored through normal binocular vision if performed at ages beyond childhood. As there is strong phylogenetic conservation of mechanisms across mammalian visual circuits, findings in the mouse model of amblyopia – i.e. MD – may lead to the development of therapeutic interventions. Furthermore, the ways in which primary visual circuits remodel in response to environmental changes can be extrapolated to general plasticity mechanisms that underlie diverse forms of learning.

REFERENCES

Abraham, W.C., and Williams, J.M. (2003). Properties and mechanisms of LTP maintenance. Neuroscientist *9*, 463-474.

Adelson, J.D., Barreto, G.E., Xu, L., Kim, T., Brott, B.K., Ouyang, Y.B., Naserke, T., Djurisic, M., Xiong, X., Shatz, C.J., *et al.* (2012). Neuroprotection from stroke in the absence of MHCI or PirB. Neuron *73*, 1100-1107.

Ahmadian, G., Ju, W., Liu, L., Wyszynski, M., Lee, S.H., Dunah, A.W., Taghibiglou, C., Wang, Y., Lu, J., Wong, T.P., *et al.* (2004). Tyrosine phosphorylation of GluR2 is required for insulin-stimulated AMPA receptor endocytosis and LTD. The EMBO journal *23*, 1040-1050.

Ajami, B., Bennett, J.L., Krieger, C., Tetzlaff, W., and Rossi, F.M. (2007). Local self-renewal can sustain CNS microglia maintenance and function throughout adult life. Nature neuroscience *10*, 1538-1543.

Akbik, F.V., Bhagat, S.M., Patel, P.R., Cafferty, W.B., and Strittmatter, S.M. (2013). Anatomical plasticity of adult brain is titrated by Nogo Receptor 1. Neuron *77*, 859-866.

Allen, N.J., and Barres, B.A. (2005). Signaling between glia and neurons: focus on synaptic plasticity. Current opinion in neurobiology *15*, 542-548.

Alliot, F., Godin, I., and Pessac, B. (1999). Microglia derive from progenitors, originating from the yolk sac, and which proliferate in the brain. Brain Res Dev Brain Res *117*, 145-152.

Antonini, A., Fagiolini, M., and Stryker, M.P. (1999). Anatomical correlates of functional plasticity in mouse visual cortex. J Neurosci *19*, 4388-4406.

Antonini, A., and Stryker, M.P. (1993). Development of individual geniculocortical arbors in cat striate cortex and effects of binocular impulse blockade. J Neurosci *13*, 3549-3573.

Antonini, A., and Stryker, M.P. (1996). Plasticity of geniculocortical afferents following brief or prolonged monocular occlusion in the cat. J Comp Neurol *369*, 64-82.

Araque, A., Sanzgiri, R.P., Parpura, V., and Haydon, P.G. (1999). Astrocyte-induced modulation of synaptic transmission. Can J Physiol Pharmacol *77*, 699-706.

Arellano, J.I., Benavides-Piccione, R., Defelipe, J., and Yuste, R. (2007). Ultrastructure of dendritic spines: correlation between synaptic and spine morphologies. Front Neurosci *1*, 131-143.

Banker, G., and Goslin, K. (1991). Culturing nerve cells (Cambridge, Mass.: MIT Press).

Bartol, T.M., Bromer, C., Kinney, J., Chirillo, M.A., Bourne, J.N., Harris, K.M., and Sejnowski, T.J. (2015). Nanoconnectomic upper bound on the variability of synaptic plasticity. eLife *4*.

Bear, M.F. (1996). NMDA-receptor-dependent synaptic plasticity in the visual cortex. Prog Brain Res *108*, 205-218.

Bear, M.F., Huber, K.M., and Warren, S.T. (2004). The mGluR theory of fragile X mental retardation. Trends in neurosciences *27*, 370-377.

Bear, M.F., Kleinschmidt, A., Gu, Q.A., and Singer, W. (1990). Disruption of experience-dependent synaptic modifications in striate cortex by infusion of an NMDA receptor antagonist. J Neurosci *10*, 909-925.

Beaulieu, C., and Colonnier, M. (1985). A laminar analysis of the number of round-asymmetrical and flat-symmetrical synapses on spines, dendritic trunks, and cell bodies in area 17 of the cat. J Comp Neurol *231*, 180-189.

Benes, F.M., and Lange, N. (2001). Two-dimensional versus three-dimensional cell counting: a practical perspective. Trends in neurosciences *24*, 11-17.

Berbel, P., and Innocenti, G.M. (1988). The development of the corpus callosum in cats: a light- and electron-microscopic study. J Comp Neurol *276*, 132-156.

Biber, K., Neumann, H., Inoue, K., and Boddeke, H.W. (2007). Neuronal 'On' and 'Off' signals control microglia. Trends in neurosciences *30*, 596-602.

Bjartmar, L., Huberman, A.D., Ullian, E.M., Renteria, R.C., Liu, X., Xu, W., Prezioso, J., Susman, M.W., Stellwagen, D., Stokes, C.C., *et al.* (2006). Neuronal pentraxins mediate synaptic refinement in the developing visual system. J Neurosci *26*, 6269-6281.

Bottenstein, J., Hayashi, I., Hutchings, S., Masui, H., Mather, J., McClure, D.B., Ohasa, S., Rizzino, A., Sato, G., Serrero, G., *et al.* (1979). The growth of cells in serum-free hormone-supplemented media. Methods Enzymol *58*, 94-109.

Boulanger, L.M. (2009). Immune proteins in brain development and synaptic plasticity. Neuron *64*, 93-109.

Bradshaw, K.D., Emptage, N.J., and Bliss, T.V. (2003). A role for dendritic protein synthesis in hippocampal late LTP. The European journal of neuroscience *18*, 3150-3152.

Braitenberg, V., Schüz, A., and Braitenberg, V. (1998). Cortex : statistics and geometry of neuronal connectivity, 2nd thoroughly rev. edn (Berlin ; New York: Springer).

Brewer, G.J. (1995). Serum-free B27/neurobasal medium supports differentiated growth of neurons from the striatum, substantia nigra, septum, cerebral cortex, cerebellum, and dentate gyrus. Journal of neuroscience research *42*, 674-683.

Brewer, G.J. (1997). Isolation and culture of adult rat hippocampal neurons. J Neurosci Methods *71*, 143-155.

Brewer, G.J., Torricelli, J.R., Evege, E.K., and Price, P.J. (1993). Optimized survival of hippocampal neurons in B27-supplemented Neurobasal, a new serum-free medium combination. Journal of neuroscience research *35*, 567-576.

Calford, M.B., Wright, L.L., Metha, A.B., and Taglianetti, V. (2003). Topographic plasticity in primary visual cortex is mediated by local corticocortical connections. J Neurosci *23*, 6434-6442.

Cang, J., Kalatsky, V.A., Lowel, S., and Stryker, M.P. (2005). Optical imaging of the intrinsic signal as a measure of cortical plasticity in the mouse. Visual neuroscience *22*, 685-691.

Cantallops, I., Haas, K., and Cline, H.T. (2000). Postsynaptic CPG15 promotes synaptic maturation and presynaptic axon arbor elaboration in vivo. Nature neuroscience *3*, 1004-1011.

Chapman, G.A., Moores, K., Harrison, D., Campbell, C.A., Stewart, B.R., and Strijbos, P.J. (2000). Fractalkine cleavage from neuronal membranes represents an acute event in the inflammatory response to excitotoxic brain damage. J Neurosci *20*, RC87.

Chen, C., and Regehr, W.G. (2000). Developmental remodeling of the retinogeniculate synapse. Neuron *28*, 955-966.

Chen, Y., Stevens, B., Chang, J., Milbrandt, J., Barres, B.A., and Hell, J.W. (2008). NS21: re-defined and modified supplement B27 for neuronal cultures. J Neurosci Methods *171*, 239-247.

Chow, D.K., Groszer, M., Pribadi, M., Machniki, M., Carmichael, S.T., Liu, X., and Trachtenberg, J.T. (2009). Laminar and compartmental regulation of dendritic growth in mature cortex. Nature neuroscience *12*, 116-118.

Christie, A., and Butler, M. (1994). Glutamine-Based Dipeptides Are Utilized in Mammalian-Cell Culture by Extracellular Hydrolysis Catalyzed by a Specific Peptidase. Journal of Biotechnology *37*, 277-290.

Chu, Y., Jin, X., Parada, I., Pesic, A., Stevens, B., Barres, B., and Prince, D.A. (2010). Enhanced synaptic connectivity and epilepsy in C1q knockout mice. Proceedings of the National Academy of Sciences of the United States of America *107*, 7975-7980.

Clark, A.K., Yip, P.K., Grist, J., Gentry, C., Staniland, A.A., Marchand, F., Dehvari, M., Wotherspoon, G., Winter, J., Ullah, J., *et al.* (2007). Inhibition of spinal microglial cathepsin S for the reversal of neuropathic pain. Proceedings of the National Academy of Sciences of the United States of America *104*, 10655-10660.

Coleman, J.E., Law, K., and Bear, M.F. (2009). Anatomical origins of ocular dominance in mouse primary visual cortex. Neuroscience *161*, 561-571.

Coleman, J.E., Nahmani, M., Gavornik, J.P., Haslinger, R., Heynen, A.J., Erisir, A., and Bear, M.F. (2010). Rapid structural remodeling of thalamocortical synapses parallels experience-dependent functional plasticity in mouse primary visual cortex. J Neurosci *30*, 9670-9682.

Colonnier, M. (1968). Synaptic patterns on different cell types in the different laminae of the cat visual cortex. An electron microscope study. Brain research *9*, 268-287.

Combadiere, C., Salzwedel, K., Smith, E.D., Tiffany, H.L., Berger, E.A., and Murphy, P.M. (1998). Identification of CX3CR1. A chemotactic receptor for the human CX3C chemokine fractalkine and a fusion coreceptor for HIV-1. The Journal of biological chemistry *273*, 23799-23804.

Cooke, S.F., and Bear, M.F. (2010). Visual experience induces long-term potentiation in the primary visual cortex. J Neurosci *30*, 16304-16313.

Cooke, S.F., and Bear, M.F. (2014). How the mechanisms of long-term synaptic potentiation and depression serve experience-dependent plasticity in primary visual cortex. Philos Trans R Soc Lond B Biol Sci *369*, 20130284.

Corriveau, R.A., Huh, G.S., and Shatz, C.J. (1998). Regulation of class I MHC gene expression in the developing and mature CNS by neural activity. Neuron *21*, 505-520.

Corriveau, R.A., Shatz, C.J., and Nedivi, E. (1999). Dynamic regulation of cpg15 during activity-dependent synaptic development in the mammalian visual system. J Neurosci *19*, 7999-8008.

Costa-Mattioli, M., Gobert, D., Harding, H., Herdy, B., Azzi, M., Bruno, M., Bidinosti, M., Ben Mamou, C., Marcinkiewicz, E., Yoshida, M., *et al.* (2005). Translational control of hippocampal synaptic plasticity and memory by the eIF2alpha kinase GCN2. Nature *436*, 1166-1173.

Coull, J.A., Beggs, S., Boudreau, D., Boivin, D., Tsuda, M., Inoue, K., Gravel, C., Salter, M.W., and De Koninck, Y. (2005). BDNF from microglia causes the shift in neuronal anion gradient underlying neuropathic pain. Nature *438*, 1017-1021.

Craig, A.M., Graf, E.R., and Linhoff, M.W. (2006). How to build a central synapse: clues from cell culture. Trends in neurosciences *29*, 8-20.

Crozier, R.A., Wang, Y., Liu, C.H., and Bear, M.F. (2007). Deprivation-induced synaptic depression by distinct mechanisms in different layers of mouse visual cortex. Proceedings of the National Academy of Sciences of the United States of America *104*, 1383-1388.

Cullheim, S., and Thams, S. (2007). The microglial networks of the brain and their role in neuronal network plasticity after lesion. Brain research reviews *55*, 89-96.

Danbolt, N.C. (2001). Glutamate uptake. Progress in neurobiology *65*, 1-105.

Darian-Smith, C., and Gilbert, C.D. (1994). Axonal sprouting accompanies functional reorganization in adult cat striate cortex. Nature *368*, 737-740.

Davalos, D., Grutzendler, J., Yang, G., Kim, J.V., Zuo, Y., Jung, S., Littman, D.R., Dustin, M.L., and Gan, W.B. (2005). ATP mediates rapid microglial response to local brain injury in vivo. Nature neuroscience *8*, 752-758.

Davis, H.P., and Squire, L.R. (1984). Protein synthesis and memory: a review. Psychol Bull *96*, 518-559.

Daw, N., Rao, Y., Wang, X.F., Fischer, Q., and Yang, Y. (2004). LTP and LTD vary with layer in rodent visual cortex. Vision Res *44*, 3377-3380.

De Paola, V., Arber, S., and Caroni, P. (2003). AMPA receptors regulate dynamic equilibrium of presynaptic terminals in mature hippocampal networks. Nature neuroscience *6*, 491-500.

De Paola, V., Holtmaat, A., Knott, G., Song, S., Wilbrecht, L., Caroni, P., and Svoboda, K. (2006). Cell type-specific structural plasticity of axonal branches and boutons in the adult neocortex. Neuron *49*, 861-875.

Declerck, P.J., Carmeliet, P., Verstreken, M., De Cock, F., and Collen, D. (1995). Generation of monoclonal antibodies against autologous proteins in gene-inactivated mice. The Journal of biological chemistry *270*, 8397-8400.

DeFelipe, J., Marco, P., Busturia, I., and Merchan-Perez, A. (1999). Estimation of the number of synapses in the cerebral cortex: methodological considerations. Cerebral cortex *9*, 722-732.

Deiva, K., Geeraerts, T., Salim, H., Leclerc, P., Hery, C., Hugel, B., Freyssinet, J.M., and Tardieu, M. (2004). Fractalkine reduces N-methyl-d-aspartate-induced calcium flux and apoptosis in human neurons through extracellular signal-regulated kinase activation. The European journal of neuroscience *20*, 3222-3232.

Denk, W., Strickler, J.H., and Webb, W.W. (1990). Two-photon laser scanning fluorescence microscopy. Science *248*, 73-76.

Dhande, O.S., Hua, E.W., Guh, E., Yeh, J., Bhatt, S., Zhang, Y., Ruthazer, E.S., Feller, M.B., and Crair, M.C. (2011). Development of single retinofugal axon arbors in normal and beta2 knock-out mice. J Neurosci *31*, 3384-3399.

Diamond, M.C., Lindner, B., Johnson, R., Bennett, E.L., and Rosenzweig, M.R. (1975). Differences in occipital cortical synapses from environmentally enriched, impoverished, and standard colony rats. Journal of neuroscience research *1*, 109-119.

Dobersen, M.J., Hammer, J.A., Noronha, A.B., MacIntosh, T.D., Trapp, B.D., Brady, R.O., and Quarles, R.H. (1985). Generation and characterization of mouse monoclonal antibodies to the myelin-associated glycoprotein (MAG). Neurochem Res *10*, 499-513.

Drager, U.C. (1974). Autoradiography of tritiated proline and fucose transported transneuronally from the eye to the visual cortex in pigmented and albino mice. Brain research *82*, 284-292.

Drager, U.C. (1975). Receptive fields of single cells and topography in mouse visual cortex. J Comp Neurol *160*, 269-290.

Dudek, S.M., and Bear, M.F. (1992). Homosynaptic long-term depression in area CA1 of hippocampus and effects of N-methyl-D-aspartate receptor blockade. Proceedings of the National Academy of Sciences of the United States of America *89*, 4363-4367.

Dunaevsky, A., Tashiro, A., Majewska, A., Mason, C., and Yuste, R. (1999). Developmental regulation of spine motility in the mammalian central nervous system. Proceedings of the National Academy of Sciences of the United States of America *96*, 13438-13443.

Elkabes, S., DiCicco-Bloom, E.M., and Black, I.B. (1996). Brain microglia/macrophages express neurotrophins that selectively regulate microglial proliferation and function. J Neurosci *16*, 2508-2521.

Elmore, M.R., Najafi, A.R., Koike, M.A., Dagher, N.N., Spangenberg, E.E., Rice, R.A., Kitazawa, M., Matusow, B., Nguyen, H., West, B.L., *et al.* (2014). Colony-stimulating factor 1 receptor signaling is necessary for microglia viability, unmasking a microglia progenitor cell in the adult brain. Neuron *82*, 380-397.

Engert, F., and Bonhoeffer, T. (1999). Dendritic spine changes associated with hippocampal long-term synaptic plasticity. Nature *399*, 66-70.

Erblich, B., Zhu, L., Etgen, A.M., Dobrenis, K., and Pollard, J.W. (2011). Absence of colony stimulation factor-1 receptor results in loss of microglia, disrupted brain development and olfactory deficits. PloS one *6*, e26317.

Erisir, A., and Dreusicke, M. (2005). Quantitative morphology and postsynaptic targets of thalamocortical axons in critical period and adult ferret visual cortex. J Comp Neurol *485*, 11-31.

Erisir, A., and Harris, J.L. (2003). Decline of the critical period of visual plasticity is concurrent with the reduction of NR2B subunit of the synaptic NMDA receptor in layer 4. J Neurosci *23*, 5208-5218.

Eysel, U.T. (1982). Functional reconnections without new axonal growth in a partially denervated visual relay nucleus. Nature *299*, 442-444.

Fagiolini, M., Pizzorusso, T., Berardi, N., Domenici, L., and Maffei, L. (1994). Functional postnatal development of the rat primary visual cortex and the role of visual experience: dark rearing and monocular deprivation. Vision Res *34*, 709-720.

Fifkova, E., and Morales, M. (1992). Actin matrix of dendritic spines, synaptic plasticity, and long-term potentiation. International review of cytology *139*, 267-307.

Fletcher, T.L., and Banker, G.A. (1989). The establishment of polarity by hippocampal neurons: the relationship between the stage of a cell's development in situ and its subsequent development in culture. Dev Biol *136*, 446-454.

Flexner, J.B., Flexner, L.B., and Stellar, E. (1963). Memory in mice as affected by intracerebral puromycin. Science *141*, 57-59.

Florence, S.L., Taub, H.B., and Kaas, J.H. (1998). Large-scale sprouting of cortical connections after peripheral injury in adult macaque monkeys. Science *282*, 1117-1121.

Frade, J.M., and Barde, Y.A. (1998). Microglia-derived nerve growth factor causes cell death in the developing retina. Neuron *20*, 35-41.

Frankland, P.W., O'Brien, C., Ohno, M., Kirkwood, A., and Silva, A.J. (2001). Alpha-CaMKII-dependent plasticity in the cortex is required for permanent memory. Nature *411*, 309-313.

Frenkel, M.Y., and Bear, M.F. (2004). How monocular deprivation shifts ocular dominance in visual cortex of young mice. Neuron *44*, 917-923.

Frenkel, M.Y., Sawtell, N.B., Diogo, A.C., Yoon, B., Neve, R.L., and Bear, M.F. (2006). Instructive effect of visual experience in mouse visual cortex. Neuron *51*, 339-349.

Frey, U., Krug, M., Reymann, K.G., and Matthies, H. (1988). Anisomycin, an inhibitor of protein synthesis, blocks late phases of LTP phenomena in the hippocampal CA1 region in vitro. Brain research *452*, 57-65.

Friedlander, M.J., Martin, K.A., and Wassenhove-McCarthy, D. (1991). Effects of monocular visual deprivation on geniculocortical innervation of area 18 in cat. J Neurosci *11*, 3268-3288.

Fujino, T., Leslie, J.H., Eavri, R., Chen, J.L., Lin, W.C., Flanders, G.H., Borok, E., Horvath, T.L., and Nedivi, E. (2011). CPG15 regulates synapse stability in the developing and adult brain. Genes Dev *25*, 2674-2685.

Galimberti, I., Gogolla, N., Alberi, S., Santos, A.F., Muller, D., and Caroni, P. (2006). Long-term rearrangements of hippocampal mossy fiber terminal connectivity in the adult regulated by experience. Neuron *50*, 749-763.

Garton, K.J., Gough, P.J., Blobel, C.P., Murphy, G., Greaves, D.R., Dempsey, P.J., and Raines, E.W. (2001). Tumor necrosis factor-alpha-converting enzyme (ADAM17) mediates the cleavage and shedding of fractalkine (CX3CL1). The Journal of biological chemistry *276*, 37993-38001.

Giese, K.P., Fedorov, N.B., Filipkowski, R.K., and Silva, A.J. (1998). Autophosphorylation at Thr286 of the alpha calcium-calmodulin kinase II in LTP and learning. Science *279*, 870-873.

Ginhoux, F., Greter, M., Leboeuf, M., Nandi, S., See, P., Gokhan, S., Mehler, M.F., Conway, S.J., Ng, L.G., Stanley, E.R., *et al.* (2010). Fate mapping analysis reveals that adult microglia derive from primitive macrophages. Science *330*, 841-845.

Gordon, J.A., and Stryker, M.P. (1996). Experience-dependent plasticity of binocular responses in the primary visual cortex of the mouse. J Neurosci *16*, 3274-3286.

Grathwohl, S.A., Kalin, R.E., Bolmont, T., Prokop, S., Winkelmann, G., Kaeser, S.A., Odenthal, J., Radde, R., Eldh, T., Gandy, S., *et al.* (2009). Formation and maintenance of Alzheimer's disease beta-amyloid plaques in the absence of microglia. Nature neuroscience *12*, 1361-1363.

Greenough, W.T., Volkmar, F.R., and Juraska, J.M. (1973). Effects of rearing complexity on dendritic branching in frontolateral and temporal cortex of the rat. Exp Neurol *41*, 371-378.

Grinberg, Y.Y., Milton, J.G., and Kraig, R.P. (2011). Spreading depression sends microglia on Levy flights. PloS one *6*, e19294.

Grutzendler, J., Kasthuri, N., and Gan, W.B. (2002). Long-term dendritic spine stability in the adult cortex. Nature *420*, 812-816.

Hanisch, U.K. (2002). Microglia as a source and target of cytokines. Glia *40*, 140-155.

Hanover, J.L., Huang, Z.J., Tonegawa, S., and Stryker, M.P. (1999). Brain-derived neurotrophic factor overexpression induces precocious critical period in mouse visual cortex. Journal of Neuroscience *19*, art. no.-RC40.

Harris, K.M. (1999). Structure, development, and plasticity of dendritic spines. Current opinion in neurobiology *9*, 343-348.

Harris, K.M., and Kater, S.B. (1994). Dendritic spines: cellular specializations imparting both stability and flexibility to synaptic function. Annu Rev Neurosci *17*, 341-371.

Harris, K.M., and Stevens, J.K. (1989). Dendritic spines of CA 1 pyramidal cells in the rat hippocampus: serial electron microscopy with reference to their biophysical characteristics. J Neurosci *9*, 2982-2997.

Harris, K.M., and Sultan, P. (1995). Variation in the number, location and size of synaptic vesicles provides an anatomical basis for the nonuniform probability of release at hippocampal CA1 synapses. Neuropharmacology *34*, 1387-1395.

Harrison, J.K., Jiang, Y., Chen, S., Xia, Y., Maciejewski, D., McNamara, R.K., Streit, W.J., Salafranca, M.N., Adhikari, S., Thompson, D.A., *et al.* (1998). Role for neuronally derived fractalkine in mediating interactions between neurons and CX3CR1-expressing microglia. Proceedings of the National Academy of Sciences of the United States of America *95*, 10896-10901.

Harrison, R.G. (1910). The development of peripheral nerve fibers in altered surroundings. Arch Entwicklung Org *30*, 15-33.

Harwell, C., Burbach, B., Svoboda, K., and Nedivi, E. (2005). Regulation of cpg15 expression during single whisker experience in the barrel cortex of adult mice. J Neurobiol *65*, 85-96.

Haskell, C.A., Cleary, M.D., and Charo, I.F. (1999). Molecular uncoupling of fractalkine-mediated cell adhesion and signal transduction. Rapid flow arrest of CX3CR1-expressing cells is independent of G-protein activation. The Journal of biological chemistry *274*, 10053-10058.

Hayashi, Y., Ishibashi, H., Hashimoto, K., and Nakanishi, H. (2006). Potentiation of the NMDA receptor-mediated responses through the activation of the glycine site by microglia secreting soluble factors. Glia *53*, 660-668.

Haynes, S.E., Hollopeter, G., Yang, G., Kurpius, D., Dailey, M.E., Gan, W.B., and Julius, D. (2006). The P2Y12 receptor regulates microglial activation by extracellular nucleotides. Nature neuroscience *9*, 1512-1519.

He, C.X., and Portera-Cailliau, C. (2013). The trouble with spines in fragile X syndrome: density, maturity and plasticity. Neuroscience *251*, 120-128.

Hebb, D.O. (1949). The organization of behavior; a neuropsychological theory (New York,: Wiley).

Heppner, F.L., Greter, M., Marino, D., Falsig, J., Raivich, G., Hovelmeyer, N., Waisman, A., Rulicke, T., Prinz, M., Priller, J., *et al.* (2005). Experimental autoimmune encephalomyelitis repressed by microglial paralysis. Nature medicine *11*, 146-152.

Herculano-Houzel, S., Collins, C.E., Wong, P., and Kaas, J.H. (2007). Cellular scaling rules for primate brains. Proceedings of the National Academy of Sciences of the United States of America *104*, 3562-3567.

Heynen, A.J., Yoon, B.J., Liu, C.H., Chung, H.J., Huganir, R.L., and Bear, M.F. (2003). Molecular mechanism for loss of visual cortical responsiveness following brief monocular deprivation. Nature neuroscience *6*, 854-862.

Hofer, S.B., Mrsic-Flogel, T.D., Bonhoeffer, T., and Hubener, M. (2006a). Lifelong learning: ocular dominance plasticity in mouse visual cortex. Current opinion in neurobiology *16*, 451-459.

Hofer, S.B., Mrsic-Flogel, T.D., Bonhoeffer, T., and Hubener, M. (2006b). Prior experience enhances plasticity in adult visual cortex. Nature neuroscience *9*, 127-132.

Hofer, S.B., Mrsic-Flogel, T.D., Bonhoeffer, T., and Hubener, M. (2009). Experience leaves a lasting structural trace in cortical circuits. Nature *457*, 313-317.

Holtmaat, A., Bonhoeffer, T., Chow, D.K., Chuckowree, J., De Paola, V., Hofer, S.B., Hubener, M., Keck, T., Knott, G., Lee, W.C., *et al.* (2009). Long-term, high-resolution imaging in the mouse neocortex through a chronic cranial window. Nat Protoc *4*, 1128-1144.

Holtmaat, A., and Svoboda, K. (2009). Experience-dependent structural synaptic plasticity in the mammalian brain. Nat Rev Neurosci *10*, 647-658.

Hooks, B.M., and Chen, C. (2007). Critical periods in the visual system: changing views for a model of experience-dependent plasticity. Neuron *56*, 312-326.

Hoshiko, M., Arnoux, I., Avignone, E., Yamamoto, N., and Audinat, E. (2012). Deficiency of the microglial receptor CX3CR1 impairs postnatal functional development of thalamocortical synapses in the barrel cortex. J Neurosci *32*, 15106-15111.

Huang, Z.J., Kirkwood, A., Pizzorusso, T., Porciatti, V., Morales, B., Bear, M.F., Maffei, L., and Tonegawa, S. (1999). BDNF regulates the maturation of inhibition and the critical period of plasticity in mouse visual cortex. Cell *98*, 739-755.

Hubel, D.H., and Wiesel, T.N. (1962). Receptive fields, binocular interaction and functional architecture in the cat's visual cortex. The Journal of physiology *160*, 106-154.

Hubel, D.H., and Wiesel, T.N. (1965). Binocular interaction in striate cortex of kittens reared with artificial squint. Journal of neurophysiology *28*, 1041-1059.

Hubel, D.H., and Wiesel, T.N. (1968). Receptive fields and functional architecture of monkey striate cortex. The Journal of physiology *195*, 215-243.

Hubel, D.H., and Wiesel, T.N. (1970). The period of susceptibility to the physiological effects of unilateral eye closure in kittens. The Journal of physiology *206*, 419-436.

Hubel, D.H., Wiesel, T.N., and LeVay, S. (1977). Plasticity of ocular dominance columns in monkey striate cortex. Philos Trans R Soc Lond B Biol Sci *278*, 377-409.

Huber, K.M., Kayser, M.S., and Bear, M.F. (2000). Role for rapid dendritic protein synthesis in hippocampal mGluR-dependent long-term depression. Science *288*, 1254-1257.

Huberman, A.D., Manu, M., Koch, S.M., Susman, M.W., Lutz, A.B., Ullian, E.M., Baccus, S.A., and Barres, B.A. (2008). Architecture and activity-mediated refinement of axonal projections from a mosaic of genetically identified retinal ganglion cells. Neuron *59*, 425-438.

Hurpin, C.M., Carosella, E.D., and Cazenave, P.A. (1992). Bactericidal activity of two IgG2a murine monoclonal antibodies with distinct fine specificities for group B Neisseria meningitidis capsular polysaccharide. Hybridoma *11*, 677-687.

Iny, K., Heynen, A.J., Sklar, E., and Bear, M.F. (2006). Bidirectional modifications of visual acuity induced by monocular deprivation in juvenile and adult rats. J Neurosci *26*, 7368-7374.

Ivanco, T.L., Racine, R.J., and Kolb, B. (2000). Morphology of layer III pyramidal neurons is altered following induction of LTP in sensorimotor cortex of the freely moving rat. Synapse *37*, 16-22.

Jacquemart, F., Millot, G., Goujet-Zalc, C., Mahouy, G., and Zalc, B. (1988). Production and characterization of a mouse monoclonal antibody to the glycolipid asialo-GM1. Hybridoma *7*, 323-331.

Jaubert-Miazza, L., Green, E., Lo, F.S., Bui, K., Mills, J., and Guido, W. (2005). Structural and functional composition of the developing retinogeniculate pathway in the mouse. Visual neuroscience *22*, 661-676.

Javaherian, A., and Cline, H.T. (2005). Coordinated motor neuron axon growth and neuromuscular synaptogenesis are promoted by CPG15 in vivo. Neuron *45*, 505-512.

Jourdain, P., Fukunaga, K., and Muller, D. (2003). Calcium/calmodulin-dependent protein kinase II contributes to activity-dependent filopodia growth and spine formation. J Neurosci *23*, 10645-10649.

Jung, S., Aliberti, J., Graemmel, P., Sunshine, M.J., Kreutzberg, G.W., Sher, A., and Littman, D.R. (2000). Analysis of fractalkine receptor CX(3)CR1 function by targeted deletion and green fluorescent protein reporter gene insertion. Molecular and cellular biology *20*, 4106-4114.

Kaech, S., and Banker, G. (2006). Culturing hippocampal neurons. Nat Protoc *1*, 2406-2415.

Kaech, S., Parmar, H., Roelandse, M., Bornmann, C., and Matus, A. (2001). Cytoskeletal microdifferentiation: a mechanism for organizing morphological plasticity in dendrites. Proceedings of the National Academy of Sciences of the United States of America *98*, 7086-7092.

Kalatsky, V.A., and Stryker, M.P. (2003). New paradigm for optical imaging: temporally encoded maps of intrinsic signal. Neuron *38*, 529-545.

Kalus, P., Muller, T.J., Zuschratter, W., and Senitz, D. (2000). The dendritic architecture of prefrontal pyramidal neurons in schizophrenic patients. Neuroreport *11*, 3621-3625.

Katayama, H., Yamamoto, A., Mizushima, N., Yoshimori, T., and Miyawaki, A. (2008). GFP-like proteins stably accumulate in lysosomes. Cell structure and function *33*, 1-12.

Kauderer, B.S., and Kandel, E.R. (2000). Capture of a protein synthesis-dependent component of long-term depression. Proceedings of the National Academy of Sciences of the United States of America *97*, 13342-13347.

Kawano, H., Kogure, T., Abe, Y., Mizuno, H., and Miyawaki, A. (2008). Two-photon dual-color imaging using fluorescent proteins. Nature methods *5*, 373-374.

Keck, T., Mrsic-Flogel, T.D., Vaz Afonso, M., Eysel, U.T., Bonhoeffer, T., and Hubener, M. (2008). Massive restructuring of neuronal circuits during functional reorganization of adult visual cortex. Nature neuroscience *11*, 1162-1167.

Kelleher, R.J., 3rd, Govindarajan, A., and Tonegawa, S. (2004). Translational regulatory mechanisms in persistent forms of synaptic plasticity. Neuron *44*, 59-73.

Kettenmann, H., Hanisch, U.K., Noda, M., and Verkhratsky, A. (2011). Physiology of microglia. Physiological reviews *91*, 461-553.

Kharazia, V.N., and Weinberg, R.J. (1999). Immunogold localization of AMPA and NMDA receptors in somatic sensory cortex of albino rat. J Comp Neurol *412*, 292-302.

Khibnik, L.A., Cho, K.K., and Bear, M.F. (2010). Relative contribution of feedforward excitatory connections to expression of ocular dominance plasticity in layer 4 of visual cortex. Neuron *66*, 493-500.

Kim, K.W., Vallon-Eberhard, A., Zigmond, E., Farache, J., Shezen, E., Shakhar, G., Ludwig, A., Lira, S.A., and Jung, S. (2011). In vivo structure/function and expression analysis of the CX3C chemokine fractalkine. Blood *118*, e156-167.

Kirkwood, A., Dudek, S.M., Gold, J.T., Aizenman, C.D., and Bear, M.F. (1993). Common forms of synaptic plasticity in the hippocampus and neocortex in vitro. Science *260*, 1518-1521.

Kleinman, H.K., Klebe, R.J., and Martin, G.R. (1981). Role of collagenous matrices in the adhesion and growth of cells. J Cell Biol *88*, 473-485.

Knott, G.W., Holtmaat, A., Wilbrecht, L., Welker, E., and Svoboda, K. (2006). Spine growth precedes synapse formation in the adult neocortex in vivo. Nature neuroscience *9*, 1117-1124.

Knott, G.W., Quairiaux, C., Genoud, C., and Welker, E. (2002). Formation of dendritic spines with GABAergic synapses induced by whisker stimulation in adult mice. Neuron *34*, 265-273.

Koch, C., and Zador, A. (1993). The function of dendritic spines: devices subserving biochemical rather than electrical compartmentalization. J Neurosci *13*, 413-422.

Koleske, A.J. (2013). Molecular mechanisms of dendrite stability. Nat Rev Neurosci *14*, 536-550.

Kono, D.H., and Theofilopoulos, A.N. (2006). Genetics of SLE in mice. Springer Semin Immunopathol *28*, 83-96.

Kupfer, C., and Palmer, P. (1964). Lateral Geniculate Nucleus - Histological + Cytochemical Changes Following Afferent Denervation + Visual Deprivation. Exp Neurol *9*, 400-&.

Lai, C.S., Franke, T.F., and Gan, W.B. (2012). Opposite effects of fear conditioning and extinction on dendritic spine remodelling. Nature *483*, 87-91.

Lang, C., Barco, A., Zablow, L., Kandel, E.R., Siegelbaum, S.A., and Zakharenko, S.S. (2004). Transient expansion of synaptically connected dendritic spines upon induction of hippocampal long-term potentiation. Proceedings of the National Academy of Sciences of the United States of America *101*, 16665-16670.

Lattal, K.M., and Abel, T. (2001). Different requirements for protein synthesis in acquisition and extinction of spatial preferences and context-evoked fear. J Neurosci *21*, 5773-5780.

Lee, S.H., Liu, L., Wang, Y.T., and Sheng, M. (2002). Clathrin adaptor AP2 and NSF interact with overlapping sites of GluR2 and play distinct roles in AMPA receptor trafficking and hippocampal LTD. Neuron *36*, 661-674.

Lee, W.C., and Nedivi, E. (2002). Extended plasticity of visual cortex in dark-reared animals may result from prolonged expression of cpg15-like genes. J Neurosci *22*, 1807-1815.

Lendvai, B., Stern, E.A., Chen, B., and Svoboda, K. (2000). Experience-dependent plasticity of dendritic spines in the developing rat barrel cortex in vivo. Nature *404*, 876-881.

Letourneau, P.C. (1975). Cell-to-substratum adhesion and guidance of axonal elongation. Dev Biol *44*, 92-101.

LeVay, S., Wiesel, T.N., and Hubel, D.H. (1980). The development of ocular dominance columns in normal and visually deprived monkeys. J Comp Neurol *191*, 1-51.

Li, Y., Du, X.F., Liu, C.S., Wen, Z.L., and Du, J.L. (2012). Reciprocal regulation between resting microglial dynamics and neuronal activity in vivo. Developmental cell *23*, 1189-1202.

Liang, K.J., Lee, J.E., Wang, Y.D., Ma, W., Fontainhas, A.M., Fariss, R.N., and Wong, W.T. (2009). Regulation of dynamic behavior of retinal microglia by CX3CR1 signaling. Investigative ophthalmology & visual science *50*, 4444-4451.

Lin, B., Kramar, E.A., Bi, X., Brucher, F.A., Gall, C.M., and Lynch, G. (2005). Theta stimulation polymerizes actin in dendritic spines of hippocampus. J Neurosci *25*, 2062-2069.

Lin, Y.C., and Koleske, A.J. (2010). Mechanisms of synapse and dendrite maintenance and their disruption in psychiatric and neurodegenerative disorders. Annu Rev Neurosci *33*, 349-378.

Lipton, P., and Raley-Susman, K.M. (1999). Autoradiographic measurements of protein synthesis in hippocampal slices from rats and guinea pigs. Methods *18*, 127-143.

Liu, B.H., Wu, G.K., Arbuckle, R., Tao, H.W., and Zhang, L.I. (2007). Defining cortical frequency tuning with recurrent excitatory circuitry. Nature neuroscience *10*, 1594-1600.

Liu, C.H., Heynen, A.J., Shuler, M.G., and Bear, M.F. (2008). Cannabinoid receptor blockade reveals parallel plasticity mechanisms in different layers of mouse visual cortex. Neuron *58*, 340-345.

Lois, C., Hong, E.J., Pease, S., Brown, E.J., and Baltimore, D. (2002). Germline transmission and tissue-specific expression of transgenes delivered by lentiviral vectors. Science *295*, 868-872.

Lynch, B.A., Lambeng, N., Nocka, K., Kensel-Hammes, P., Bajjalieh, S.M., Matagne, A., and Fuks, B. (2004). The synaptic vesicle protein SV2A is the binding site for the antiepileptic drug levetiracetam. Proceedings of the National Academy of Sciences of the United States of America *101*, 9861-9866.

Maciejewski-Lenoir, D., Chen, S., Feng, L., Maki, R., and Bacon, K.B. (1999). Characterization of fractalkine in rat brain cells: migratory and activation signals for CX3CR-1-expressing microglia. Journal of immunology *163*, 1628-1635.

Maggi, L., Trettel, F., Scianni, M., Bertollini, C., Eusebi, F., Fredholm, B.B., and Limatola, C. (2009). LTP impairment by fractalkine/CX3CL1 in mouse hippocampus is mediated through the activity of adenosine receptor type 3 (A3R). Journal of neuroimmunology *215*, 36-42.

Majewska, A.K., Newton, J.R., and Sur, M. (2006). Remodeling of synaptic structure in sensory cortical areas in vivo. J Neurosci *26*, 3021-3029.

Malenka, R.C., and Bear, M.F. (2004). LTP and LTD: an embarrassment of riches. Neuron *44*, 5-21.

Maletic-Savatic, M., Malinow, R., and Svoboda, K. (1999). Rapid dendritic morphogenesis in CA1 hippocampal dendrites induced by synaptic activity. Science *283*, 1923-1927.

Mallat, M., Chamak, B., and Thery, C. (1994). Influences of brain macrophages on the survival, growth and regeneration of neurons. Neurodegenerative Diseases, 91-104.

Mallat, M., Houlgatte, R., Brachet, P., and Prochiantz, A. (1989). Lipopolysaccharide-stimulated rat brain macrophages release NGF in vitro. Dev Biol *133*, 309-311.

Manahan-Vaughan, D., Kulla, A., and Frey, J.U. (2000). Requirement of translation but not transcription for the maintenance of long-term depression in the CA1 region of freely moving rats. J Neurosci *20*, 8572-8576.

Mangini, N.J., and Pearlman, A.L. (1980). Laminar distribution of receptive field properties in the primary visual cortex of the mouse. J Comp Neurol *193*, 203-222.

Markus, E.J., Petit, T.L., and LeBoutillier, J.C. (1987). Synaptic structural changes during development and aging. Brain research *432*, 239-248.

Matsuzaki, M., Honkura, N., Ellis-Davies, G.C., and Kasai, H. (2004). Structural basis of long-term potentiation in single dendritic spines. Nature *429*, 761-766.

Matus, A. (2000). Actin-based plasticity in dendritic spines. Science *290*, 754-758.

May, O.L., Erisir, A., and Hill, D.L. (2008). Modifications of gustatory nerve synapses onto nucleus of the solitary tract neurons induced by dietary sodium-restriction during development. J Comp Neurol *508*, 529-541.

McCurry, C.L., Shepherd, J.D., Tropea, D., Wang, K.H., Bear, M.F., and Sur, M. (2010). Loss of Arc renders the visual cortex impervious to the effects of sensory experience or deprivation. Nature neuroscience *13*, 450-457.

McKinney, R.A., Capogna, M., Durr, R., Gahwiler, B.H., and Thompson, S.M. (1999). Miniature synaptic events maintain dendritic spines via AMPA receptor activation. Nature neuroscience *2*, 44-49.

Merchan-Perez, A., Rodriguez, J.R., Alonso-Nanclares, L., Schertel, A., and Defelipe, J. (2009). Counting Synapses Using FIB/SEM Microscopy: A True Revolution for Ultrastructural Volume Reconstruction. Frontiers in neuroanatomy *3*, 18.

Metin, C., Godement, P., and Imbert, M. (1988). The primary visual cortex in the mouse: receptive field properties and functional organization. Experimental brain research *69*, 594-612.

Mioche, L., and Singer, W. (1989). Chronic recordings from single sites of kitten striate cortex during experience-dependent modifications of receptive-field properties. Journal of neurophysiology *62*, 185-197.

Mitchell, D.E. (1988). The extent of visual recovery from early monocular or binocular visual deprivation in kittens. The Journal of physiology *395*, 639-660.

Mitchell, D.E., Cynader, M., and Movshon, J.A. (1977). Recovery from the effects of monocular deprivation in kittens. J Comp Neurol *176*, 53-63.

Mitzdorf, U., and Singer, W. (1980). Monocular activation of visual cortex in normal and monocularly deprived cats: an analysis of evoked potentials. The Journal of physiology *304*, 203-220.

Montarolo, P.G., Goelet, P., Castellucci, V.F., Morgan, J., Kandel, E.R., and Schacher, S. (1986). A critical period for macromolecular synthesis in long-term heterosynaptic facilitation in Aplysia. Science *234*, 1249-1254.

Mostany, R., and Portera-Cailliau, C. (2008). A craniotomy surgery procedure for chronic brain imaging. J Vis Exp.

Mrsic-Flogel, T.D., Hofer, S.B., Ohki, K., Reid, R.C., Bonhoeffer, T., and Hubener, M. (2007). Homeostatic regulation of eye-specific responses in visual cortex during ocular dominance plasticity. Neuron *54*, 961-972.

Muhammed, R. (2009). The mouse visually evoked potential : neural correlates and functional applications. In Massachusetts Institute of Technology Dept of Brain and Cognitive Sciences (Cambridge, Massachusetts: Massachusetts Institute of Technology).

Mulkey, R.M., and Malenka, R.C. (1992). Mechanisms underlying induction of homosynaptic long-term depression in area CA1 of the hippocampus. Neuron *9*, 967-975.

Nader, K., Schafe, G.E., and Le Doux, J.E. (2000). Fear memories require protein synthesis in the amygdala for reconsolidation after retrieval. Nature *406*, 722-726.

Nagerl, U.V., Eberhorn, N., Cambridge, S.B., and Bonhoeffer, T. (2004). Bidirectional activity-dependent morphological plasticity in hippocampal neurons. Neuron *44*, 759-767.

Nahmani, M., and Erisir, A. (2005). VGluT2 immunochemistry identifies thalamocortical terminals in layer 4 of adult and developing visual cortex. J Comp Neurol *484*, 458-473.

Nedivi, E., Fieldust, S., Theill, L.E., and Hevron, D. (1996). A set of genes expressed in response to light in the adult cerebral cortex and regulated during development. Proceedings of the National Academy of Sciences of the United States of America *93*, 2048-2053.

Nedivi, E., Hevroni, D., Naot, D., Israeli, D., and Citri, Y. (1993). Numerous candidate plasticity-related genes revealed by differential cDNA cloning. Nature *363*, 718-722.

Nedivi, E., Wu, G.Y., and Cline, H.T. (1998). Promotion of dendritic growth by CPG15, an activity-induced signaling molecule. Science *281*, 1863-1866.

Nguyen, A.T., Braschi, S., Geoffrion, M., Fong, L.G., Crooke, R.M., Graham, M.J., Young, S.G., and Milne, R. (2006). A mouse monoclonal antibody specific for mouse apoB48 and apoB100 produced by immunizing "apoB39-only" mice with mouse apoB48. Biochim Biophys Acta *1761*, 182-185.

Nimmerjahn, A., Kirchhoff, F., and Helmchen, F. (2005). Resting microglial cells are highly dynamic surveillants of brain parenchyma in vivo. Science *308*, 1314-1318.

Nishiyori, A., Minami, M., Ohtani, Y., Takami, S., Yamamoto, J., Kawaguchi, N., Kume, T., Akaike, A., and Satoh, M. (1998). Localization of fractalkine and CX3CR1 mRNAs in rat brain: does fractalkine play a role in signaling from neuron to microglia? FEBS letters *429*, 167-172.

Obata, S., Obata, J., Das, A., and Gilbert, C.D. (1999). Molecular correlates of topographic reorganization in primary visual cortex following retinal lesions. Cerebral cortex *9*, 238-248.

Okamoto, K., Nagai, T., Miyawaki, A., and Hayashi, Y. (2004). Rapid and persistent modulation of actin dynamics regulates postsynaptic reorganization underlying bidirectional plasticity. Nature neuroscience *7*, 1104-1112.

Osterweil, E.K., Krueger, D.D., Reinhold, K., and Bear, M.F. (2010). Hypersensitivity to mGluR5 and ERK1/2 leads to excessive protein synthesis in the hippocampus of a mouse model of fragile X syndrome. J Neurosci *30*, 15616-15627.

Pagani, F., Paolicelli, R.C., Murana, E., Cortese, B., Di Angelantonio, S., Zurolo, E., Guiducci, E., Ferreira, T.A., Garofalo, S., Catalano, M., *et al.* (2015). Defective microglial development in the hippocampus of Cx3cr1 deficient mice. Frontiers in cellular neuroscience *9*, 111.

Paolicelli, R.C., Bolasco, G., Pagani, F., Maggi, L., Scianni, M., Panzanelli, P., Giustetto, M., Ferreira, T.A., Guiducci, E., Dumas, L., *et al.* (2011). Synaptic pruning by microglia is necessary for normal brain development. Science *333*, 1456-1458.

Parkhurst, C.N., Yang, G., Ninan, I., Savas, J.N., Yates, J.R., 3rd, Lafaille, J.J., Hempstead, B.L., Littman, D.R., and Gan, W.B. (2013). Microglia promote learning-dependent synapse formation through brain-derived neurotrophic factor. Cell *155*, 1596-1609.

Parnavelas, J.G., Globus, A., and Kaups, P. (1973). Continuous illumination from birth affects spine density of neurons in the visual cortex of the rat. Exp Neurol *40*, 742-747.

Pascual, O., Ben Achour, S., Rostaing, P., Triller, A., and Bessis, A. (2012). Microglia activation triggers astrocyte-mediated modulation of excitatory neurotransmission. Proceedings of the National Academy of Sciences of the United States of America *109*, E197-205.

Perea, G., and Araque, A. (2010). GLIA modulates synaptic transmission. Brain research reviews *63*, 93-102.

Peri, F., and Nusslein-Volhard, C. (2008). Live imaging of neuronal degradation by microglia reveals a role for v0-ATPase a1 in phagosomal fusion in vivo. Cell *133*, 916-927.

Peters, A., Palay, S.L., and Webster, H.d. (1991). The fine structure of the nervous system : neurons and their supporting cells, 3rd edn (New York: Oxford University Press).

Pham, T.A., Rubenstein, J.L., Silva, A.J., Storm, D.R., and Stryker, M.P. (2001). The CRE/CREB pathway is transiently expressed in thalamic circuit development and contributes to refinement of retinogeniculate axons. Neuron *31*, 409-420.

Pittenger, C., and Kandel, E.R. (2003). In search of general mechanisms for long-lasting plasticity: Aplysia and the hippocampus. Philos Trans R Soc Lond B Biol Sci *358*, 757-763.

Pocock, J.M., and Kettenmann, H. (2007). Neurotransmitter receptors on microglia. Trends in neurosciences *30*, 527-535.

Porter, N.M., Thibault, O., Thibault, V., Chen, K.C., and Landfield, P.W. (1997). Calcium channel density and hippocampal cell death with age in long-term culture. J Neurosci *17*, 5629-5639.

Portera-Cailliau, C., Weimer, R.M., De Paola, V., Caroni, P., and Svoboda, K. (2005). Diverse modes of axon elaboration in the developing neocortex. PLoS Biol *3*, e272.

Prusky, G.T., and Douglas, R.M. (2003). Developmental plasticity of mouse visual acuity. The European journal of neuroscience *17*, 167-173.

Prusky, G.T., West, P.W., and Douglas, R.M. (2000). Behavioral assessment of visual acuity in mice and rats. Vision Res *40*, 2201-2209.

Purpura, D.P. (1974). Dendritic spine "dysgenesis" and mental retardation. Science *186*, 1126-1128.

Putz, U., Harwell, C., and Nedivi, E. (2005). Soluble CPG15 expressed during early development rescues cortical progenitors from apoptosis. Nature neuroscience *8*, 322-331.

Ragozzino, D., Di Angelantonio, S., Trettel, F., Bertollini, C., Maggi, L., Gross, C., Charo, I.F., Limatola, C., and Eusebi, F. (2006). Chemokine fractalkine/CX3CL1 negatively modulates active glutamatergic synapses in rat hippocampal neurons. J Neurosci *26*, 10488-10498.

Rakic, P., Bourgeois, J.P., Eckenhoff, M.F., Zecevic, N., and Goldman-Rakic, P.S. (1986). Concurrent overproduction of synapses in diverse regions of the primate cerebral cortex. Science *232*, 232-235.

Ramón y Cajal, S., DeFelipe, J., and Jones, E.G. (1988). Cajal on the cerebral cortex : an annotated translation of the complete writings (New York: Oxford University Press).

Reimer, G., Pollard, K.M., Penning, C.A., Ochs, R.L., Lischwe, M.A., Busch, H., and Tan, E.M. (1987). Monoclonal autoantibody from a (New Zealand black x New Zealand white)F1 mouse and some human scleroderma sera target an Mr 34,000 nucleolar protein of the U3 RNP particle. Arthritis Rheum *30*, 793-800.

Rezaie, P., and Male, D. (1999). Colonisation of the developing human brain and spinal cord by microglia: a review. Microsc Res Tech *45*, 359-382.

Rittenhouse, C.D., Siegler, B.A., Voelker, C.C., Shouval, H.Z., Paradiso, M.A., and Bear, M.F. (2006). Stimulus for rapid ocular dominance plasticity in visual cortex. Journal of neurophysiology *95*, 2947-2950.

Rogers, J.T., Morganti, J.M., Bachstetter, A.D., Hudson, C.E., Peters, M.M., Grimmig, B.A., Weeber, E.J., Bickford, P.C., and Gemma, C. (2011). CX3CR1 deficiency leads to impairment of hippocampal cognitive function and synaptic plasticity. J Neurosci *31*, 16241-16250.

Romijn, H.J., van Huizen, F., and Wolters, P.S. (1984). Towards an improved serum-free, chemically defined medium for long-term culturing of cerebral cortex tissue. Neurosci Biobehav Rev *8*, 301-334.

Roth, S., Zhang, S., Chiu, J., Wirth, E.K., and Schweizer, U. (2010). Development of a serum-free supplement for primary neuron culture reveals the interplay of selenium and vitamin E in neuronal survival. J Trace Elem Med Biol *24*, 130-137.

Rubio-Garrido, P., Perez-de-Manzo, F., Porrero, C., Galazo, M.J., and Clasca, F. (2009). Thalamic input to distal apical dendrites in neocortical layer 1 is massive and highly convergent. Cerebral cortex *19*, 2380-2395.

Sajikumar, S., and Frey, J.U. (2003). Anisomycin inhibits the late maintenance of long-term depression in rat hippocampal slices in vitro. Neurosci Lett *338*, 147-150.

Sajikumar, S., Navakkode, S., and Frey, J.U. (2005). Protein synthesis-dependent long-term functional plasticity: methods and techniques. Current opinion in neurobiology *15*, 607-613.

Sakaguchi, S., Yamaguchi, T., Nomura, T., and Ono, M. (2008). Regulatory T cells and immune tolerance. Cell *133*, 775-787.

Sato, M., and Stryker, M.P. (2008). Distinctive features of adult ocular dominance plasticity. J Neurosci *28*, 10278-10286.

Sawtell, N.B., Frenkel, M.Y., Philpot, B.D., Nakazawa, K., Tonegawa, S., and Bear, M.F. (2003). NMDA receptor-dependent ocular dominance plasticity in adult visual cortex. Neuron *38*, 977-985.

Schafer, D.P., Lehrman, E.K., Kautzman, A.G., Koyama, R., Mardinly, A.R., Yamasaki, R., Ransohoff, R.M., Greenberg, M.E., Barres, B.A., and Stevens, B. (2012). Microglia sculpt postnatal neural circuits in an activity and complement-dependent manner. Neuron *74*, 691-705.

Schafer, D.P., Lehrman, E.K., and Stevens, B. (2013). The "quad-partite" synapse: microglia-synapse interactions in the developing and mature CNS. Glia *61*, 24-36.

Schikorski, T., and Stevens, C.F. (1997). Quantitative ultrastructural analysis of hippocampal excitatory synapses. J Neurosci *17*, 5858-5867.

Schluter, O.M., Xu, W., and Malenka, R.C. (2006). Alternative N-terminal domains of PSD-95 and SAP97 govern activity-dependent regulation of synaptic AMPA receptor function. Neuron *51*, 99-111.

Schneider, M., Marison, I.W., and von Stockar, U. (1996). The importance of ammonia in mammalian cell culture. J Biotechnol *46*, 161-185.

Schuett, S., Bonhoeffer, T., and Hubener, M. (2002). Mapping retinotopic structure in mouse visual cortex with optical imaging. J Neurosci *22*, 6549-6559.

Schuz, A., and Munster, A. (1985). Synaptic density on the axonal tree of a pyramidal cell in the cortex of the mouse. Neuroscience *15*, 33-39.

Shatz, C.J., and Stryker, M.P. (1978). Ocular dominance in layer IV of the cat's visual cortex and the effects of monocular deprivation. The Journal of physiology *281*, 267-283.

Sheridan, G.K., and Murphy, K.J. (2013). Neuron-glia crosstalk in health and disease: fractalkine and CX3CR1 take centre stage. Open biology *3*, 130181.

Shimojo, M., Nakajima, K., Takei, N., Hamanoue, M., and Kohsaka, S. (1991). Production of basic fibroblast growth factor in cultured rat brain microglia. Neurosci Lett *123*, 229-231.

Shirai, T., and Mellors, R.C. (1971). Natural thymocytotoxic autoantibody and reactive antigen in New Zealand black and other mice. Proceedings of the National Academy of Sciences of the United States of America *68*, 1412-1415.

Singer, W. (1977). Effects of monocular deprivation on excitatory and inhibitory pathways in cat striate cortex. Experimental brain research *30*, 25-41.

Smith, G.B., Heynen, A.J., and Bear, M.F. (2009). Bidirectional synaptic mechanisms of ocular dominance plasticity in visual cortex. Philos Trans R Soc Lond B Biol Sci *364*, 357-367.

Sogn, C.J., Puchades, M., and Gundersen, V. (2013). Rare contacts between synapses and microglial processes containing high levels of Iba1 and actin--a postembedding immunogold study in the healthy rat brain. The European journal of neuroscience *38*, 2030-2040.

Somogyi, E., Sotonyi, P., Balogh, I., Nemes, A., and Rubanyi, G. (1978). Comparative polarized-light and electron microscopic studies of changes in the structure of the intercalate disc following various experimental lesions. Acta morphologica Academiae Scientiarum Hungaricae *26*, 197-210.

Song, L., Lee, C., and Schindler, C. (2011). Deletion of the murine scavenger receptor CD68. Journal of lipid research *52*, 1542-1550.

Squirrell, J.M., Wokosin, D.L., White, J.G., and Bavister, B.D. (1999). Long-term two-photon fluorescence imaging of mammalian embryos without compromising viability. Nature biotechnology *17*, 763-767.

Stellwagen, D., and Malenka, R.C. (2006). Synaptic scaling mediated by glial TNF-alpha. Nature *440*, 1054-1059.

Stettler, D.D., Yamahachi, H., Li, W., Denk, W., and Gilbert, C.D. (2006). Axons and synaptic boutons are highly dynamic in adult visual cortex. Neuron *49*, 877-887.

Stevens, B., Allen, N.J., Vazquez, L.E., Howell, G.R., Christopherson, K.S., Nouri, N., Micheva, K.D., Mehalow, A.K., Huberman, A.D., Stafford, B., *et al.* (2007). The classical complement cascade mediates CNS synapse elimination. Cell *131*, 1164-1178.

Stockmeier, C.A., Mahajan, G.J., Konick, L.C., Overholser, J.C., Jurjus, G.J., Meltzer, H.Y., Uylings, H.B., Friedman, L., and Rajkowska, G. (2004). Cellular changes in the postmortem hippocampus in major depression. Biol Psychiatry *56*, 640-650.

Sun, W., Tan, Z., Mensh, B.D., and Ji, N. (2016). Thalamus provides layer 4 of primary visual cortex with orientation- and direction-tuned inputs. Nature neuroscience *19*, 308-315.

Svoboda, K., Denk, W., Kleinfeld, D., and Tank, D.W. (1997). In vivo dendritic calcium dynamics in neocortical pyramidal neurons. Nature *385*, 161-165.

Svoboda, K., and Yasuda, R. (2006). Principles of two-photon excitation microscopy and its applications to neuroscience. Neuron *50*, 823-839.

Tagawa, Y., Kanold, P.O., Majdan, M., and Shatz, C.J. (2005). Multiple periods of functional ocular dominance plasticity in mouse visual cortex. Nature neuroscience *8*, 380-388.

Takumi, Y., Ramirez-Leon, V., Laake, P., Rinvik, E., and Ottersen, O.P. (1999). Different modes of expression of AMPA and NMDA receptors in hippocampal synapses. Nature neuroscience *2*, 618-624.

Talal, N., and Steinberg, A.D. (1974). The pathogenesis of autoimmunity in New Zealand black mice. Curr Top Microbiol Immunol *64*, 79-103.

Tanaka, J., Horiike, Y., Matsuzaki, M., Miyazaki, T., Ellis-Davies, G.C., and Kasai, H. (2008). Protein synthesis and neurotrophin-dependent structural plasticity of single dendritic spines. Science *319*, 1683-1687.

Tanaka, Y., Matsuwaki, T., Yamanouchi, K., and Nishihara, M. (2013). Increased lysosomal biogenesis in activated microglia and exacerbated neuronal damage after traumatic brain injury in progranulin-deficient mice. Neuroscience *250*, 8-19.

Terry, R.D., Masliah, E., Salmon, D.P., Butters, N., DeTeresa, R., Hill, R., Hansen, L.A., and Katzman, R. (1991). Physical basis of cognitive alterations in Alzheimer's disease: synapse loss is the major correlate of cognitive impairment. Ann Neurol *30*, 572-580.

Theodosis, D.T., Poulain, D.A., and Oliet, S.H. (2008). Activity-dependent structural and functional plasticity of astrocyte-neuron interactions. Physiological reviews *88*, 983-1008.

Thomas, W.E. (1992). Brain macrophages: evaluation of microglia and their functions. Brain research Brain research reviews *17*, 61-74.

Tondravi, M.M., McKercher, S.R., Anderson, K., Erdmann, J.M., Quiroz, M., Maki, R., and Teitelbaum, S.L. (1997). Osteopetrosis in mice lacking haematopoietic transcription factor PU.1. Nature *386*, 81-84.

Trachtenberg, J.T., Chen, B.E., Knott, G.W., Feng, G., Sanes, J.R., Welker, E., and Svoboda, K. (2002). Long-term in vivo imaging of experience-dependent synaptic plasticity in adult cortex. Nature *420*, 788-794.

Trachtenberg, J.T., and Stryker, M.P. (2001). Rapid anatomical plasticity of horizontal connections in the developing visual cortex. J Neurosci *21*, 3476-3482.

Trachtenberg, J.T., Trepel, C., and Stryker, M.P. (2000). Rapid extragranular plasticity in the absence of thalamocortical plasticity in the developing primary visual cortex. Science *287*, 2029-2032.

Tremblay, M.E., Lowery, R.L., and Majewska, A.K. (2010). Microglial interactions with synapses are modulated by visual experience. PLoS Biol *8*, e1000527.

Tremblay, M.E., and Majewska, A.K. (2011). A role for microglia in synaptic plasticity? Commun Integr Biol *4*, 220-222.

Tritsch, G.L., and Moore, G.E. (1962). Spontaneous decomposition of glutamine in cell culture media. Exp Cell Res *28*, 360-364.

Tsui, J., and Malenka, R.C. (2006). Substrate localization creates specificity in calcium/calmodulin-dependent protein kinase II signaling at synapses. The Journal of biological chemistry *281*, 13794-13804.

Tsumoto, T., and Suda, K. (1978). Evidence for excitatory connections from the deprived eye to the visual cortex in monocularly deprived kittens. Brain research *153*, 150-156.

Ueno, M., Fujita, Y., Tanaka, T., Nakamura, Y., Kikuta, J., Ishii, M., and Yamashita, T. (2013). Layer V cortical neurons require microglial support for survival during postnatal development. Nature neuroscience *16*, 543-551.

van der Valk, J., Brunner, D., De Smet, K., Fex Svenningsen, A., Honegger, P., Knudsen, L.E., Lindl, T., Noraberg, J., Price, A., Scarino, M.L., *et al.* (2010). Optimization of chemically defined cell culture media--replacing fetal bovine serum in mammalian in vitro methods. Toxicol In Vitro *24*, 1053-1063.

Van Harreveld, A., and Fifkova, E. (1975). Swelling of dendritic spines in the fascia dentata after stimulation of the perforant fibers as a mechanism of post-tetanic potentiation. Exp Neurol *49*, 736-749.

Vanderklish, P.W., and Edelman, G.M. (2002). Dendritic spines elongate after stimulation of group 1 metabotropic glutamate receptors in cultured hippocampal neurons. Proceedings of the National Academy of Sciences of the United States of America *99*, 1639-1644.

Wake, H., Moorhouse, A.J., Jinno, S., Kohsaka, S., and Nabekura, J. (2009). Resting microglia directly monitor the functional state of synapses in vivo and determine the fate of ischemic terminals. J Neurosci *29*, 3974-3980.

Wallace, W., and Bear, M.F. (2004). A morphological correlate of synaptic scaling in visual cortex. J Neurosci *24*, 6928-6938.

Wang, L., Kloc, M., Gu, Y., Ge, S., and Maffei, A. (2013). Layer-specific experience-dependent rewiring of thalamocortical circuits. J Neurosci *33*, 4181-4191.

Waung, M.W., Pfeiffer, B.E., Nosyreva, E.D., Ronesi, J.A., and Huber, K.M. (2008). Rapid translation of Arc/Arg3.1 selectively mediates mGluR-dependent LTD through persistent increases in AMPAR endocytosis rate. Neuron *59*, 84-97.

Wiesel, T.N., and Hubel, D.H. (1963). Single-Cell Responses in Striate Cortex of Kittens Deprived of Vision in One Eye. Journal of neurophysiology *26*, 1003-1017.

Wiesel, T.N., and Hubel, D.H. (1965). Comparison of the effects of unilateral and bilateral eye closure on cortical unit responses in kittens. Journal of neurophysiology *28*, 1029-1040.

Wilbrecht, L., Holtmaat, A., Wright, N., Fox, K., and Svoboda, K. (2010). Structural plasticity underlies experience-dependent functional plasticity of cortical circuits. J Neurosci *30*, 4927-4932.

Xu, T., Yu, X., Perlik, A.J., Tobin, W.F., Zweig, J.A., Tennant, K., Jones, T., and Zuo, Y. (2009). Rapid formation and selective stabilization of synapses for enduring motor memories. Nature *462*, 915-919.

Yamahachi, H., Marik, S.A., McManus, J.N., Denk, W., and Gilbert, C.D. (2009). Rapid axonal sprouting and pruning accompany functional reorganization in primary visual cortex. Neuron *64*, 719-729.

Yang, Y., Wang, X.B., Frerking, M., and Zhou, Q. (2008). Spine expansion and stabilization associated with long-term potentiation. J Neurosci *28*, 5740-5751.

Yang, Y., and Zhou, Q. (2009). Spine modifications associated with long-term potentiation. Neuroscientist *15*, 464-476.

Yona, S., Kim, K.W., Wolf, Y., Mildner, A., Varol, D., Breker, M., Strauss-Ayali, D., Viukov, S., Guilliams, M., Misharin, A., *et al.* (2013). Fate mapping reveals origins and dynamics of monocytes and tissue macrophages under homeostasis. Immunity *38*, 79-91.

Yoon, B.J., Smith, G.B., Heynen, A.J., Neve, R.L., and Bear, M.F. (2009). Essential role for a long-term depression mechanism in ocular dominance plasticity. Proceedings of the National Academy of Sciences of the United States of America *106*, 9860-9865.

Zhan, Y., Paolicelli, R.C., Sforazzini, F., Weinhard, L., Bolasco, G., Pagani, F., Vyssotski, A.L., Bifone, A., Gozzi, A., Ragozzino, D., *et al.* (2014). Deficient neuron-microglia signaling results in impaired functional brain connectivity and social behavior. Nature neuroscience *17*, 400-406.

Zhou, H., Wang, Y., Wang, W., Jia, J., Li, Y., Wang, Q., Wu, Y., and Tang, J. (2009). Generation of monoclonal antibodies against highly conserved antigens. PloS one *4*, e6087.

Zhou, Q., Homma, K.J., and Poo, M.M. (2004). Shrinkage of dendritic spines associated with long-term depression of hippocampal synapses. Neuron *44*, 749-757.

Zito, K., Knott, G., Shepherd, G.M., Shenolikar, S., and Svoboda, K. (2004). Induction of spine growth and synapse formation by regulation of the spine actin cytoskeleton. Neuron *44*, 321-334.

Zuo, Y., Lin, A., Chang, P., and Gan, W.B. (2005). Development of long-term dendritic spine stability in diverse regions of cerebral cortex. Neuron *46*, 181-189.